CONFIDENTIAL

Copy
RM L9J05

NACA RM L9J05

NACA

RESEARCH MEMORANDUM

INVESTIGATION AT MACH NUMBER 1.62 OF THE PRESSURE DISTRIBUTION OVER A RECTANGULAR WING WITH SYMMETRICAL CIRCULAR-ARC SECTION AND 30-PERCENT-CHORD TRAILING-EDGE FLAP

By K. R. Czarnecki and James N. Mueller

Langley Aeronautical Laboratory
Langley Air Force Base, Va.

NATIONAL ADVISORY COMMITTEE
FOR AERONAUTICS

WASHINGTON

January 25, 1950

CONFIDENTIAL

NATIONAL ADVISORY COMMITTEE FOR AERONAUTICS

RESEARCH MEMORANDUM

INVESTIGATION AT MACH NUMBER 1.62 OF THE PRESSURE DISTRIBUTION OVER A RECTANGULAR WING WITH SYMMETRICAL CIRCULAR-ARC SECTION AND 30-PERCENT-CHORD TRAILING-EDGE FLAP

By K. R. Czarnecki and James N. Mueller

SUMMARY

An investigation has been made of the pressure distribution over a rectangular wing with a 9-percent-thick symmetrical circular-arc section and a 30-percent-chord trailing-edge flap; schlieren and liquid-film flow studies have also been made. Results obtained at a Mach number of 1.62 and a Reynolds number range of 0.55 to 1.07 $\times 10^6$ indicate good agreement between theoretical and experimental pressure distributions except on the low-pressure side of the flap near the trailing edge and on the high-pressure side of the flap and wing near the hinge line. In these regions, laminar separation occurred. As a result of the flow separations, the experimental increments in aerodynamic coefficients due to angle of attack or flap deflection were generally smaller and the slopes of the experimental curves lower than the theoretical coefficient increments and slopes. The experimental section-coefficient curves also exhibit a break or shift that may result in undesirable stability and control characteristics such as snaking and nonlinear stick force-deflection relationships.

INTRODUCTION

As a result of the large number of airplanes and missiles being designed for the supersonic speed range, a great need has arisen for information on which to base the design of supersonic controls. In order to meet this need, a number of theoretical and experimental investigations of the aerodynamic characteristics of controls at supersonic speeds have been initiated. Theoretical flap characteristics alone are inadequate, however, because of the existence of shock-boundary-layer interaction effects not considered in the theory. Most

of the experimental investigations so far reported, on the other hand, have been limited to three-dimensional control surfaces and techniques that determine only the over-all characteristics of the control and give little or no insight into the reasons for the discrepancies between the theoretical and experimental results. An investigation of the interaction effects by means of pressure distributions and schlieren and liquid-film flow observations has, therefore, been undertaken to determine the nature and magnitude of the interaction effects for a three-dimensional rectangular wing with a trailing-edge flap.

The tests were made in the Langley 9-inch supersonic tunnel at Mach numbers of 1.62, 1.93, and 2.40 over a Reynolds number range from 0.55 to 1.07×10^6. Airfoils of 9- and 6-percent-chord thickness were investigated. Each airfoil had a rectangular plan form, a symmetrical circular-arc section, and a 30-percent-chord trailing-edge flap. The present paper gives the results obtained with the 9-percent-thick airfoil at the Mach number of 1.62.

SYMBOLS

p_L	local static pressure on airfoil
p	stream static pressure
M	stream Mach number
γ	ratio of specific heats for air (1.4)
q	dynamic pressure $\left(\frac{\gamma}{2}M^2 p\right)$
P	pressure coefficient $\left(\frac{p_L - p}{q}\right)$
c	chord of airfoil
c_f	chord of flap
n	section normal force (positive upward)
m	section pitching moment about midchord (positive when it tends to rotate the leading edge of airfoil upward)

h flap section hinge moment (positive when it tends to deflect the flap downward)

c_n section normal-force coefficient (n/qc)

c_m section pitching-moment coefficient about midchord $\left(m/qc^2\right)$

c_h flap section hinge-moment coefficient $\left(h/qc_f^2\right)$

ρ mass density of free stream

μ stream coefficient of viscosity

V free-stream velocity

R Reynolds number $(\rho Vc/\mu)$

α airfoil angle of attack

δ deflection of flap chord with respect to airfoil chord (positive in downward direction)

t/c ratio of maximum thickness of airfoil section to airfoil chord length

x/c distance from leading edge in terms of chord length

Slope parameters:

c_{n_α} variation of section normal-force coefficient with angle of attack $\left(\frac{\partial c_n}{\partial \alpha}\right)_\delta$

c_{m_α} variation of section pitching-moment coefficient with angle of attack $\left(\frac{\partial c_m}{\partial \alpha}\right)_\delta$

c_{h_α} variation of flap section hinge-moment coefficient with angle of attack $\left(\frac{\partial c_h}{\partial \alpha}\right)_\delta$

c_{n_δ} variation of section normal-force coefficient with flap deflection $\left(\frac{\partial c_n}{\partial \delta}\right)_\alpha$

c_{m_δ} variation of section pitching-moment coefficient with flap deflection $\left(\frac{\partial c_m}{\partial \delta}\right)_\alpha$

c_{h_δ} variation of flap section hinge-moment coefficient with flap deflection $\left(\frac{\partial c_h}{\partial \delta}\right)_\alpha$

$\left(\frac{\partial c_m}{\partial c_n}\right)_\delta$ variation of section pitching-moment coefficient with section normal-force coefficient for constant flap deflection

$\left(\frac{\partial c_h}{\partial c_n}\right)_\delta$ variation of section hinge-moment coefficient with section normal-force coefficient for constant flap deflection

$\left(\frac{\partial c_m}{\partial c_n}\right)_\alpha$ variation of section pitching-moment coefficient with section normal-force coefficient for constant angle of attack

$\left(\frac{\partial c_h}{\partial c_n}\right)_\alpha$ variation of section hinge-moment coefficient with section normal-force coefficient for constant angle of attack

APPARATUS AND METHODS

Wind Tunnel

The investigation was conducted in the Langley 9-inch supersonic tunnel, which is of the continuous-operation closed-return type with provisions for the control of the humidity and pressure of the enclosed air. Changes in test Mach number are provided by interchangeable two-dimensional nozzle blocks forming test sections approximately 9 inches

square. Eleven fine-mesh screens in the settling chamber ahead of the nozzles aid in keeping the turbulence in the tunnel test section at a low level. For qualitative, visual-flow observations, a schlieren optical system is provided. During the present tests, the quantity of water vapor in the tunnel air was kept to values sufficiently low so that the effects of condensation in the supersonic nozzle were negligible. The pressure in the tunnel was adjusted to provide the desired variations in Reynolds numbers for the tests.

Models

Two models were used in the investigation: a pressure-distribution model for pressure measurements and a schileren model for visual and liquid-film flow observations. Both models had 3-inch chords and rectangular plan forms and were equipped with 30-percent-chord full-span trailing-edge flaps. The airfoil sections in streamwise planes were symmetrical circular arcs with a thickness of 9 percent of the chord. The included angle between the wing upper and lower surfaces at the leading and trailing edges was 20.6°. All wing tips were cut off in planes parallel to the free-stream direction and perpendicular to the airfoil span.

The models were machined from steel with the leading and trailing edges ground to a thickness of less than 0.002 inch. The wing contours were cut to within 0.002 inch of the specified values, and the wing surfaces were free of scratches and highly polished. There was, however, a very slight spanwise twist over the length of the model, and the upper flap surface did not fair smoothly into the wing surface at all points by an amount smaller than the tolerance of 0.002 inch but great enough to be noticeable in the pressure distributions. The gap between the flap and the fixed portion of the airfoil was 0.005 inch or about 0.0017 chord. This gap was not sealed during the tests.

A dimensional sketch of the pressure-distribution model is shown in figure 1. For convenience in carrying pressure leads from the model to the outside of the tunnel and in setting angles of attack and flap-deflection angles, the model was mounted in the tunnel directly from the tunnel wall, as illustrated in figures 2 and 3. Inasmuch as no provision was made to bypass the tunnel-wall boundary layer, it was expected that there would be an interaction between the flow over the model and the tunnel boundary layer which would result in pressure disturbances similar to those reported in reference 1. In order to avoid making pressure measurements in regions strongly affected by such disturbances, the model was so proportioned that the disturbances from the model-tunnel-wall juncture would not intersect the Mach cone (based on linear theory) from the wing tip (e.g., fig. 3). The span of the

model was so chosen that the disturbance from the wing tip would not be reflected from the boundary layer on the tunnel wall opposite the tip to any point close to the trailing edge of the wing.

The pressure-distribution model was equipped with static-pressure orifices on both the upper and lower surfaces at two spanwise stations. One of the stations was located in the region between the Mach cones from the tip disturbances (fig. 3) where the flow was two-dimensional at low angles of attack and small flap deflections. At high angles of attack and large flap deflections the disturbances from the model-tunnel-wall juncture and from the wing tip actually merge on the high-pressure side of the wing or flap because of lower local velocities and higher local Mach angles and the flow at the station is no longer strictly two-dimensional. However, for the range of α and δ investigated the effects of the tip disturbances were negligible and the flow remained essentially two-dimensional even at the largest angles of the tests. The other orifice station was located within the Mach cone from the wing tip but outside the Mach cone from the leading edge of the flap. (See fig. 3.) At each station each wing surface contained 16 pressure orifices of 0.014-inch diameter drilled perpendicular to the surface. Twelve of the orifices were on the main airfoil and four on the flap. The locations of the orifices and the orifice stations are given in figure 1. All pressure leads from the orifices were ducted to the outside of the tunnel internally through the model and through the steel supporting plate.

Figure 4 shows the schlieren model and illustrates the method used to mount the wing in the tunnel for schlieren observations. For these tests the schlieren model was mounted horizontally from the lower nozzle block by means of a single, vertical, sweptback strut. In order to avoid interference from any shock-boundary-layer interaction at the airfoil-tunnel-wall juncture, the model was designed to span only the middle 60 percent of the tunnel and did not extend too close to the tunnel-wall boundary layers. For liquid-film flow studies the airfoil was mounted vertically from the tunnel wall in a similar manner by replacing one of the observation windows with a steel plate to which the model support strut was anchored.

Pressure Measurements and Reduction of Data

The pressures on the wing and the total pressure in the tunnel settling chamber were recorded simultaneously by photographing a multiple-tube mercury manometer on which the pressures were indicated. Subsequently, the pressures were read directly from the film as pressure coefficients through the use of a film reader.

Aerodynamic coefficients were obtained by plotting the pressures normal to the wing or flap chord and by mechanically integrating the faired curves. The chordwise components of the pressure forces were not computed because of the great labor required to reduce these pressures to coefficients and because it was found that the contribution of these chordwise components to all aerodynamic coefficients presented was relatively small and in no way affected any of the comparisons.

Test Methods and Range of Tests

During the investigation all pressure distributions and schlieren and liquid-film flow photographs were obtained by setting and holding constant the angle of attack of the airfoil and by varying the flap deflection in sequence from 0° to the limit of the positive or negative flap deflections. It was possible to change both the angle of attack and flap-deflection angle of the pressure-distribution wing from outside the tunnel while the tunnel was in operation. Angles of attack and flap angles on the schlieren model, on the other hand, had to be set while the tunnel was shut down and checked while the tunnel was operating. The angle settings of the pressure-distribution model were, therefore, somewhat more accurate than those on the schlieren wing because it was possible to use a more accurate technique for determining the angles.

All schlieren photographs were obtained with the model in profile with the knife edges in the schlieren system both horizontal and vertical. In the liquid-film flow investigation, the model was on one occasion photographed at different time intervals while drying in the tunnel during testing to check techniques, but usually it was photographed after being removed from the tunnel after a long time interval at which time the film was representative of flow conditions. A more detailed description of the basic technique can be found in reference 2.

Pressure-distribution tests were made over a range of α from -0.65° to 4.35° at 1° intervals. The highest angle of attack is slightly below the angle at which the leading-edge shock theoretically detached from the airfoil. The flap-deflection range was usually from about -16° to 18°, with the angles set in 2° increments in the small positive flap-deflection range and about 4° increments over the rest of the range.

Schlieren photographs with flap neutral were obtained over approximately the same range and interval of angle of attack as in the case of the pressure distributions. With the flap deflected, photographs were obtained at several flap angles, usually at angles of

attack of 0.35°, 2.35°, and 4.35°. Liquid-film flow studies were confined to $\alpha = 0°$ and 5° with flap neutral and to $\delta = 5°$, 10°, and 15° at an angle of attack of 0°.

Most of the pressure-distribution tests were made with the stagnation pressure in the tunnel set at one atmosphere, three-quarters of an atmosphere, and one-half atmosphere. Based on the airfoil chord of 3 inches, the test Reynolds numbers corresponding to the above pressures were 1.07, 0.81, and 0.55 million, respectively. Schlieren photographs and liquid-film flow studies were made only at the high Reynolds number although some visual schlieren observations also were made at the lower Reynolds numbers.

Precision of Data

Stream surveys obtained with the test section empty indicate that the mean value of the Mach number in the region occupied by the test models is 1.62 and that the variation about this mean is no more than 0.7 of 1 percent. There was no evidence of any large irregularities in stream flow direction. For the pressure-distribution model, the angle-of-attack and flap-deflection settings at station 1 are believed to be accurate to ±0.05° and ±0.1°, respectively. At station 2 the angle of attack is greater than that at station 1 by about 0.15° to 0.20° owing to the twist resulting from wing fabrication difficulties, and the angle settings are less certain owing to greater deflections under load than those which occurred at the inboard station. As a result of these uncertainties all angles, regardless of station, are based on those of station 1. For the schlieren model the angle settings are considered somewhat less accurate than those of the pressure-distribution model at station 1. Individual pressure coefficients are usually accurate to ±0.01, and consistent discrepancies of greater magnitude are not due to errors in reading pressures but due to local surface irregularities which were deliberately neglected in fairing the experimental curves. The pressure-coefficient increments resulting from the slight misalinement of the upper flap surface with the wing were not neglected. The aerodynamic coefficients are indicated usually to vary less than ±0.005 in c_n, ±0.002 in c_m, and ±0.01 in c_h with the greatest error resulting from inaccuracies in fairing the pressure curves in the region of the flap hinge line and near the flap trailing edge. Installation of pressure orifices close to these points would have been very difficult, owing to physical limitations imposed by the methods of model construction and tube installation.

RESULTS AND DISCUSSION

Pressure Distributions

Two-dimensional-flow region.- Some experimental pressure distributions selected from a considerably larger number obtained at the two-dimensional-flow station (station 1) are presented in figures 5 and 6 for a Reynolds number of 1.07×10^6 to show the effects of changing the angle of attack and flap deflection. In figure 7 are presented a few typical experimental pressure distributions to illustrate the effects of changes in Reynolds number. The theoretical pressure distributions included in figures 5 and 6 were calculated from oblique-shock theory and the Prandtl-Meyer equations for the expansion of a two-dimensional supersonic flow. The theoretical calculations neglect the fact that on circular-arc airfoils the shocks at the wing leading edge and at the flap hinge line are curved and the flow behind the shocks is rotational. Calculations by the method of reference 3 indicate, nevertheless, that for the range of angles of attack and flap-deflection angles of interest in this investigation at $M = 1.62$ the effects of neglecting shock curvature should be negligible for the most part.

The results shown in figure 5 for varying δ at constant α generally indicate very good agreement between theory and experiment over the forward portion of the airfoil but show a large deviation of the experimental pressures from the theoretical over the rear portion of the wing. When the flap was deflected, the experimental pressures on the suction side of the flap agreed with theory up to approximately the 85-percent-chord point at small flap angles but only to about the hinge line at high flap deflections. Beyond this point a slight compression not predicted by the theory occurred, and the pressure then remained approximately constant over the flap surface to the trailing edge. At the higher δ's, a similar small but abrupt pressure increase occurred on the main wing ahead of the flap hinge line on the flap high-pressure side, while the pressure rise expected on the flap surface did not occur until some distance aft of the hinge line. As the flap angle was decreased the region of the main wing affected by this phenomena diminished in size and it was no longer possible to distinguish the pressure changes accurately because of the lack of pressure orifices in the immediate vicinity of the hinge line.

Experimental pressure distributions having the characteristic small but abrupt pressure rise followed by a constant pressure just described above have been observed in reference 4 in supersonic tests of airfoils without flaps and in references 5 and 6 in investigations at transonic speeds of shock-boundary layer interactions. In all cases, these characteristic pressure distributions were found to be associated with flow separation. Further, in references 5 and 6 it was found that this

type of pressure distribution occurred only when the boundary layer on the wing was laminar. The occurrence of separation ahead of the hinge line on the high-pressure side and ahead of the trailing edge on the low-pressure side of the flap is possible because of the transmission of the high pressures behind the flap and trailing-edge shocks upstream through the subsonic boundary layer.

At the highest positive δ's shown in figure 5 the flap shock is detached from the lower flap surface according to the nonviscid shock-expansion theory. The slight disagreement between the theoretical and experimental pressure distributions over the forward portion of the airfoil at $\alpha = 4.35^\circ$ and $\delta = 13^\circ$ and 16° may most probably be ascribed to twist in the model between the pressure and angle measurement stations under the extremely high load.

Typical effects of angle of attack on the wing pressures with δ held constant are illustrated in figure 6. It may be seen that for $\delta = 0^\circ$ (fig. 6(b)) a small region of negative pressures greater than the theoretical was present on the upper flap surface ahead of the separated-flow region at all angles of attack. This apparent discrepancy between theory and experiment is believed to result from the fact that the upper flap-surface contour deviates from that of the wing by a small amount due to fabrication difficulties. The results also indicate that, when the flap was in the center of the wake and the flap load was nearly zero, flow separation was present simultaneously on both sides of the flap near the trailing edge. (See fig. 6(b), $\alpha = -0.65^\circ$ and 0.35° with $\delta = 0^\circ$.)

The effect of decreasing the Reynolds number from 1.07 to 0.55×10^6 (fig. 7) was to move the point of initial separation forward on both the suction side of the flap and the flap high-pressure side of the wing. The magnitudes of the pressure rises behind the separation points as characterized by the flat portions of the pressure distributions also increased. Pressure distributions obtained at a Reynolds number of 0.81×10^6 had characteristics intermediate to those at the higher and lower Reynolds numbers. Inasmuch as the changes in pressures from the pressures for the other Reynolds number conditions were small, no pressure-distribution data for the intermediate Reynolds number are shown. For the range of angles of attack, flap angles, and Reynolds numbers investigated the most forward point on the wing at which flow separation occurred was at the 50-percent-chord point or two-thirds of the flap chord ahead of the flap hinge line on the side of the wing toward which the flap was deflected.

Wing-tip region.- Pressure distributions obtained at station 2 in the region influenced by the wing tip are shown in figures 8 to 10. In order to make it possible to compare the pressure distributions at

the inboard and outboard stations directly, the combinations of angle of attack, flap deflection, and Reynolds number for which data are presented in figures 8 to 10 correspond exactly to the combinations of α, δ, and Reynolds number used in figures 5 to 7. For $\delta = 0^\circ$, the theoretical pressure-distribution curves for the outboard station were computed by the method of reference 7. A method of corresponding precision for the calculations of pressures on the flap in the region influenced by the wing tip for the case when the flap is deflected is not available. Hence, for this investigation, the theoretical flap pressures were obtained arbitrarily by adding to the pressure-distribution curves computed by the method of reference 7 for $\delta = 0^\circ$ (station 2) the increments in pressure coefficient due to flap deflection determined from two-dimensional shock-expansion theory. The Mach number at the hinge line was assumed to be that computed for the station by the method of reference 7, and the pressure increments are defined as the differences in flap pressures between $\delta = 0^\circ$ and δ equals the required angle.

In general, the experimental results indicate that the previously described phenomena of flow separation at station 1 were also present at station 2. The foremost point at station 2 influenced by the wing tip is apparent from the abrupt change in chordwise pressure gradient that occurs at that point. As the angle of attack was increased, the point moved forward on the lower wing surface and rearward on the upper surface, but its location was always in good agreement with theory.

Figure 10 indicates that at positive flap angles the pressure distributions that occurred on the upper or low-pressure side of the flap at the outboard station were of a different type at the two test Reynolds numbers shown. At $R = 0.55 \times 10^6$ the pressure distribution was of the same type as that found at the two-dimensional station at all Reynolds numbers. At $R = 1.07 \times 10^6$ the pressure distribution was no longer flat but the pressure increased continuously toward the flap trailing edge where it attained a magnitude considerably greater than that of the pressure found at the lower Reynolds number. Inasmuch as this phenomenon occurred only at positive δ (figs. 8 to 10), even at angles of attack near 0°, it is ascribed, at least partly, to the effects of model asymmetry.

Comparison between stations.- A comparison between the experimental pressure distributions at stations 1 and 2 indicates that, on the flap high-pressure side, flow separation occurred at approximately the same chordwise point on the main wing for comparable α's and δ's. (Compare figs. 5 to 7 with corresponding figs. 8 to 10.) The small but abrupt pressure increases behind the separation points also were approximately equal at the two stations for the test conditions where they could be accurately established. Thus, the pressure in the separated-flow region at station 1 was usually considerably greater

than that at station 2. The agreement between theory and experiment, however, is generally not quite as good at the outboard station as it was at the two-dimensional-flow station. The increased discrepancy apparently results partly from the fact that the experimental angle of attack at station 2 is somewhat higher than the nominal angle because of twist in the model and partly because of the inadequacy of the theory used to calculate the pressure. If the model twist is accounted for, then the agreement between theory and experiment at the outboard station is almost as good as that at station 1, despite the arbitrariness of the method of calculating the pressures.

On the flap suction surface, the flow again was found to separate at about the same chordwise location at the two pressure-measurement stations for all test conditions except possibly on the upper flap surface at positive flap angles when the Reynolds number was 1.07×10^6. While not shown, the results obtained at $R = 0.81 \times 10^6$ were very similar to those obtained at $R = 0.55 \times 10^6$. If the results on the flap upper surface at positive δ at $R = 1.07 \times 10^6$ are excluded, it is found that the pressures in the separated-flow region are nearly equal at the two stations, although the pressure at station 1 is consistently the greater of the two by a very small amount. It appears from an analysis of these results, therefore, that the flow-separation phenomenon generally should be fairly uniform across the span of the model even in the three-dimensional-flow region.

Schlieren and Liquid-Film Studies

Schlieren observations.- A group of typical schlieren flow photographs obtained at a Reynolds number of 1.07×10^6 is presented in figures 11 and 12. It should be noted that the schlieren flow observations were made on a three-dimensional model and that at the Mach number of the tests the regions of the wing influenced by the wing tip extended nearly across the span of the model at the trailing edge.

An examination of figure 11, which shows the nature of the flow about the model with flap at 0°, reveals a short dark line (marked mixing line on one photograph) radiating at a small angle from the upper flap surface in the photographs with the knife edge horizontal. In the photographs obtained with the knife edge vertical, the line is less clear and is light in color. At the origin of this line a weak compression shock, barely discernible at low angles of attack, is present. As α was increased, the origin of the line moved forward toward the hinge line, the angle between the line and flap surface enlarged, and the intensity of the forward shock increased.

This double or forked shock phenomenon just described was also present in the tests of references 4 to 6 and was found to be associated with flow separation, as had been the corresponding pressure distributions with the characteristic small but abrupt compression followed by a region of constant pressure. Again, it was found in references 5 and 6 that the double or forked shock appeared only when the boundary layer on the model was laminar. The short line radiating at the small angle from the flap is in reality a mixing line between the flow above the line and the essentially dead-air space below the line. The apparent sharpness of the line signifies that, regardless of the spanwise variation in Mach number, the separation phenomenon was fairly uniform across most of the wing span. This conclusion is in agreement with that derived from the pressure distributions. In contrast to the uniformity of flow separation across the span, the breadth and fanlike appearance of the disturbances at the hinge line and the shocks at the trailing edge indicate the dependence of other quantities upon the spanwise variation in Mach number. In some of the photographs it is possible to see some curved disturbance lines originating at the upper airfoil surface just ahead of the flap hinge line. These lines are caused by reflections of the bow wave from the tunnel observation windows.

With the flap deflected, the same general considerations applied (fig. 12). As δ was increased, the origin of the separation or mixing line on the suction side of the flap moved toward the hinge line, the angle between the line and the flap chord became larger, and the shock at the separation point became stronger. At the hinge line a strong expansion region is visible on the flap suction side extending approximately to the shock from the separation point at the larger flap angles, while a strong shock can be seen on the high-pressure side. The character of the flow on the compression side of the flap is obscured in many of the pictures by the support strut. It can be seen clearly, however, in the photograph for $\alpha = -5.00^\circ$ and $\delta = -18^\circ$ which was obtained with the wing and flap deflected in a direction to eliminate the support interference from the high-pressure side of the wing. This schlieren picture indicates that separation occurred on the main wing ahead of the hinge line while the main shock has moved to the rear of the wing-flap juncture.

At the trailing edge with the flap deflected, the schlieren flow pictures show the presence of shocks just behind both the upper and lower surfaces even at the highest flap angles. At these high flap angles, nonviscid airfoil theory predicts the occurrence of a shock at the trailing edge on the suction side of the flap and only an expansion on the high-pressure side. A closer examination of a large number of photographs showed that, although not too clear in most of the pictures, the expansion not only actually existed but the flow

overexpanded to a velocity greater than that of the free stream. Consequently, when the flow met that from the other wing surface, it was deflected back to approximately stream direction through a shock some distance downstream of the flap trailing edge.

A clearer concept of the character of the flow over the model can be obtained by referring to the sketch in figure 13 which has been prepared from an analysis of schlieren photographs and from pressure distributions at station 1 for $\alpha = 3.35^\circ$ and $\delta = 10^\circ$. Because of interaction between the shock at the upper trailing edge of the model and the subsonic boundary layer and wake of the airfoil, the flow separates from the upper surface of the flap almost at the hinge line. On the lower surface a similar separation, due to shock boundary-layer interaction at the flap hinge line, occurs on the main wing some distance ahead of the hinge line while the main shock moves slightly to the rear. In both instances the occurrence of flow separation at a point so far ahead of the main shock is probably associated with a laminar boundary layer on the model inasmuch as all experimental results to date indicate that, in the case of turbulent boundary layers, disturbances are transmitted upstream only a relatively short distance and the characteristic forked or double shock does not exist. Both the low Reynolds number of the tests and the favorable pressure gradients along the chord tend to keep the boundary layer laminar. Between the model and the separated flow is a region of dead air, where the pressure is constant in the chordwise direction. The boundary between the dead-air region and the separated flow usually shows up very clearly as a sharp mixing line on the schlieren photographs and is appropriately designated in figure 13. At the flap trailing edge the flows from the two wing surfaces evidently reach an equilibrium pressure and are deflected back to approximately stream direction through a mechanism as yet not clearly understood but entirely different from that predicted by nonviscid airfoil theory. As a result, the center of the wake may be displaced upward from the flap trailing edge.

The schlieren flow photographs presented and discussed above were for a Reynolds number of 1.07×10^6. Flows at the lower Reynolds numbers of the tests were not photographed because the changes in character of the flow for the small Reynolds number range of the investigation were small and difficult to distinguish. Visual schlieren flow observations did establish the fact, however, that the separation points moved forward and the angles of flow separation relative to the wing or flap chord increased with a decrease in Reynolds number. Pressure calculations based on angles of flow determined from the schlieren pictures agreed fairly well with the measured values.

Liquid-film flow studies.- The liquid-film technique used to investigate the boundary-layer-flow characteristics of the airfoil is

still in the development stage; hence no photographs of the studies are given and no effort is made to describe the apparent characteristics of the boundary-layer flow in great detail. In general, however, the studies indicated that with the wing and flap set at 0° the boundary layer was laminar everywhere over the model at a Reynolds number of 1.07×10^6 except in the separated-flow regions and except for a very narrow triangular region of turbulent flow at each wing tip with the apex of the triangle located at approximately the midchord point of the wing tip. Evidently, the slight discontinuity in the airfoil surfaces at the hinge line was not sufficient to precipitate transition at the Reynolds number and Mach number of the tests. The turbulent boundary layer in the tip regions may result from a cross flow in the inboard direction over the sharp corner at the square tip of the wing. Theoretical calculations indicate the existence of a pressure gradient in this direction all along the wing tip which increased in magnitude toward the trailing edge.

Separated-flow regions could be distinguished from the laminar boundary-layer-flow areas only by increasing the drying time in the tests until the liquid film had evaporated from both the turbulent and laminar boundary-layer-flow regions. Because of the lack of velocity and surface shearing action in the separated-flow region, the liquid film in this area was still visible after it had completely dried in all other regions. A test made in this manner at α near 4.35° and $\delta = 0^\circ$ indicated the presence of a separated-flow region, the location and extent of which agreed well with those determined from schlieren flow photographs and pressure distributions.

Tests made with the flap deflected showed that the boundary layer became turbulent on the high-pressure side of the flap at a point corresponding approximately to the location of the main shock a short distance behind the hinge line. Attention is here directed to the fact that all three modes of experimentation, pressure surveys, schlieren flow observations, and liquid-film studies, lead to the conclusion that the boundary-layer flow on the model is primarily laminar in character.

Wing Section Characteristics

Variation of aerodynamic coefficients with δ.- Aerodynamic characteristics obtained by integrating the theoretical pressure distributions and the experimental pressure distributions for the Reynolds number of 1.07×10^6 are presented in figures 14 to 16 as a function of flap deflection, in figures 17 to 19 as a function of angle of attack, and in figures 20 to 23 as a function of section normal-force coefficient. At this point it is desirable to mention that where

the fairing of the curves presented is not obvious the trends have been established from analyses of a considerably larger amount of data, much of which was intermediate to that shown.

Inspection of figure 14 indicates that as a result of the flow separations discussed in the previous sections the lifting effectiveness of the flap was less than that predicted from theory and was actually zero for a very small range of flap angles when the flap was in the center of the wake near a total flap deflection ($\alpha + \delta$) of 0°. The loss in lift effectiveness is connected with a very rapid shift in flow separation from one side of the flap to the other. For most of the deflection range where the flap is ineffective, separation usually was present simultaneously on both sides of the flap near the trailing edge. As α was increased from 0°, the flap-deflection range for which the flap was ineffective diminished more rapidly at the outboard station than at the inboard location. Figure 14 also shows that for small flap deflections the slopes of the theoretical and experimental curves for the two-dimensional station were nearly equal. At the higher angles, however, the curves diverged, thus indicating the increasing intensity of the separation as δ was increased. At the outboard station the discrepancy between theory and experiment was somewhat greater than at the two-dimensional station. As pointed out previously, a part of this increased discrepancy between the theoretical and experimental curves is probably due to the slightly larger angle of attack at station 2 resulting from twist in the model and a part due to the inadequacy of the theory. A comparison of the experimental curves for the two stations shows that the breaks in the curves for station 2 occur at smaller flap angles than at those of the inboard station. It appears, therefore, that the flap lift-effectiveness curve of the complete three-dimensional airfoil will not have a sharp break as the curves of the section characteristics but will have a more gradual change in slope over a larger flap-deflection range.

Parallel to the break or shift in the normal-force-coefficient curves, a shift occurred in the plots of airfoil pitching-moment (fig. 15) and flap hinge-moment coefficients (fig. 16) against flap deflection. In general, the same considerations discussed for the normal-force-coefficient curves apply here except for the fact that the ranges of the moment breaks in terms of flap angles did not diminish as rapidly with increase in α as they did in the case of the normal-force coefficient. It may be seen that, in effect, there is a shift between the portions of the curves associated with positive or negative hinge moments equivalent to 2° to 3° flap deflection. As for the case of the normal-force coefficient, the pitching- and hinge-moment-coefficient curves for a complete wing probably will have a more gradual change in slope over a larger flap-deflection range. The occurrence of a similar break in the hinge moments of an all-movable control surface of

different plan form and section is reported in reference 8. It is possible that the appearance of such a phenomenon may be associated with, among other things, the magnitude of the included trailing-edge angle.

Further examination of the experimental results for both spanwise stations shows that, for the pitching-moment curves in particular (fig. 15), there was a difference in slopes between the portions of the curves associated with positive or negative hinge moments. This phenomenon occurred even at α near 0° where from symmetry considerations the slopes were expected to be equal, and, furthermore, it tended to increase in intensity with Reynolds number. The reason for its occurrence is not entirely clear but may be due, at least in part, to a slight model asymmetry.

Variation of aerodynamic coefficients with α.- The agreement between the theoretical and experimental curves when plotted against angle of attack (figs. 17 to 19) was good as regards the slopes of the curves for station 1 but poor as regards the displacement of the curves. At station 2 the agreement between theory and experiment was slightly poorer as regards the slopes of the normal-force- and pitching-moment-coefficient curves and about as good as regards the hinge-moment curves. In relation to the displacements of the theoretical and experimental curves, the agreement at the two stations was about the same. As in the case at constant α, the curves for some of the smaller flap angles show discontinuities in the region where the flap was approximately in the center of the wing wake. From the shape of the curves with the discontinuities it is evident that the breaks are caused by the lack of changes in loading on the flap and not on the main wing. For clearer identification the regions in which the breaks in the curves appear have been shown by a short-dash line. It is apparent that, particularly for the case of an airfoil without flap, it may be a very simple matter to fair the curves erroneously and not perceive the effects of shock-boundary-layer interaction. For the three-dimensional wing as a whole, the breaks in the force curves will again be more gradual and will extend over a greater angle-of-attack range. At the same time the identification of the separation effects will be more difficult.

Variation of aerodynamic coefficients with c_n.- In order to determine whether the breaks in the force curves were present when the angle of attack and flap deflection were eliminated as primary variables, the section pitching- and hinge-moment coefficients were plotted against the normal-force coefficient (figs. 20 to 23). For clarity the curves for constant angle of attack and constant flap deflection are presented on separate figures. The experimental results do not show any readily definable discontinuities for constant α but indicate the occurrence of breaks in the curves at constant δ. The figures also indicate a

better agreement between theory and experiment at station 1 than at station 2, which stems primarily, as pointed out several times previously, from the neglect of the slightly greater angle of attack at the outboard station and the inadequacy of the theory for the three-dimensional-flow region.

Effect of changes in Reynolds number.- Some idea as to the effects of scale on the aerodynamic characteristics of the wing may be obtained by comparing a few typical curves from the low Reynolds number tests (figs. 24 to 28) with the corresponding figures obtained at the high Reynolds number (figs. 14 to 16 and 18 to 19). In general, it was found that the conclusions derived from the tests at $R = 1.07 \times 10^6$ applied directly to the results obtained at $R = 0.55 \times 10^6$. The only major differences were that the magnitudes of the flap ineffectiveness range at the lower Reynolds numbers were about 1° to 2° greater in terms of flap angle, around 1° greater in terms of α, and the breaks occurred at more nearly the same angles of attack and flap deflection at both the inboard and outboard stations. It thus appears that the adverse effects of shock-boundary-layer interaction will be more severe at the lower Reynolds number even in the case of the full three-dimensional wing.

Although the Reynolds number of the investigation is low, it is nearly within the range of Reynolds numbers for control surfaces of missiles flown at high altitudes. This fact can be seen more clearly if it is realized that at an altitude of 50,000 feet and at the Mach number of the tests, 1.62, the Reynolds number of 1.07×10^6 corresponds to flight of a wing having a chord a little over 7 inches in length. It is apparent, therefore, from the results of this investigation that, as a result of the possible complete loss in control effectiveness over a very narrow range of flap deflections due to flow separation, undesirable stability and control characteristics such as snaking and nonlinear stick force-deflection relationships may be encountered in supersonic flight if control surfaces similar to the ones investigated are used.

Slope parameters.- Because of the discontinuities in the curves and the definite differences in slope between the portions of the curves associated with positive or negative flap hinge moments the slope parameters derived from the experimental curves have little significance in the usual sense. However, some important general conclusions can be derived from a study of the parameters and, therefore, curves which show the variations of the various parameters with α and δ are presented in figures 29 to 32. The slope parameters were normally taken as tangents to the curves at α and $c_n = 0$ when the flap angle was held constant and at δ and c_m or $c_h = 0$ when the angle of attack

remained fixed. In the case of the experimental curves when discontinuities in slope occurred in the curves near the reference points, only the slopes associated with positive flap angles were used.

A comparison of the results of station 1 with those of station 2 indicates that in general the agreement between theory and experiment was better at the two-dimensional than at the three-dimensional flow station. The poorer agreement between theory and experiment at the tip station can be accounted for only partly by the twist in the model, thus indicating some inadequacy on the part of the theory. Also, the theoretical and experimental slopes c_{m_δ}, c_{n_δ}, and c_{h_δ} are smaller at station 2 than the theoretical and experimental slopes at station 1 (fig. 30), indicating a lower flap effectiveness in the region influenced by the wing tip. In conventional theories of control effectiveness, such as the usual linear theories and the two-dimensional theories with flap-tip corrections, the effects of the wing tip are disregarded. In these tests, the loss in flap effectiveness in the region theoretically influenced by the wing tip but not by the flap side edge was found to occur as a result of the higher Mach number at the flap hinge line produced by the influence of the wing tip and, hence, was not connected with viscous effects or, to any great extent, with flap-tip effects. As a consequence, the loss in flap effectiveness on a three-dimensional wing may be greater than that normally expected from the use of the conventional linearized and second-order control-effectiveness theories even after the normal allowances for inaccuracies in the theory including viscous effects. The loss in flap effectiveness at the outboard station as compared to that at the inboard location is predicted, however, by the method employed in this paper for estimating the pressures and forces.

The figures also show that the effects of Reynolds number are considerably greater in the region affected by the wing tip than at the two-dimensional station. The effects of Reynolds number on a three-dimensional rectangular wing, therefore, will probably increase as the aspect ratio decreases and may also increase as the Mach number decreases and the area of the region influenced by the wing tip expands. Since the character and magnitude of the Reynolds number effects may differ with Mach number, final conclusions regarding the latter points require further study.

CONCLUSIONS

An investigation has been made of the aerodynamic characteristics of a rectangular wing with a 9-percent-thick symmetrical circular-arc section and a 30-percent-chord trailing-edge flap by means of pressure

distributions and schlieren and liquid-film flow observations. An analysis of the results obtained at a Mach number of 1.62 and a Reynolds number range from 0.55 to 1.07 $\times 10^6$ indicated that:

1. The theoretical and experimental pressure distributions were in good agreement except on the low-pressure side of the flap near the trailing edge and on the high-pressure side of the flap and wing at the hinge line. In these regions the experimental pressures deviated from the theoretical because of laminar separation resulting from shock-boundary-layer interaction.

2. As a result of the boundary-layer separation, the experimental increments in aerodynamic coefficients due to angle of attack or flap deflection were generally smaller and the slopes of the experimental curves lower than the theoretical coefficient increments and slopes.

3. Owing to shock-boundary-layer interaction, there was a break or shift in the experimental section force and moment curves when the flap was approximately in the center of the wake that may result in undesirable stability and control characteristics such as snaking and nonlinear stick force-deflection relationships. However, the experimental results also tend to indicate that these adverse characteristics will not be quite as severe in the case of a three-dimensional wing.

4. At the outboard station, which is theoretically influenced by the wing tip but not by the side edge of the flap, there was a loss in experimental normal-force coefficient due to flap deflection as compared with that at the two-dimensional station which is not predicted by any of the usual linearized and second-order control-effectiveness theories and is not connected with viscous effects. It is possible, therefore, that the actual effectiveness of a flap near the tip of a three-dimensional wing may be less than that estimated from the conventional control-effectiveness theories even after the normal allowances for inaccuracies in the theory and viscous effects are applied.

5. In general, the boundary layer on the model was laminar in character. With the flap deflected, the boundary layer became turbulent behind the main shock just behind the hinge line on the high-pressure side of the flap.

6. The effect of decreasing the Reynolds number was to move the points of initial separation forward and to cause the breaks or shifts in the force and moment curves to appear at more nearly the same angle of attack or flap deflection at the two test stations.

7. The effects of Reynolds number were considerably greater at the station influenced by the wing tip, indicating the probability that the aerodynamic characteristics of three-dimensional wings will be affected

by Reynolds number to a greater extent if the aspect ratio is low. It is also possible that for a constant aspect ratio the influence of the Reynolds number may increase as the Mach number decreases and the area of the region influenced by the wing tip expands.

Langley Aeronautical Laboratory
National Advisory Committee for Aeronautics
Langley Air Force Base, Va.

REFERENCES

1. Czarnecki, K. R., and Schueller, C. F.: Investigation of Interaction Effects Arising from Side-Wall Boundary Layers in Supersonic Wind-Tunnel Tests of Airfoils. NACA RM L8G27, 1948.

2. Gray, W. E.: A Simple Visual Method of Recording Boundary Layer Transition (Liquid Film). TN No. Aero. 1816, British R.A.E., Aug. 1946.

3. Munk, M. M., and Prim, R. C.: Surface-Pressure Gradient and Shock-Front Curvature at the Edge of a Plane Ogive with Attached Shock Front. Jour. Aero. Sci., vol. 15, no. 11, Nov. 1948, pp. 691-695.

4. Ferri, Antonio: Experimental Results with Airfoils Tested in the High-Speed Tunnel at Guidonia. NACA TM 946, 1940.

5. Ackeret, J., Feldmann, F., and Rott, N.: Investigations of Compression Shocks and Boundary Layers in Gases Moving at High Speed. NACA TM 1113, 1947.

6. Liepmann, Hans Wolfgang: The Interaction between Boundary Layer and Shock Waves in Transonic Flow. Jour. Aero. Sci., vol. 13, no. 12, Dec. 1946, pp. 623-638.

7. Czarnecki, K. R., and Mueller, James N.: An Approximate Method of Calculating Pressures in the Tip Region of a Rectangular Wing of Circular-Arc Section at Supersonic Speeds. NACA RM L9J10, 1950.

8. Vaccaro, R. J., and Upton, J., Jr.: Hinge Moment Tests of V-349 Model at a Mach Number of 1.72. Rep. No. 5799, Chance Vought Aircraft, Div. of United Aircraft Corp. (Stratford, Conn.), Nov. 21, 1947.

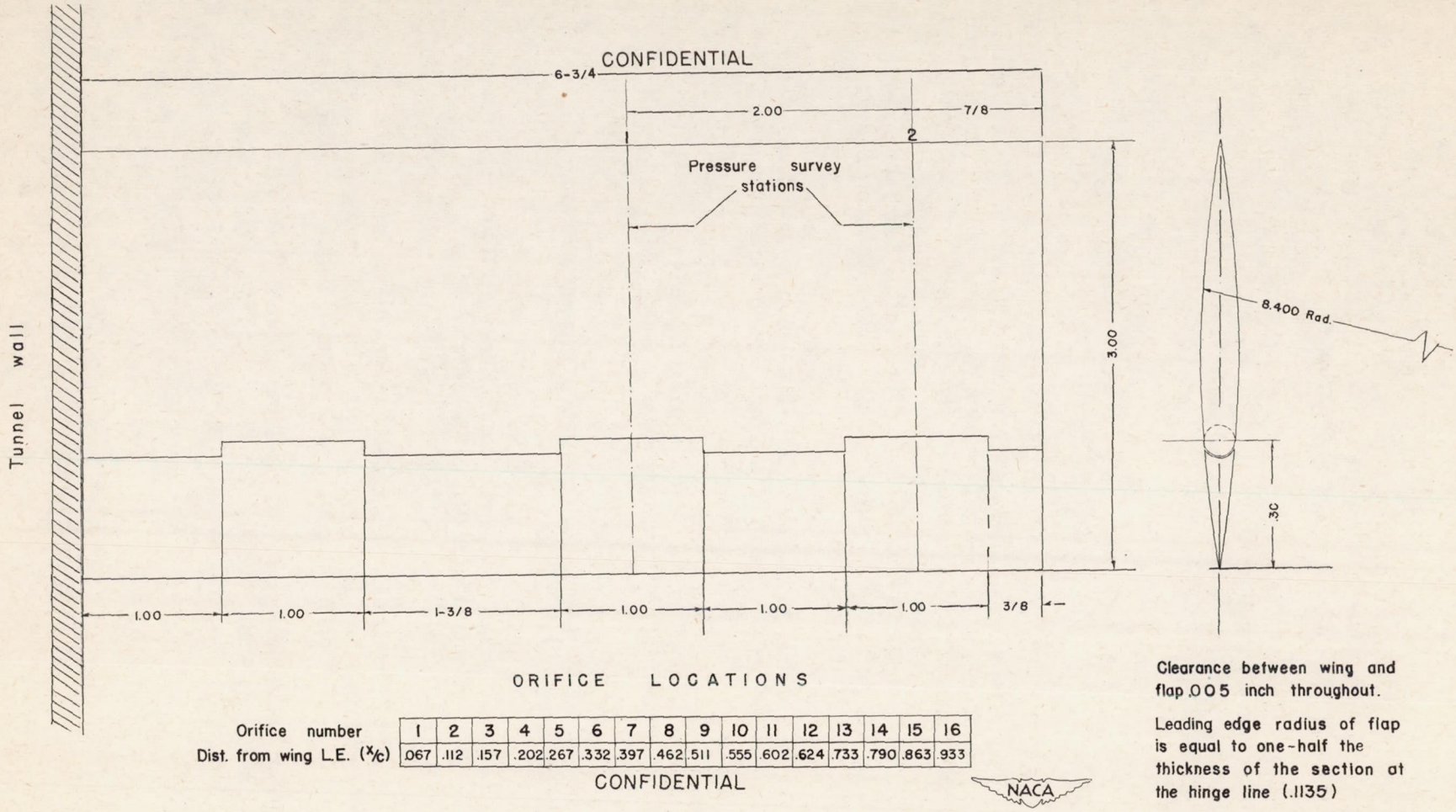

Figure 1.- Dimensional sketch of pressure distribution model with plain flap.

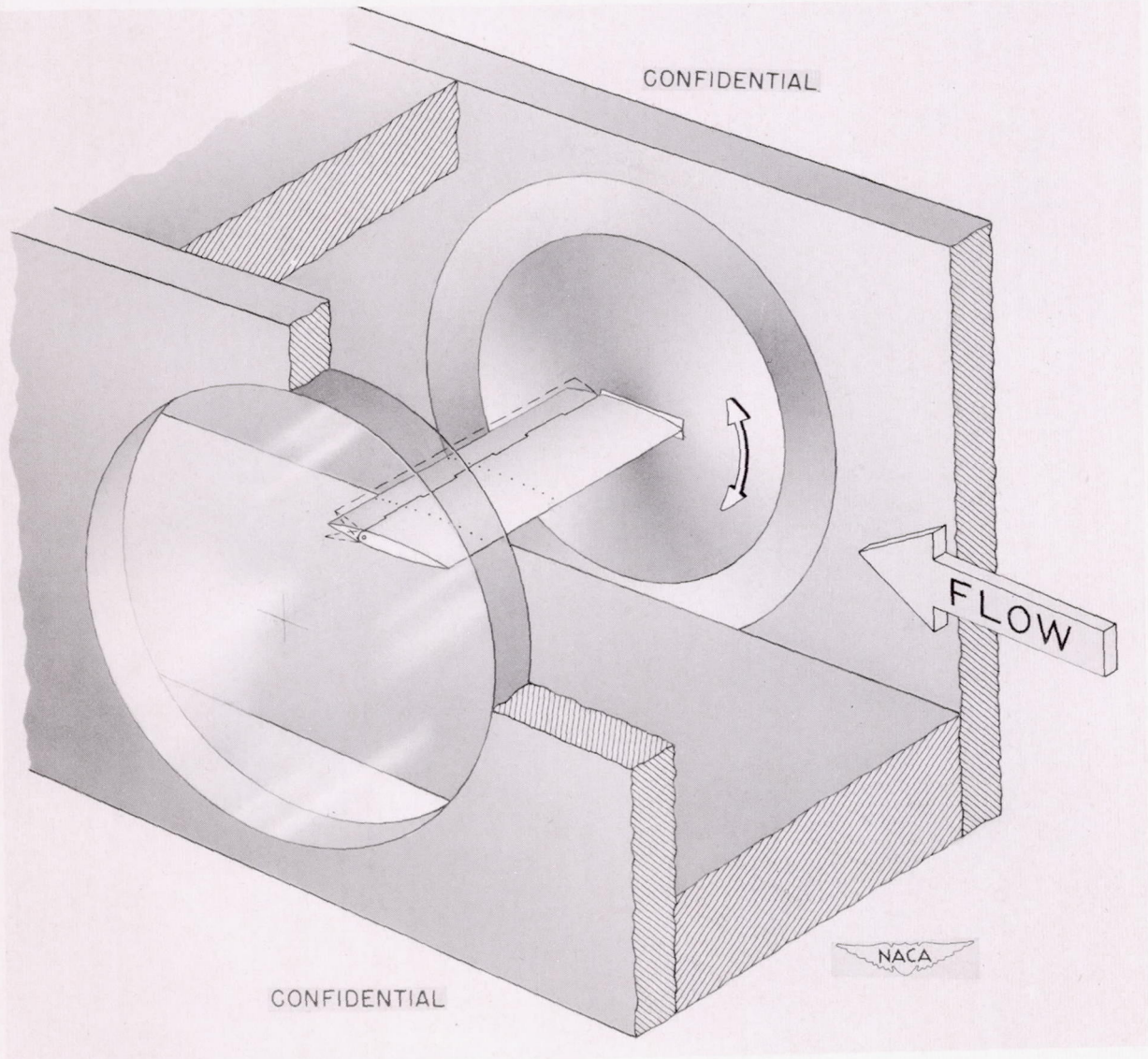

Figure 2.- Wing mounted in tunnel for testing.

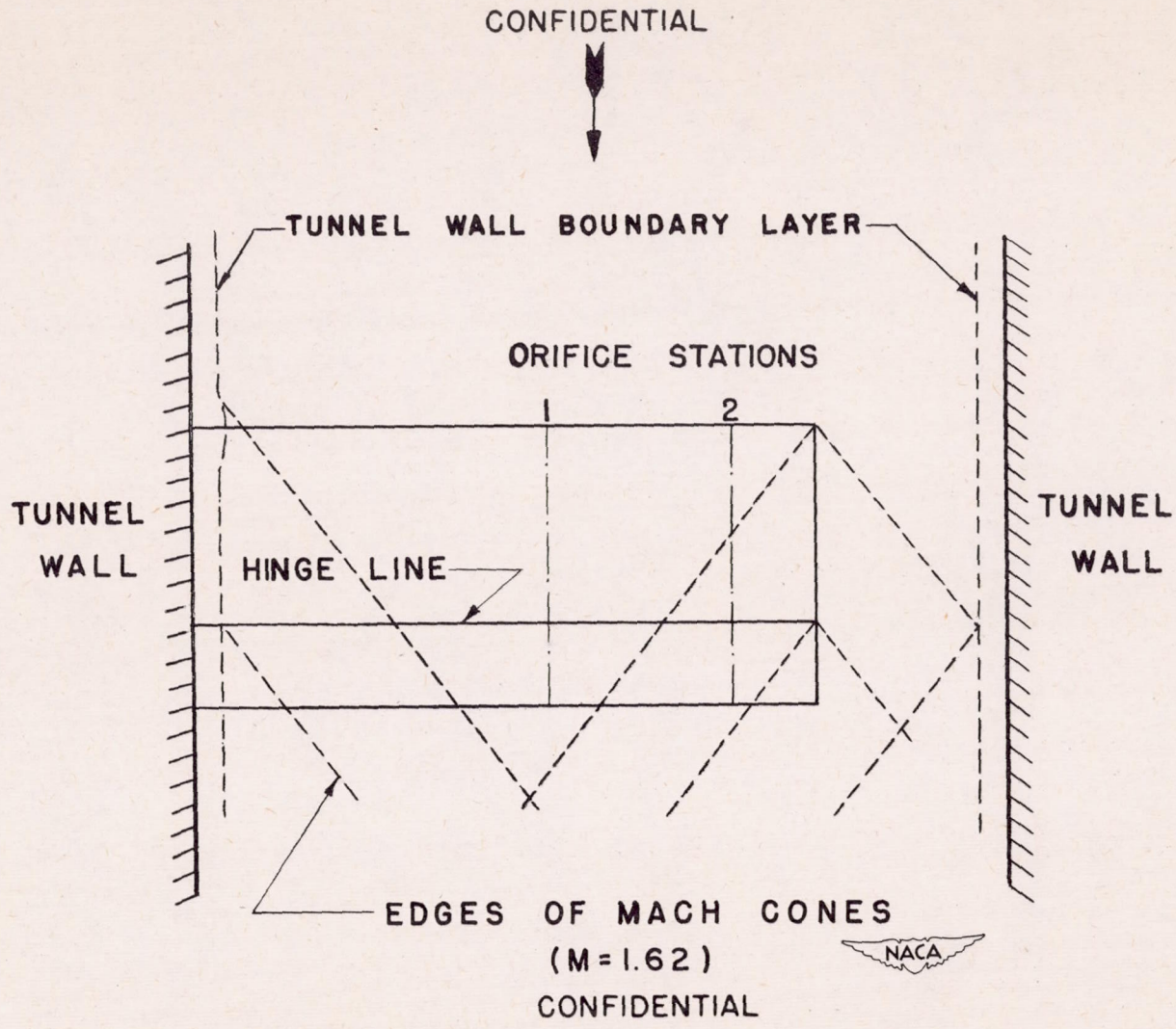

Figure 3.- Pressure-distribution model and its relative location in the wind tunnel.

CONFIDENTIAL

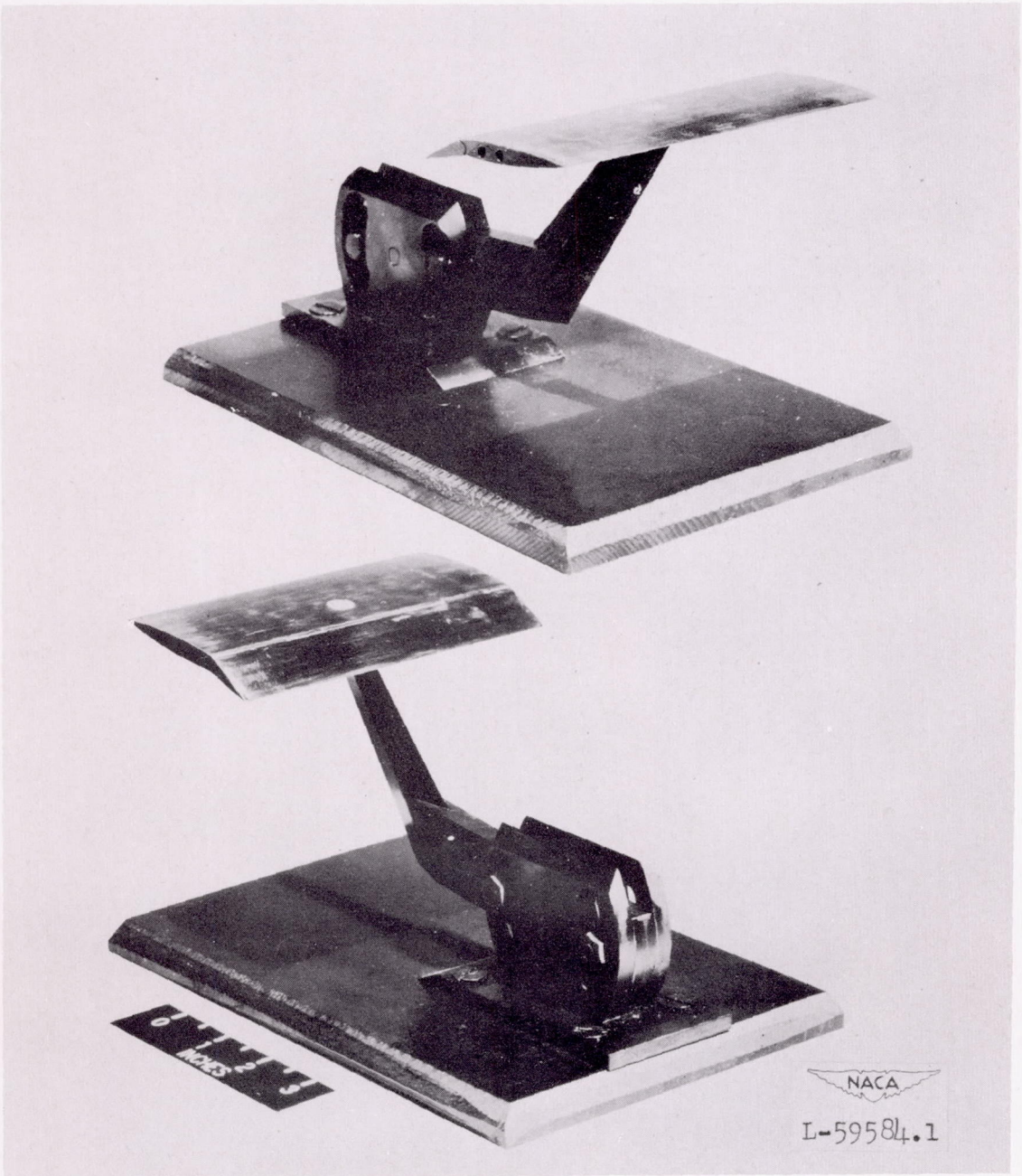

Figure 4.- Front and rear three-quarter views of schlieren model used in tests. Symmetrical circular-arc airfoil, 9-percent thick.

CONFIDENTIAL

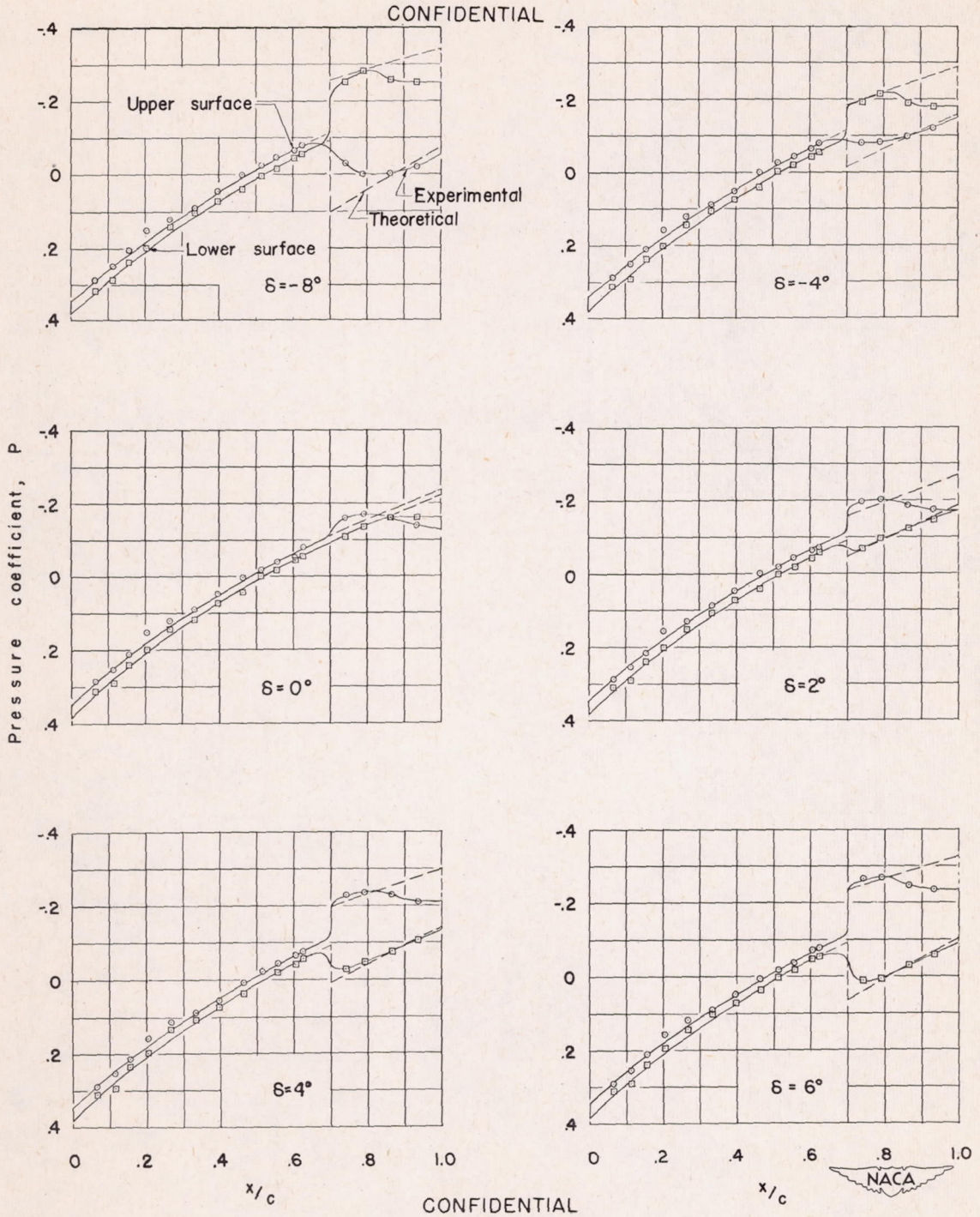

(a) $\alpha = 0.35^{\circ}$.

Figure 5.- Effect of flap deflection on experimental and theoretical pressure distributions. Symmetrical circular-arc airfoil, 9-percent thick; station 1; M, 1.62; R, 1.07×10^6.

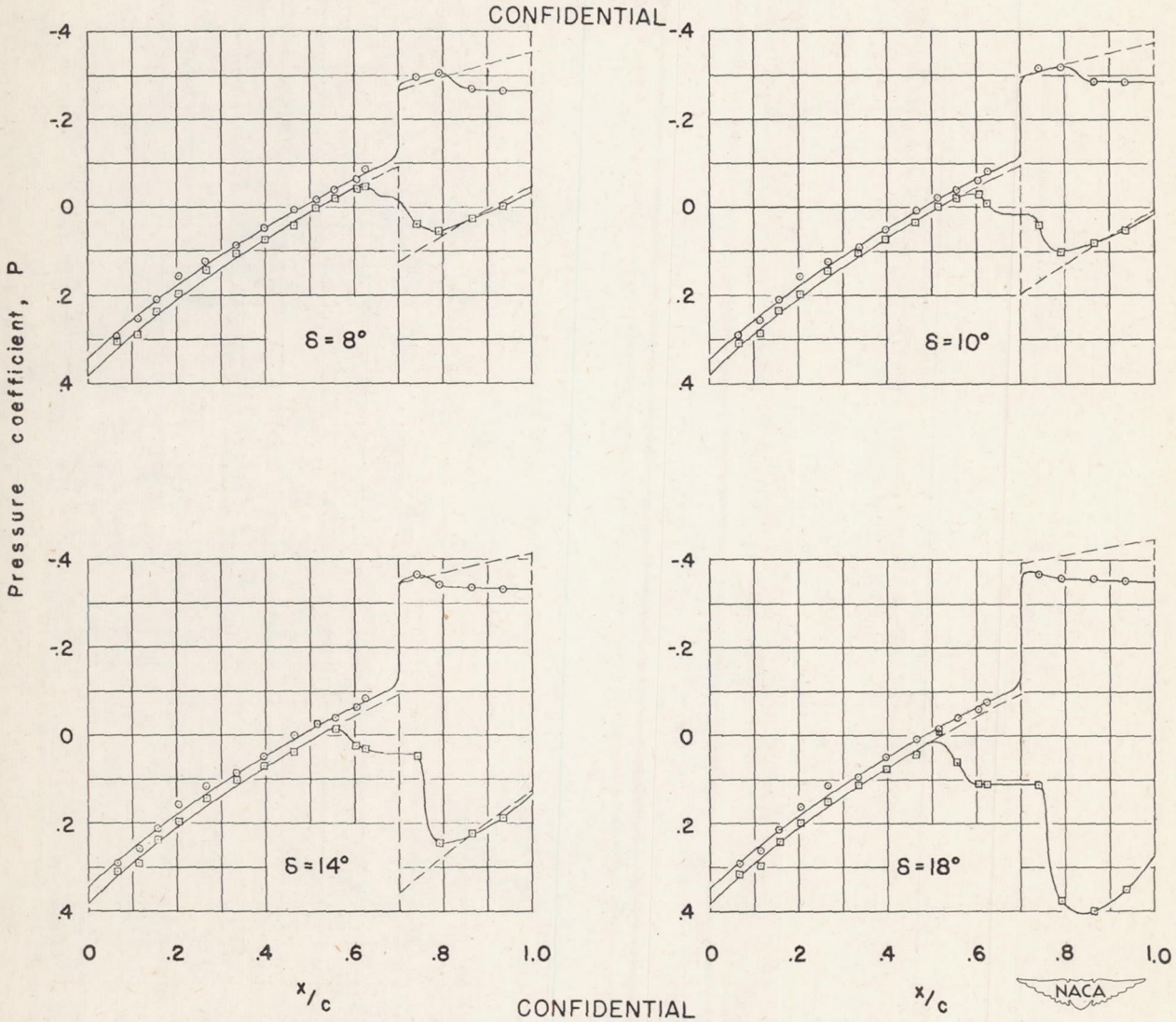

(a) Concluded.

Figure 5.- Continued.

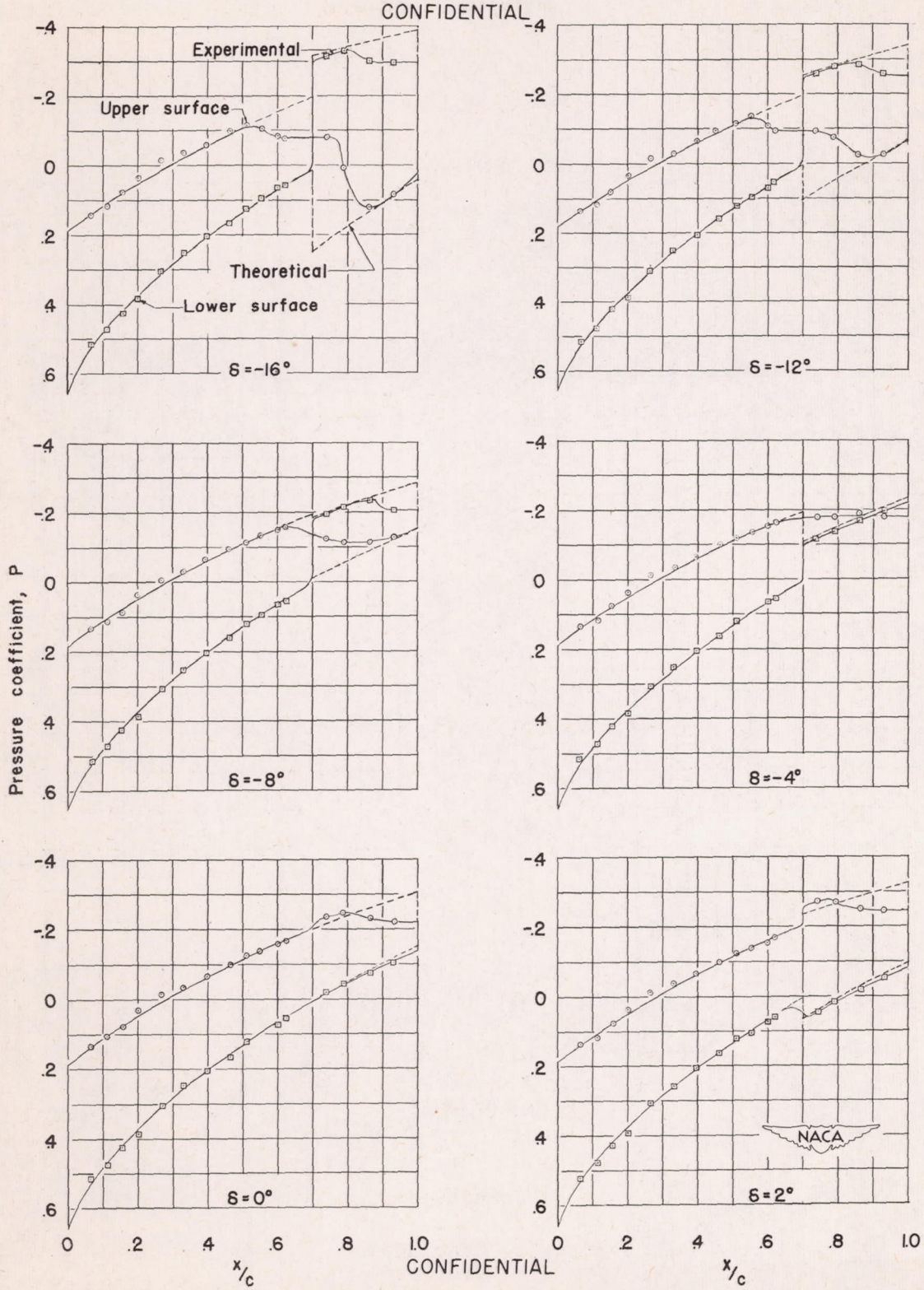

(b) $\alpha = 4.35^{\circ}$.

Figure 5.- Continued.

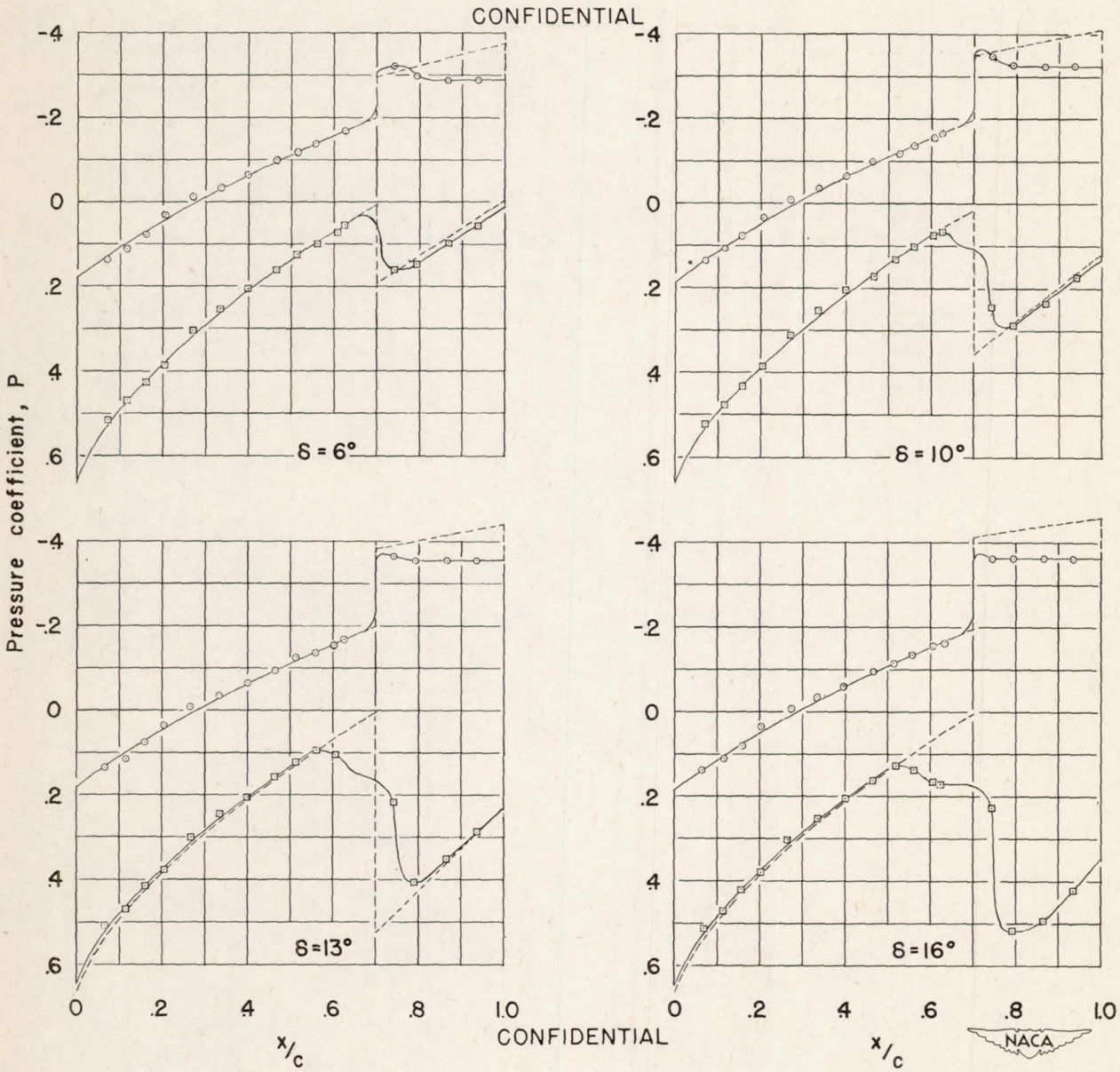

(b) Concluded.

Figure 5.- Concluded.

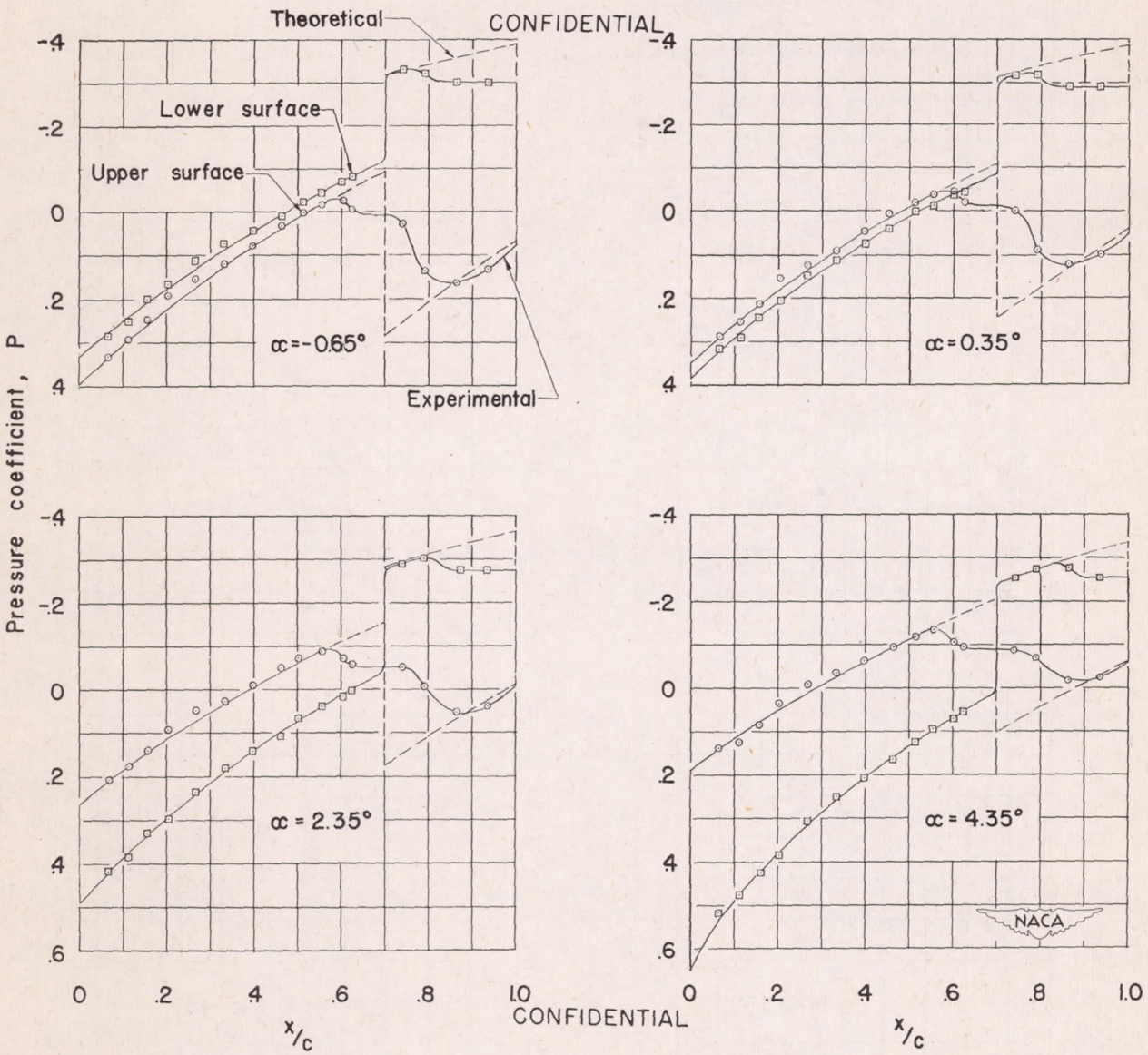

(a) $\delta = -12^{\circ}$.

Figure 6.- Effect of angle of attack on experimental and theoretical pressure distributions. Symmetrical circular-arc airfoil, 9-percent thick; station 1; M, 1.62; R, 1.07×10^6.

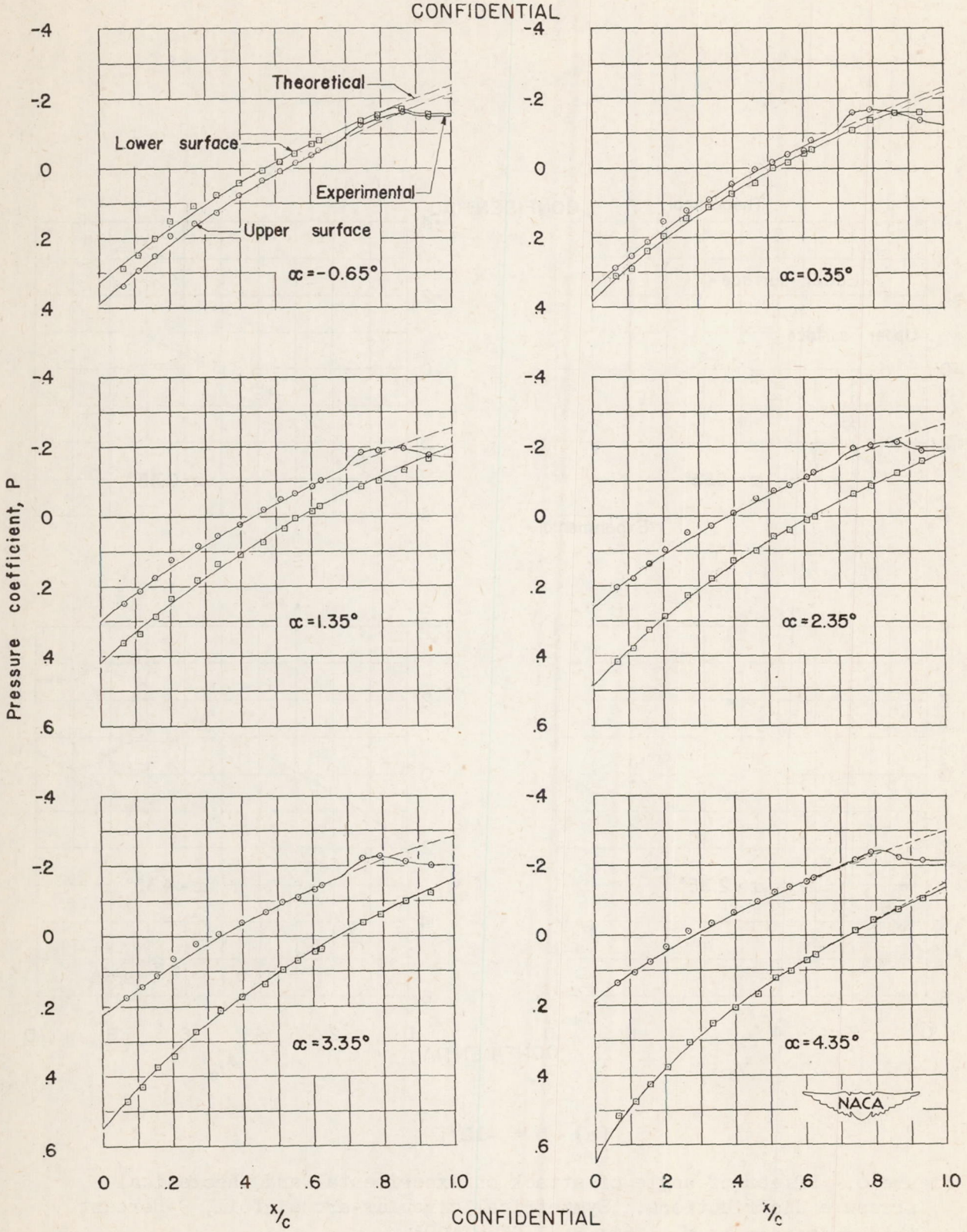

(b) $\delta = 0^{\circ}$.

Figure 6.- Continued.

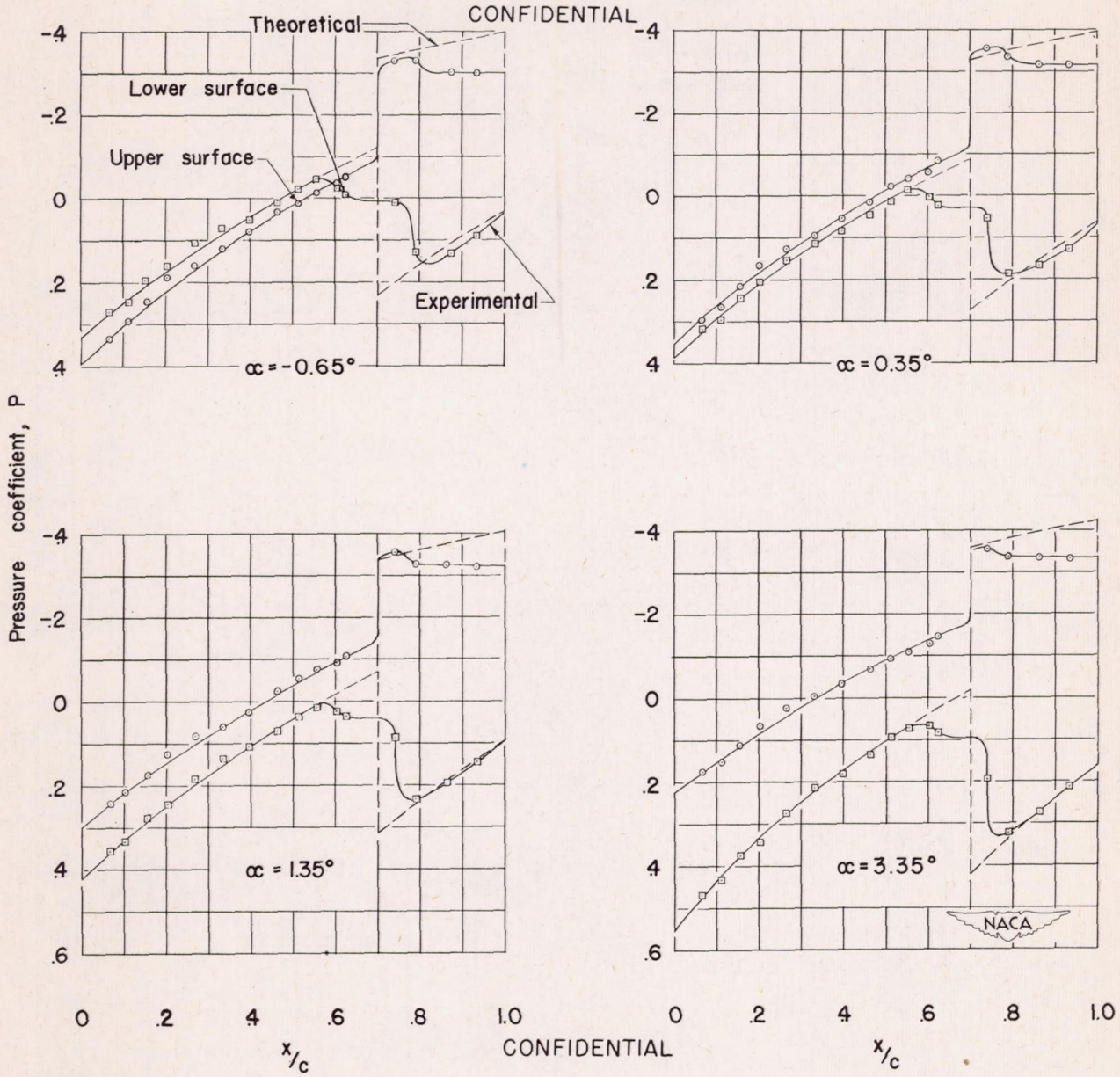

(c) $\delta = 12^{\circ}$.

Figure 6.- Concluded.

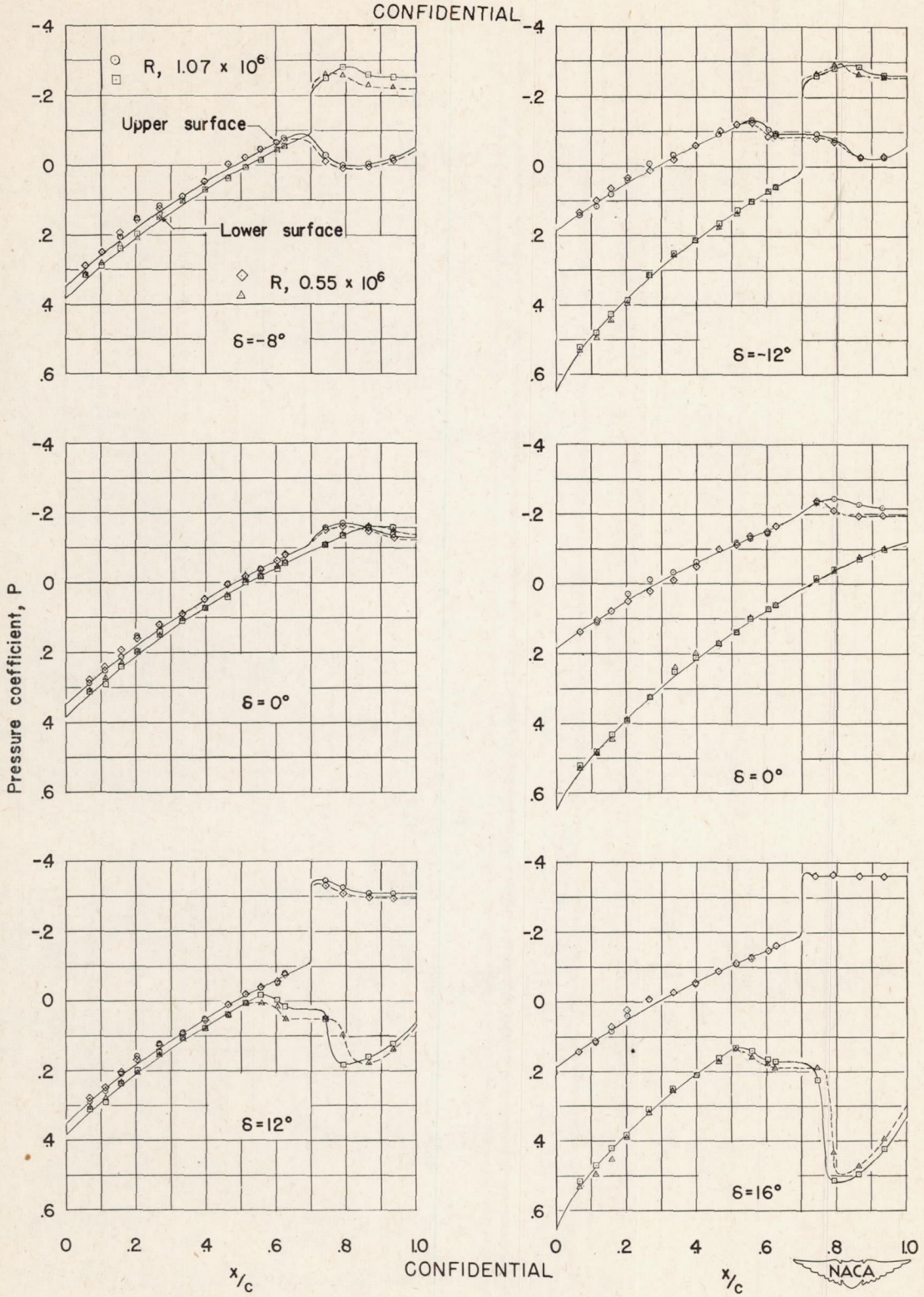

(a) $\alpha = 0.35^{\circ}$. (b) $\alpha = 4.35^{\circ}$.

Figure 7.- Effect of Reynolds number on experimental pressure distributions. Symmetrical circular-arc airfoil, 9-percent thick; station 1; M, 1.62.

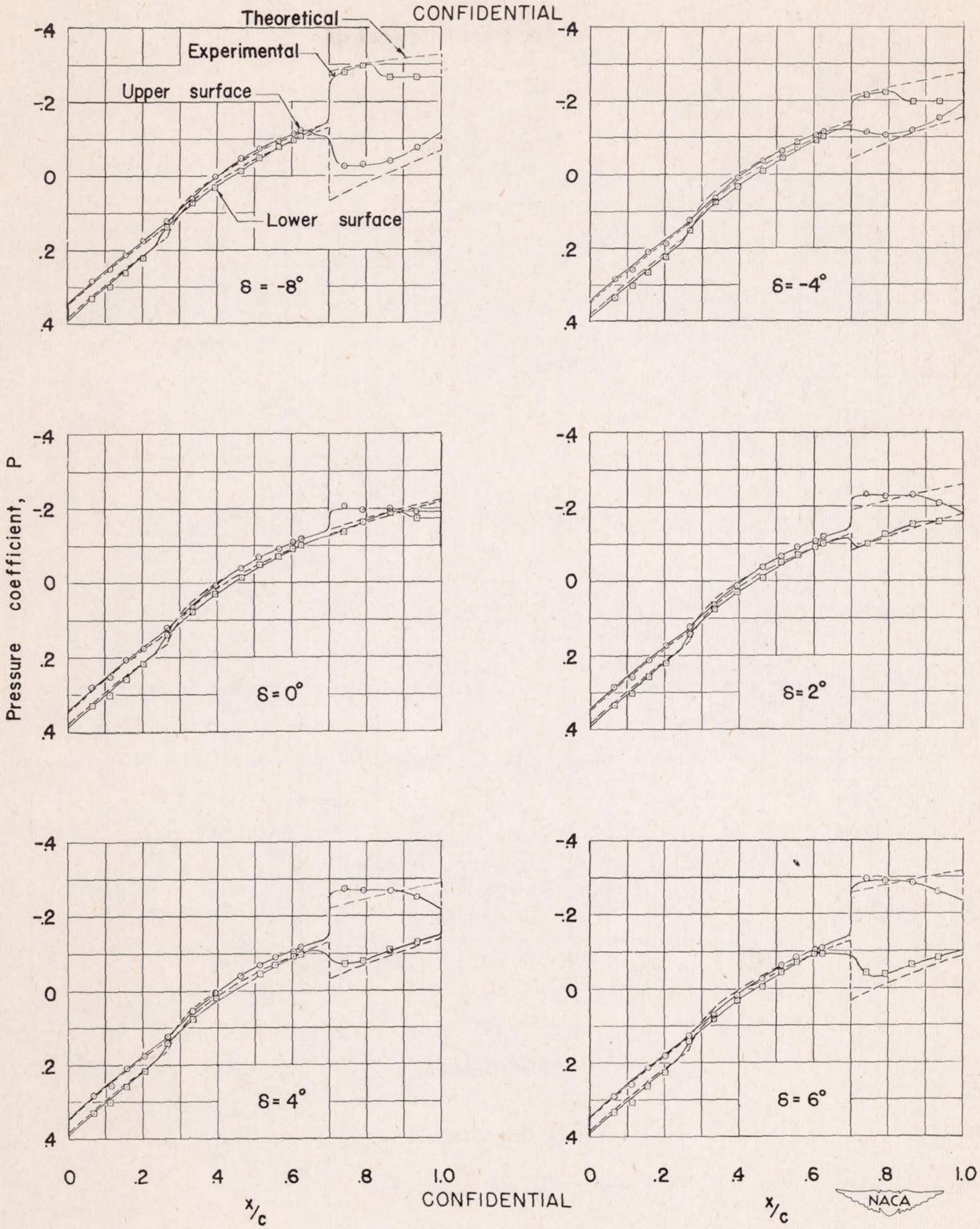

(a) $\alpha = 0.35^{\circ}$.

Figure 8.- Effect of flap deflection on experimental and theoretical pressure distributions. Symmetrical circular-arc airfoil, 9-percent thick; station 2; M, 1.62; R, 1.07×10^6.

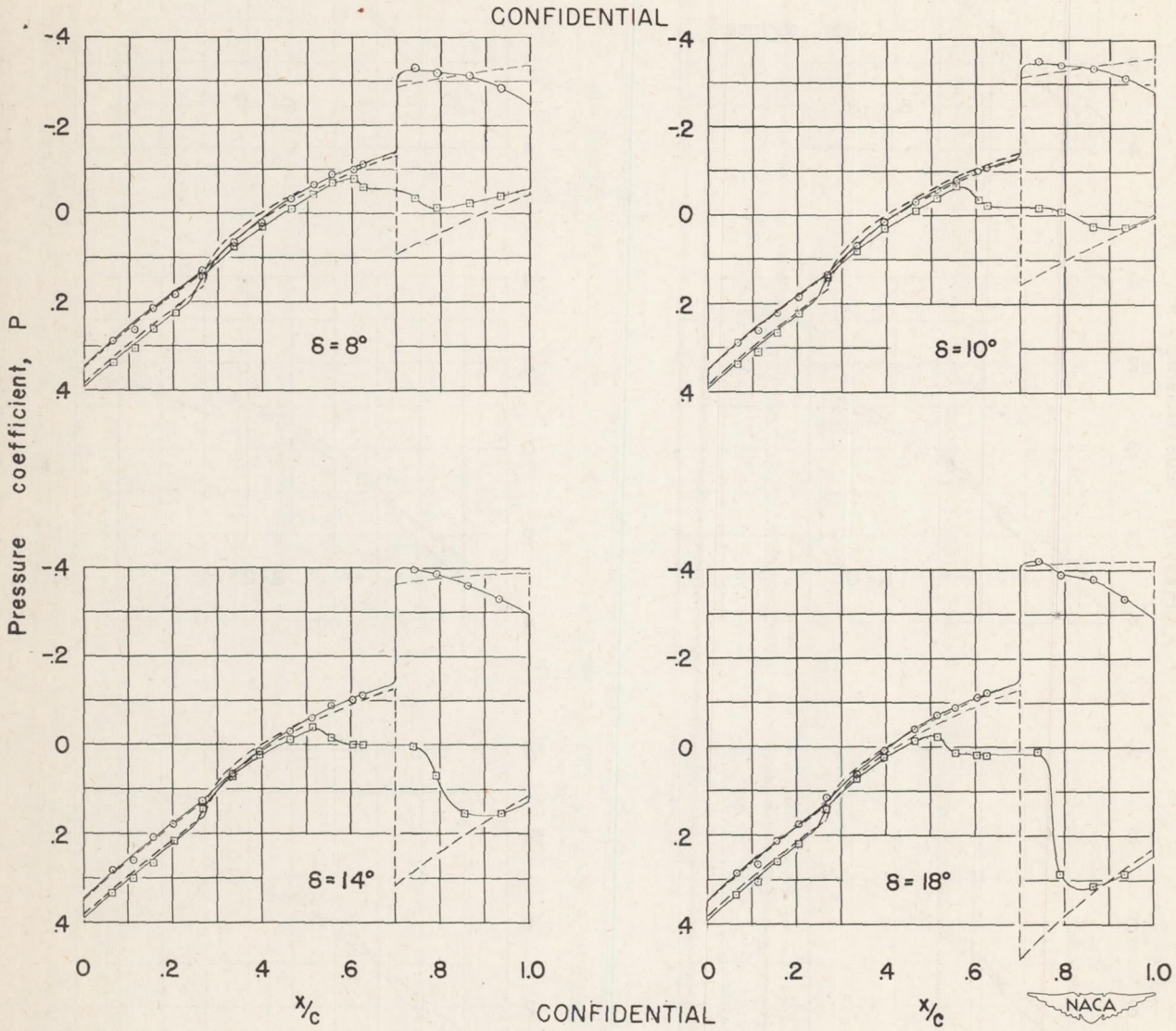

(a) Concluded.

Figure 8.- Continued.

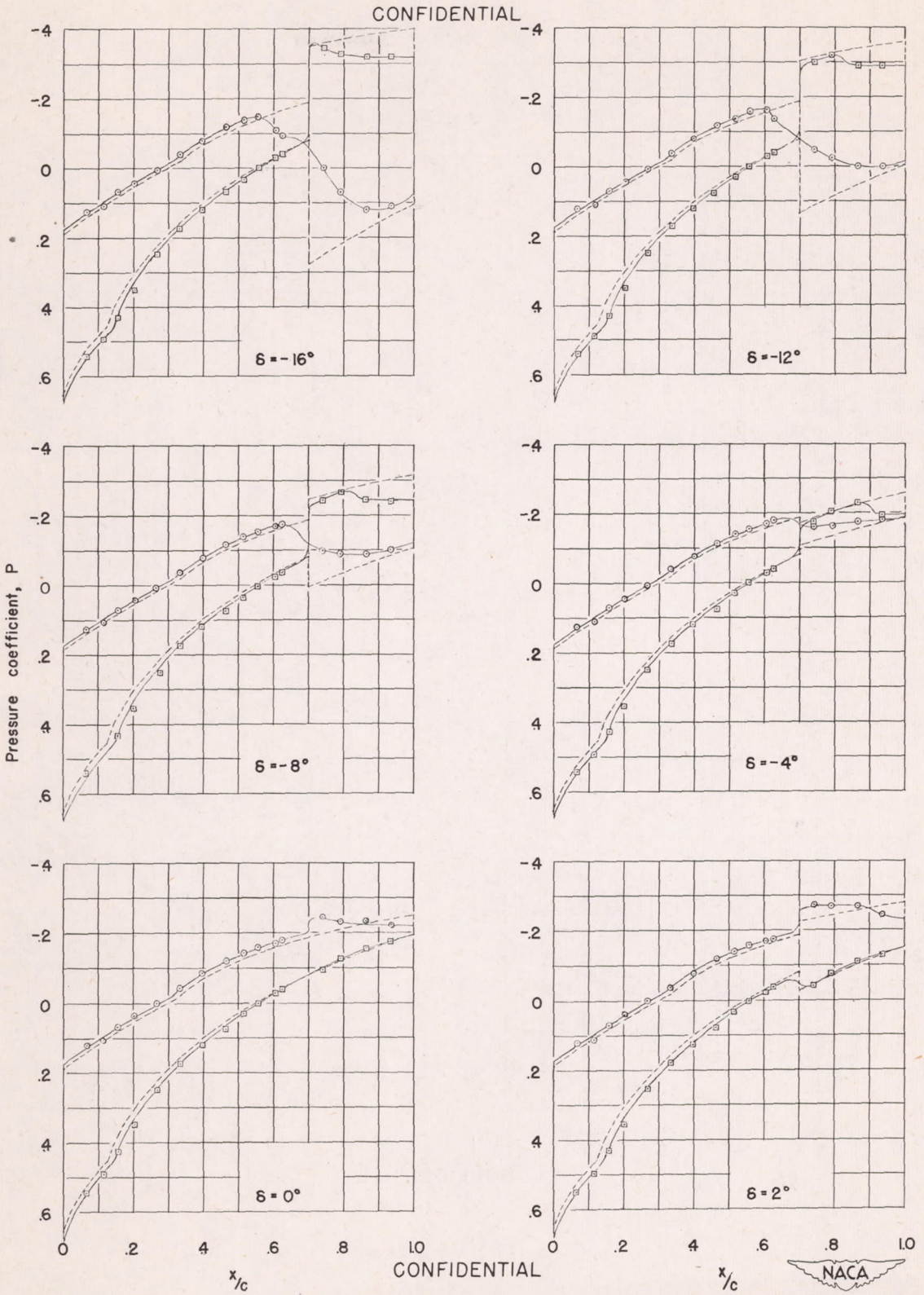

(b) $\alpha = 4.35^{\circ}$.

Figure 8.- Continued.

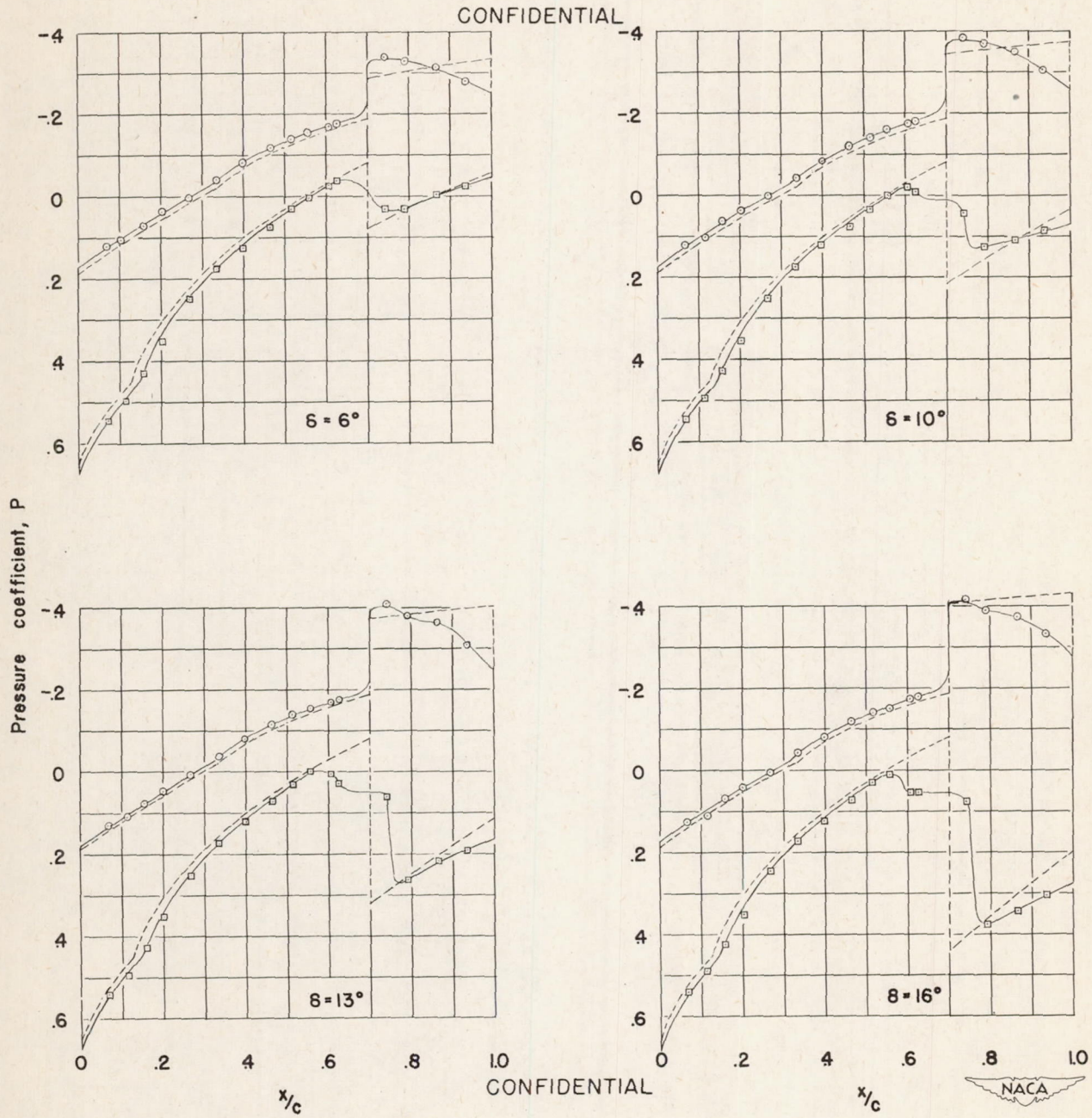

(b) Concluded.

Figure 8.- Concluded.

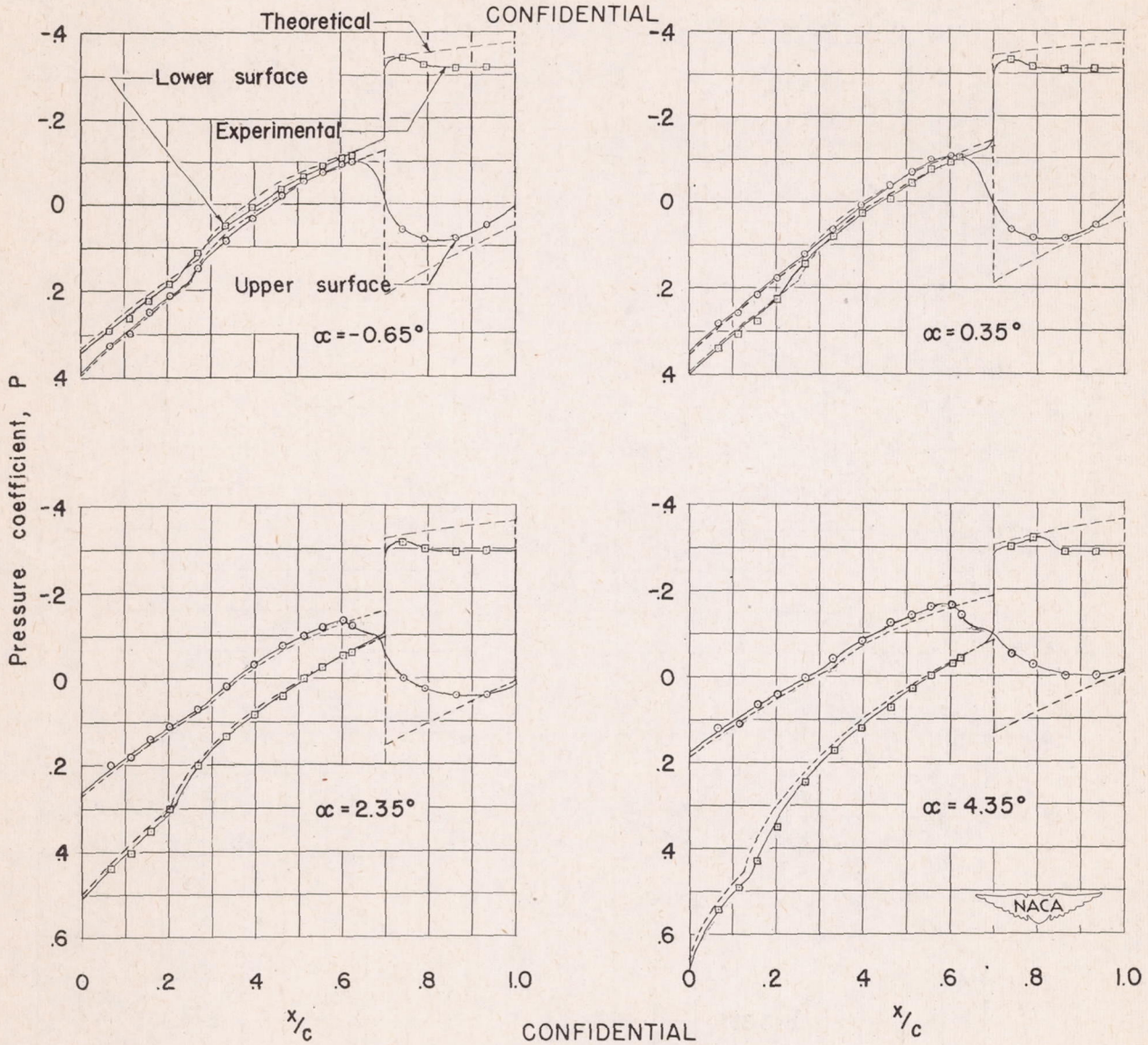

(a) $\delta = -12^{\circ}$.

Figure 9.- Effect of angle of attack on experimental and theoretical pressure distributions. Symmetrical circular-arc airfoil, 9-percent thick; station 2; M, 1.62; R, 1.07×10^{6}.

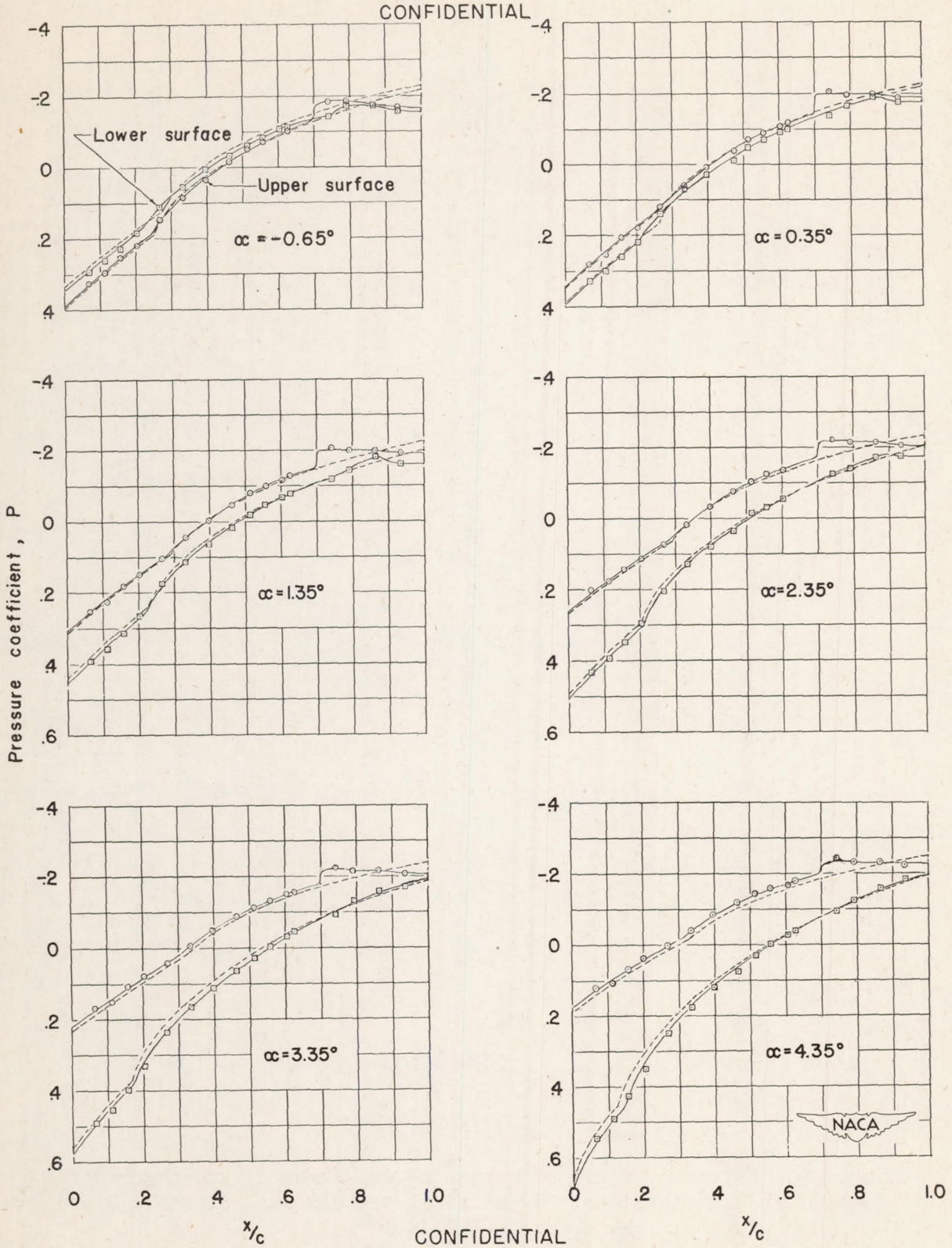

(b) $\delta = 0^{\circ}$.

Figure 9.- Continued.

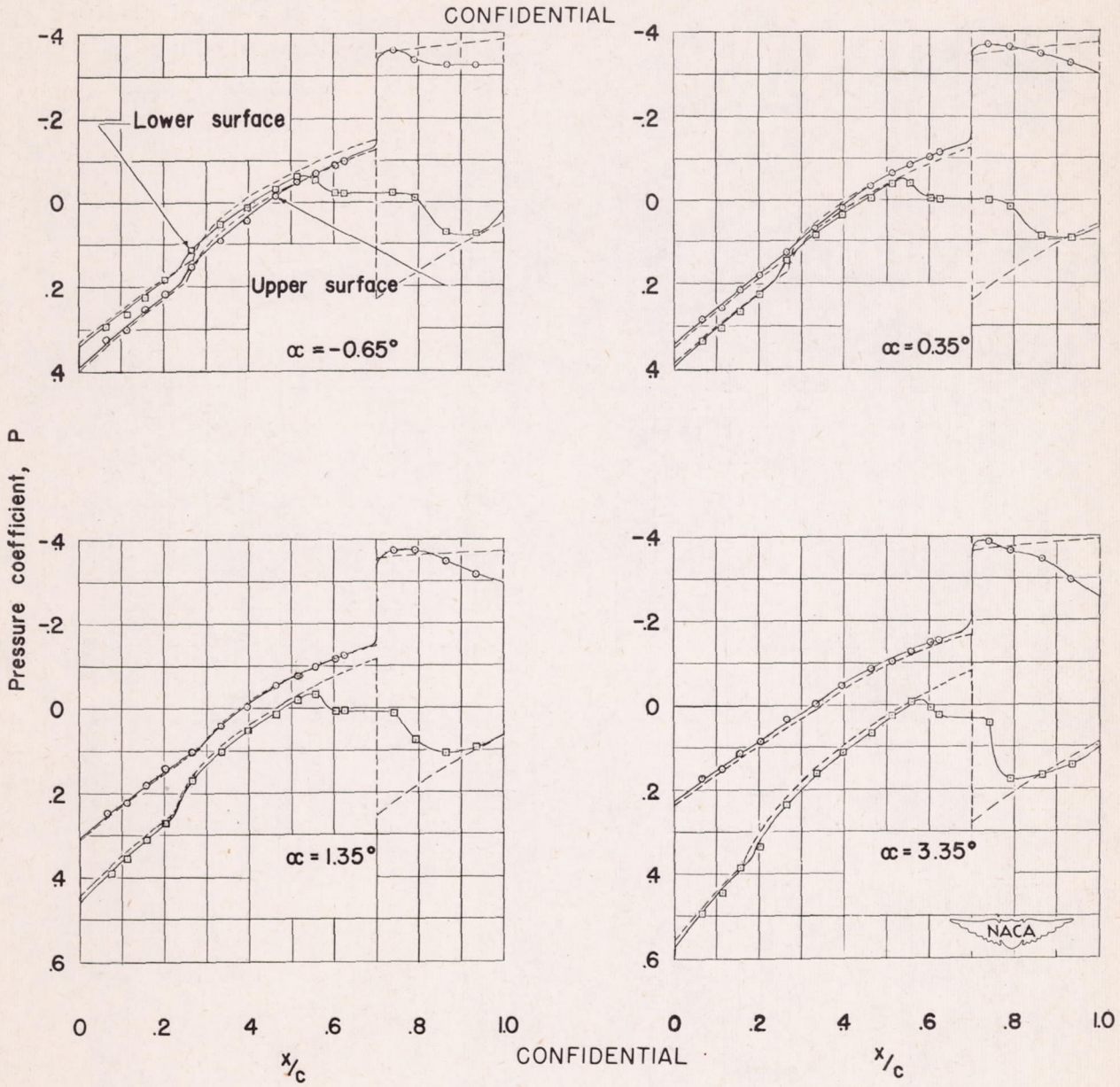

(c) $\delta = 12^{\circ}$.

Figure 9.- Concluded.

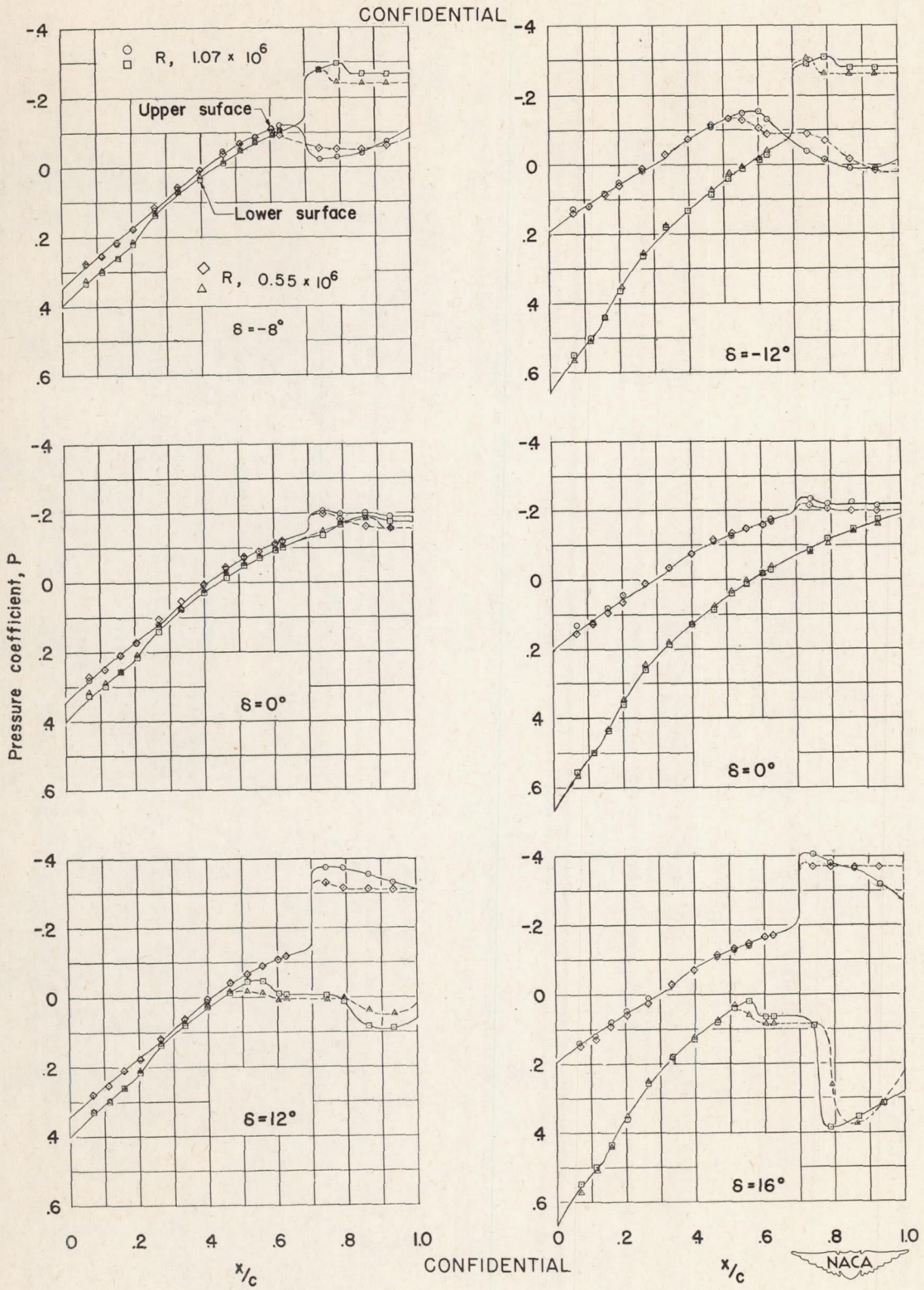

(a) $\alpha = 0.35°$. (b) $\alpha = 4.35°$.

Figure 10.- Effect of Reynolds number on experimental pressure distributions. Symmetrical circular-arc airfoil, 9-percent thick; station 2; M, 1.62.

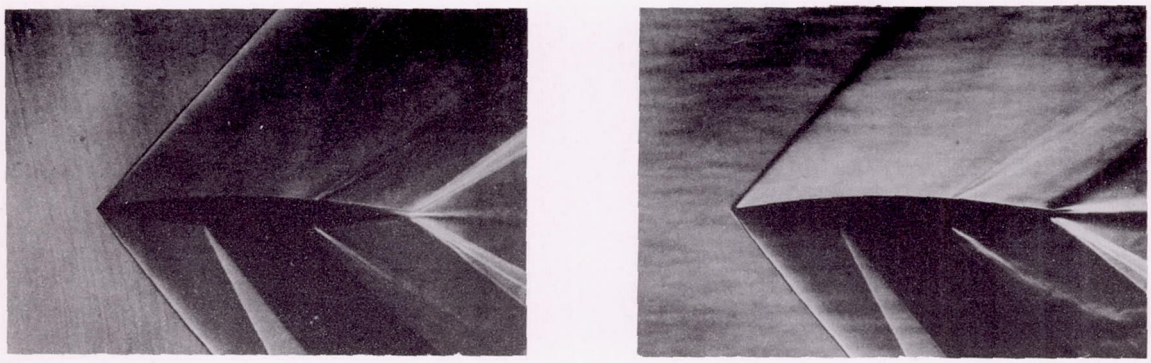

$\alpha = 1.00^{\circ}$, $\delta = 0^{\circ}$.

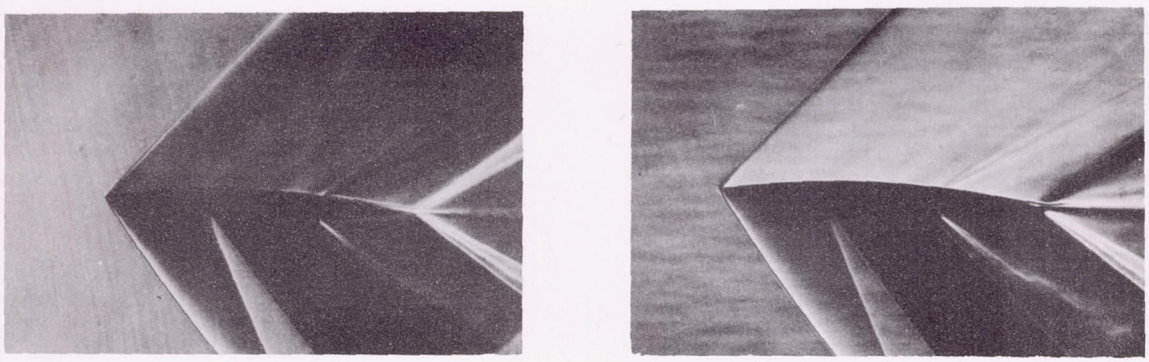

$\alpha = 3.00^{\circ}$, $\delta = 0^{\circ}$.

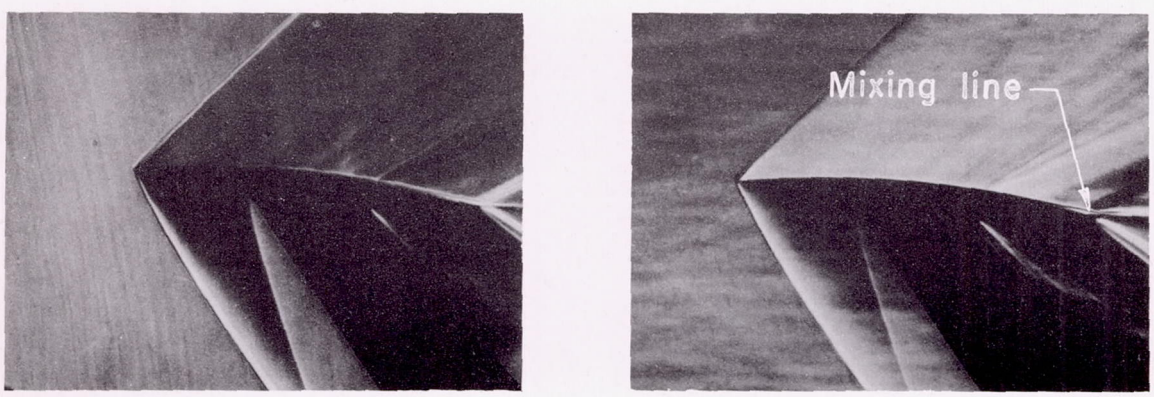

$\alpha = 5.00^{\circ}$, $\delta = 0^{\circ}$.

Vertical knife edge. Horizontal knife edge.

NACA L-62156

Figure 11.- Typical schlieren photographs of flow about a symmetrical circular-arc airfoil, 9-percent thick with flap neutral. R, 1.07×10^6; M, 1.62.

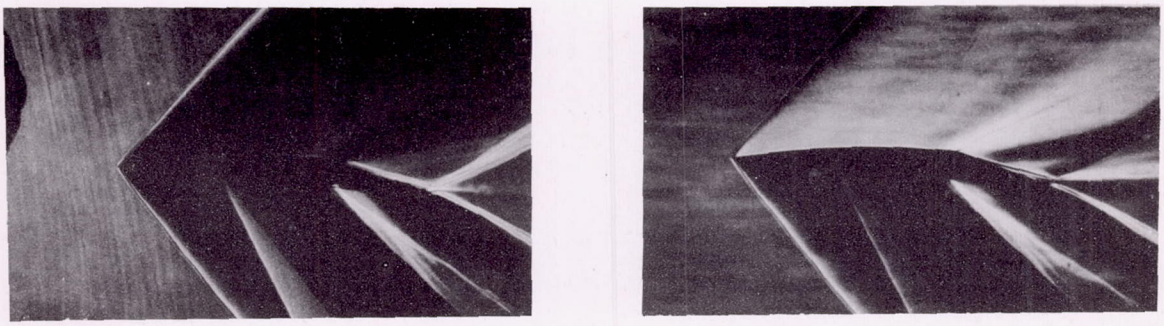

$\alpha = 1.00^{\circ}$, $\delta = 10^{\circ}$.

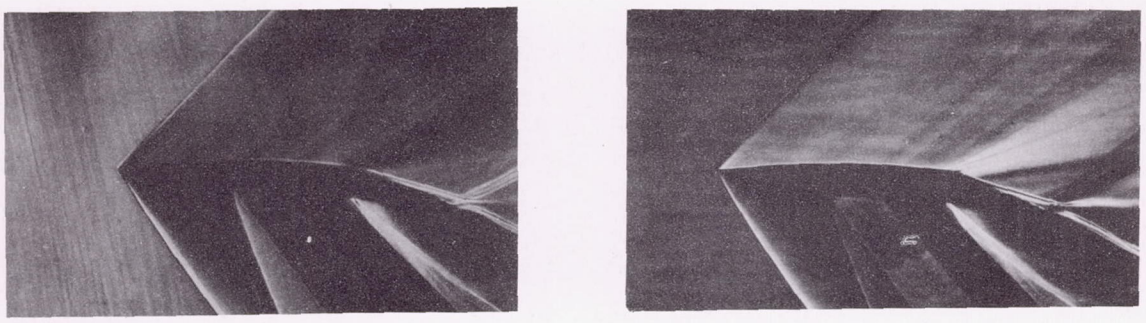

$\alpha = 4.00^{\circ}$, $\delta = 10^{\circ}$.

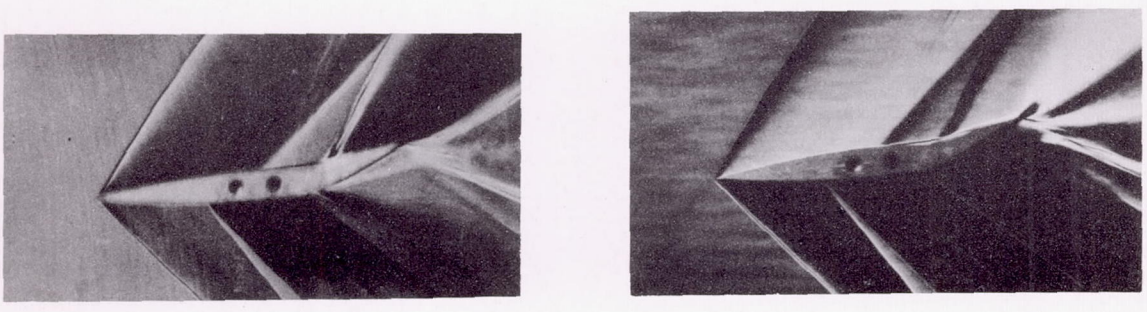

$\alpha = -5^{\circ}$, $\delta = -18^{\circ}$.

Vertical knife edge. Horizontal knife edge.

NACA L-62157

Figure 12.- Typical schlieren photographs of flow about a symmetrical circular-arc airfoil, $\frac{t}{c} = 0.09$ with flap deflected. R, 1.07×10^{6}; M, 1.62.

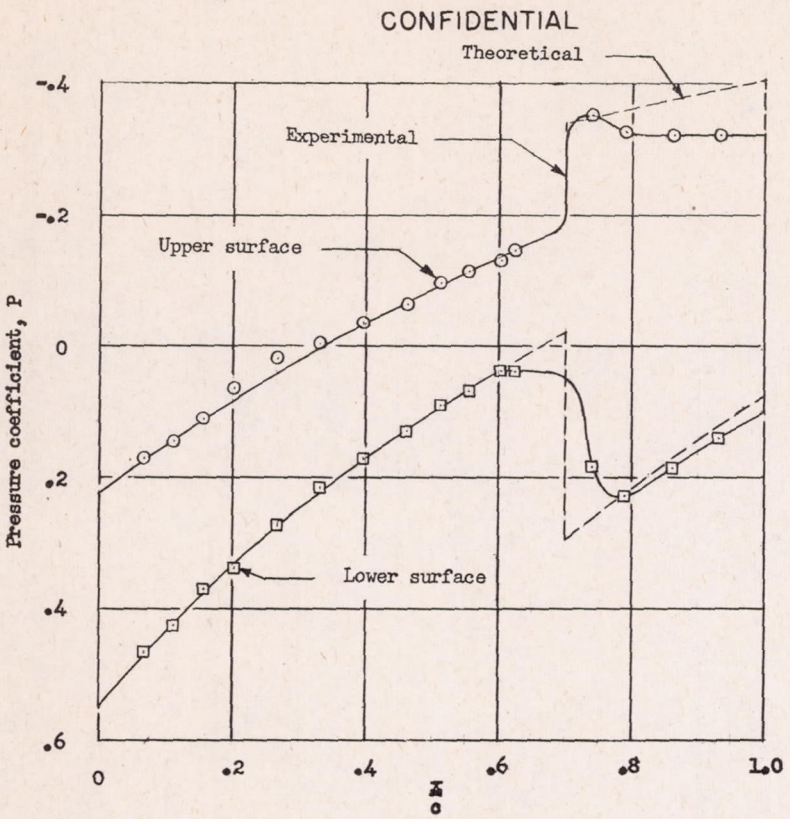

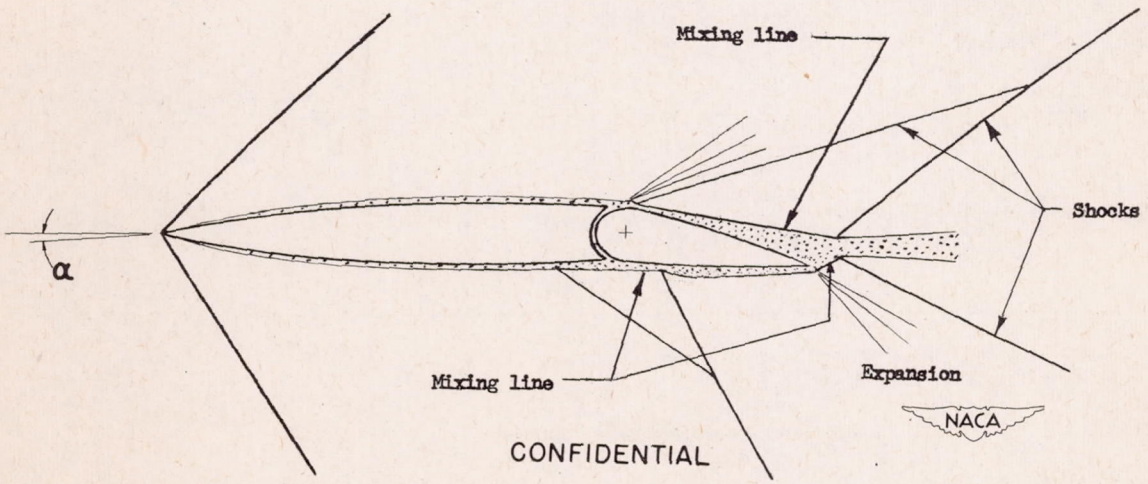

Figure 13.- Character of flow over wing at $\alpha = 3.35^{\circ}$ and $\delta = 10^{\circ}$. Symmetrical circular-arc airfoil, 9-percent thick; station 1; M, 1.62; R, 1.07×10^{6}.

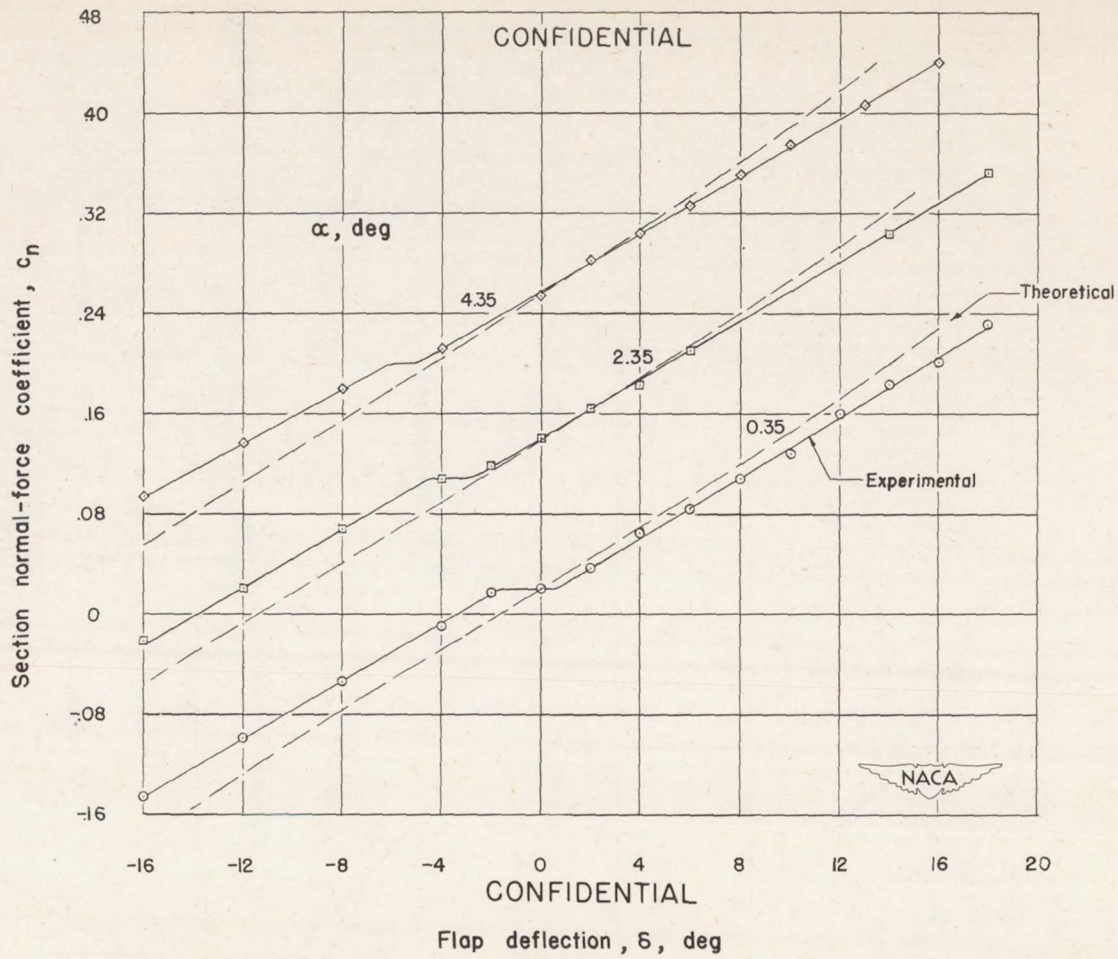

(a) Station 1.

Figure 14.- Variation of section normal-force coefficient with flap deflection. Symmetrical circular-arc airfoil, 9-percent thick; M, 1.62; R, 1.07×10^6.

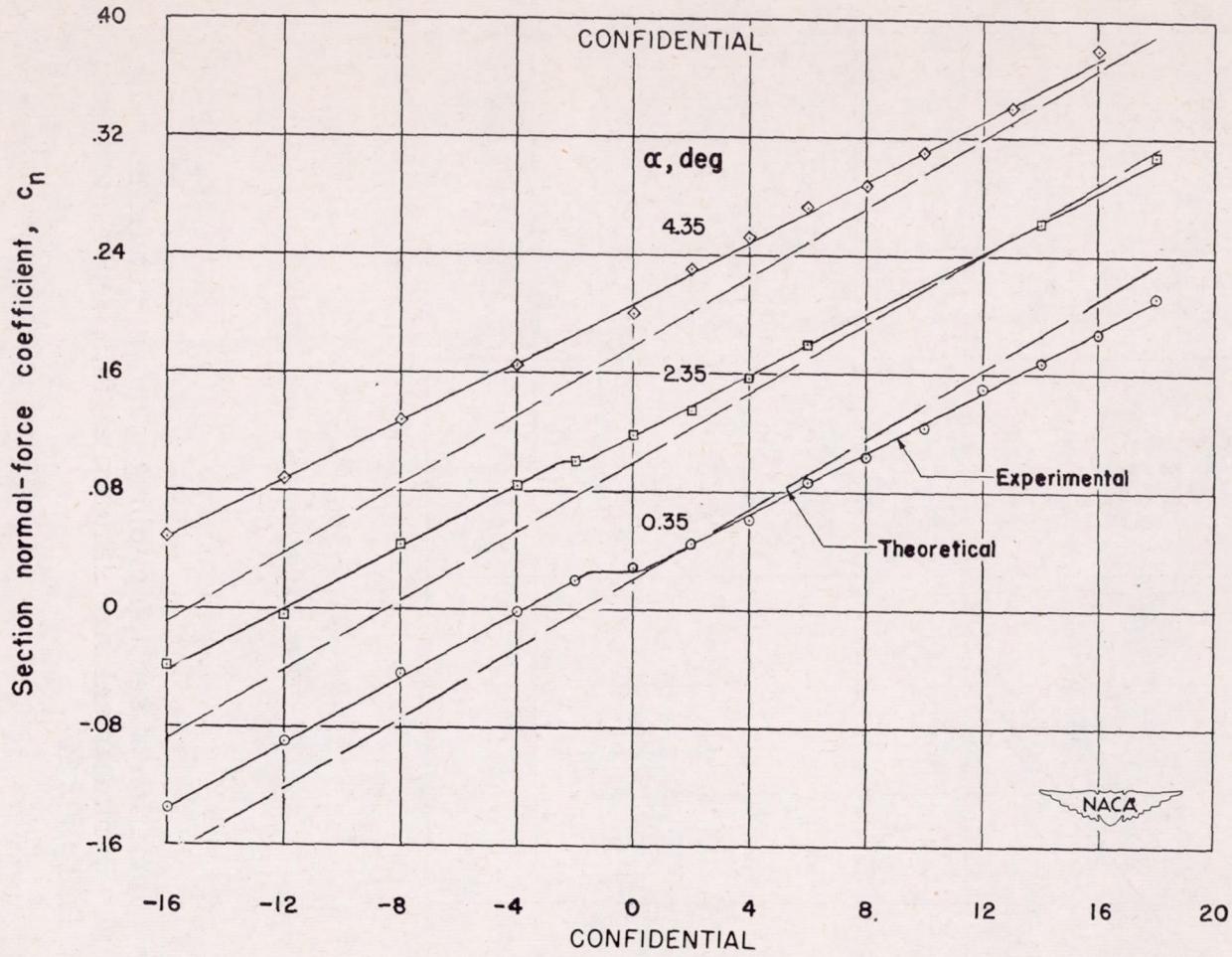

(b) Station 2.

Figure 14.- Concluded.

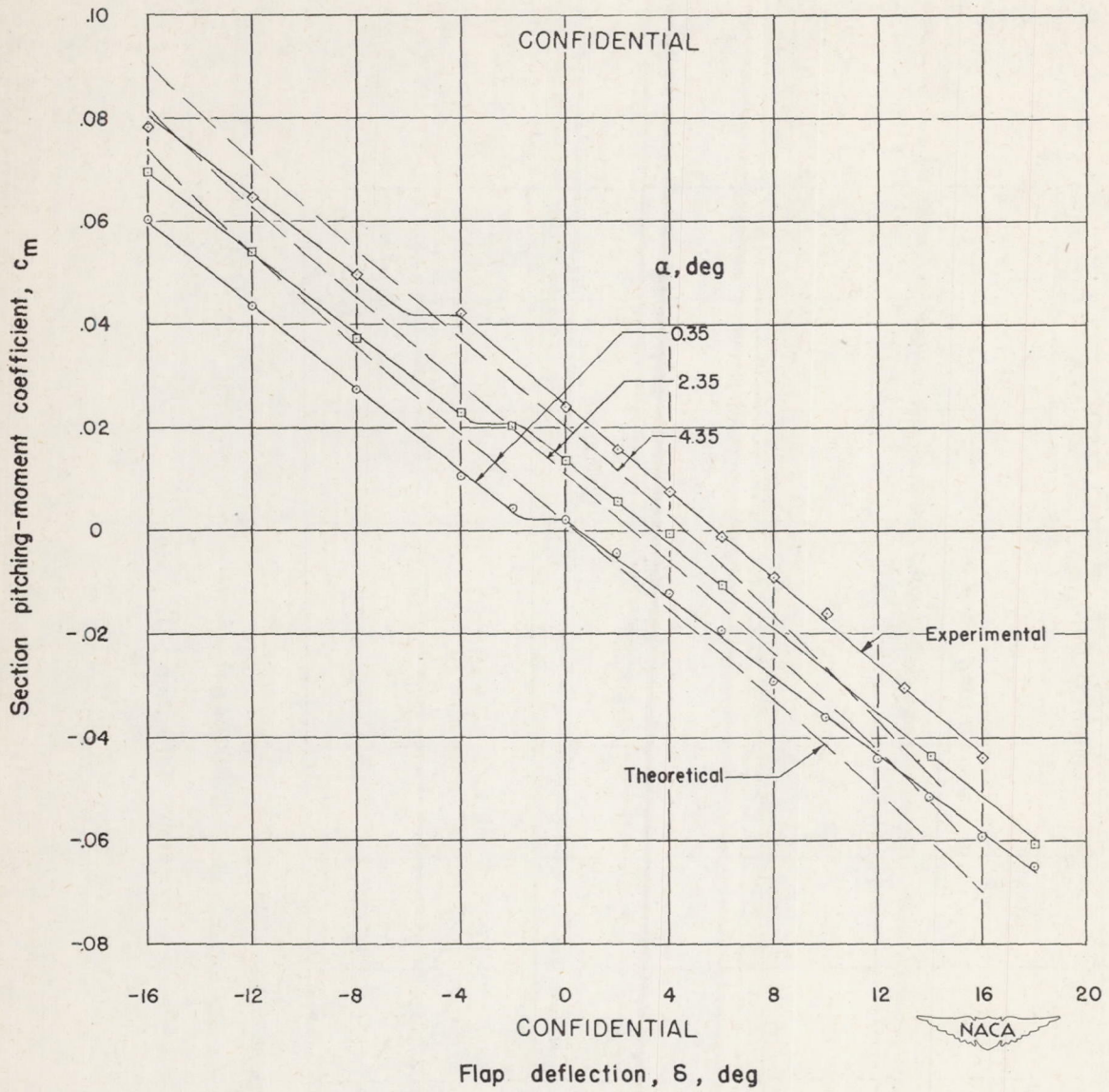

(a) Station 1.

Figure 15.- Variation of section pitching-moment coefficient with flap deflection. Symmetrical circular-arc airfoil, 9-percent thick; M, 1.62; R, 1.07×10^6.

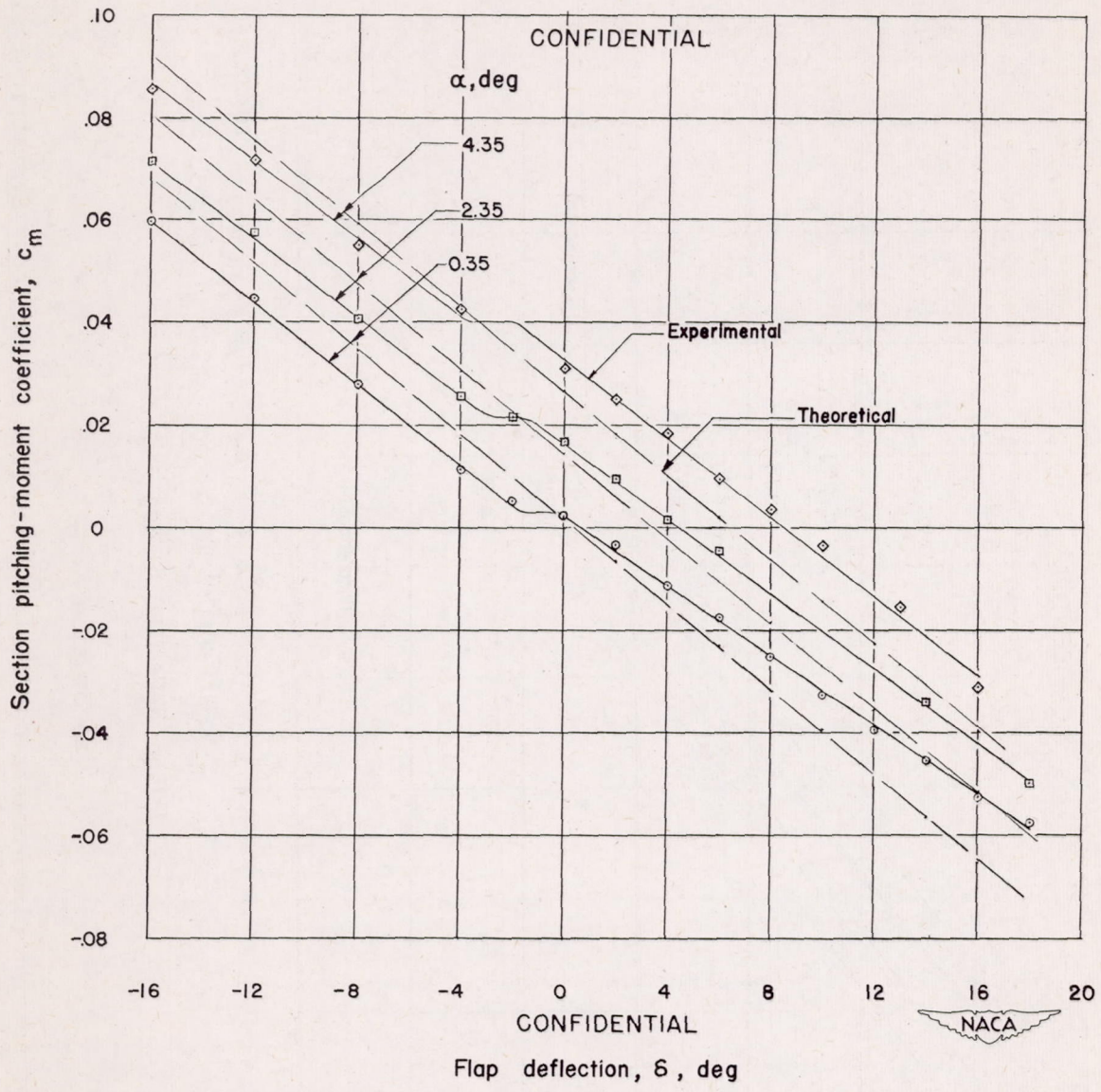

(b) Station 2.

Figure 15.- Concluded.

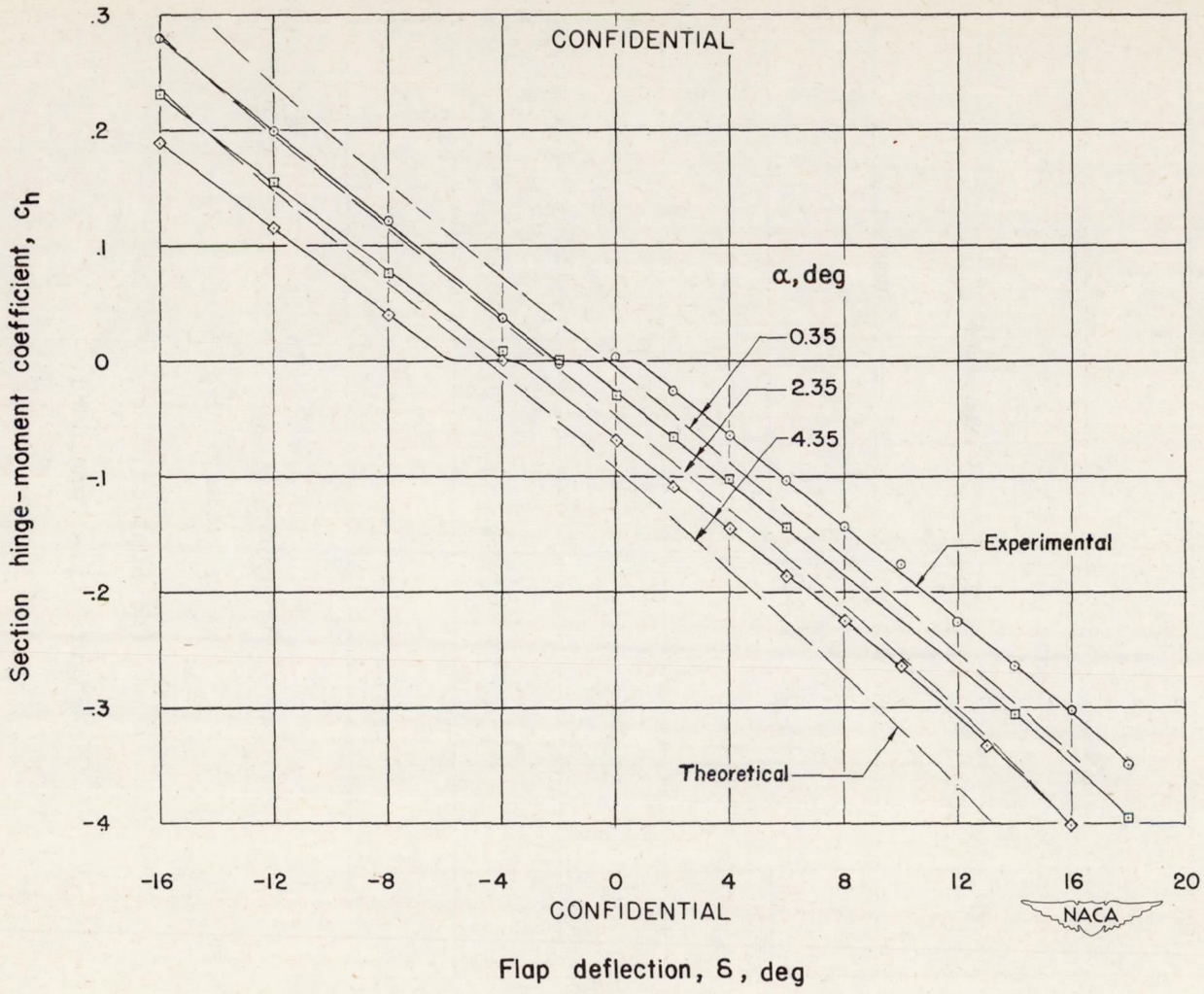

(a) Station 1.

Figure 16.- Variation of section hinge-moment coefficient with flap deflection. Symmetrical circular-arc airfoil, 9-percent thick; M, 1.62; R, 1.07 × 10^6.

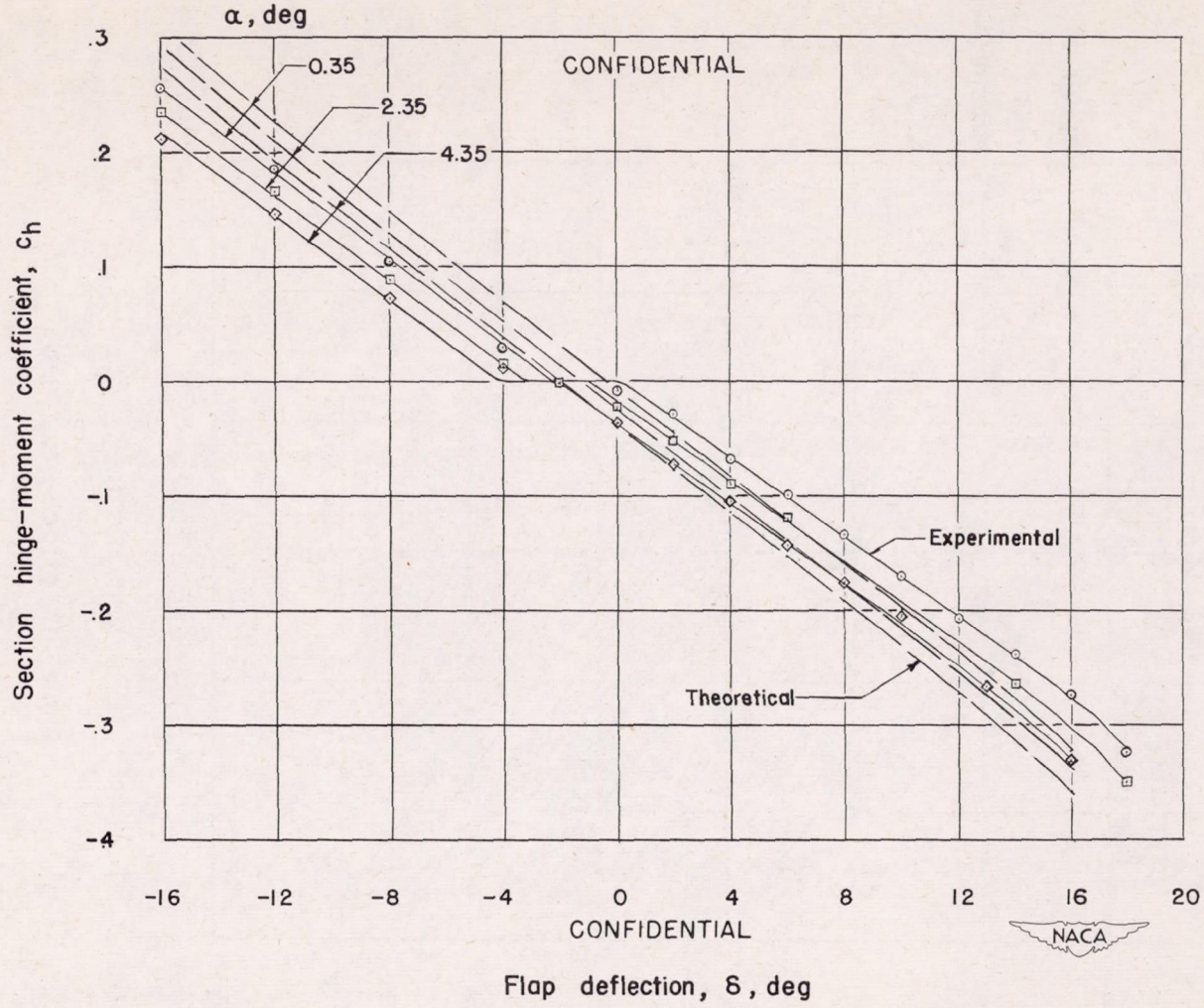

(b) Station 2.

Figure 16.- Concluded.

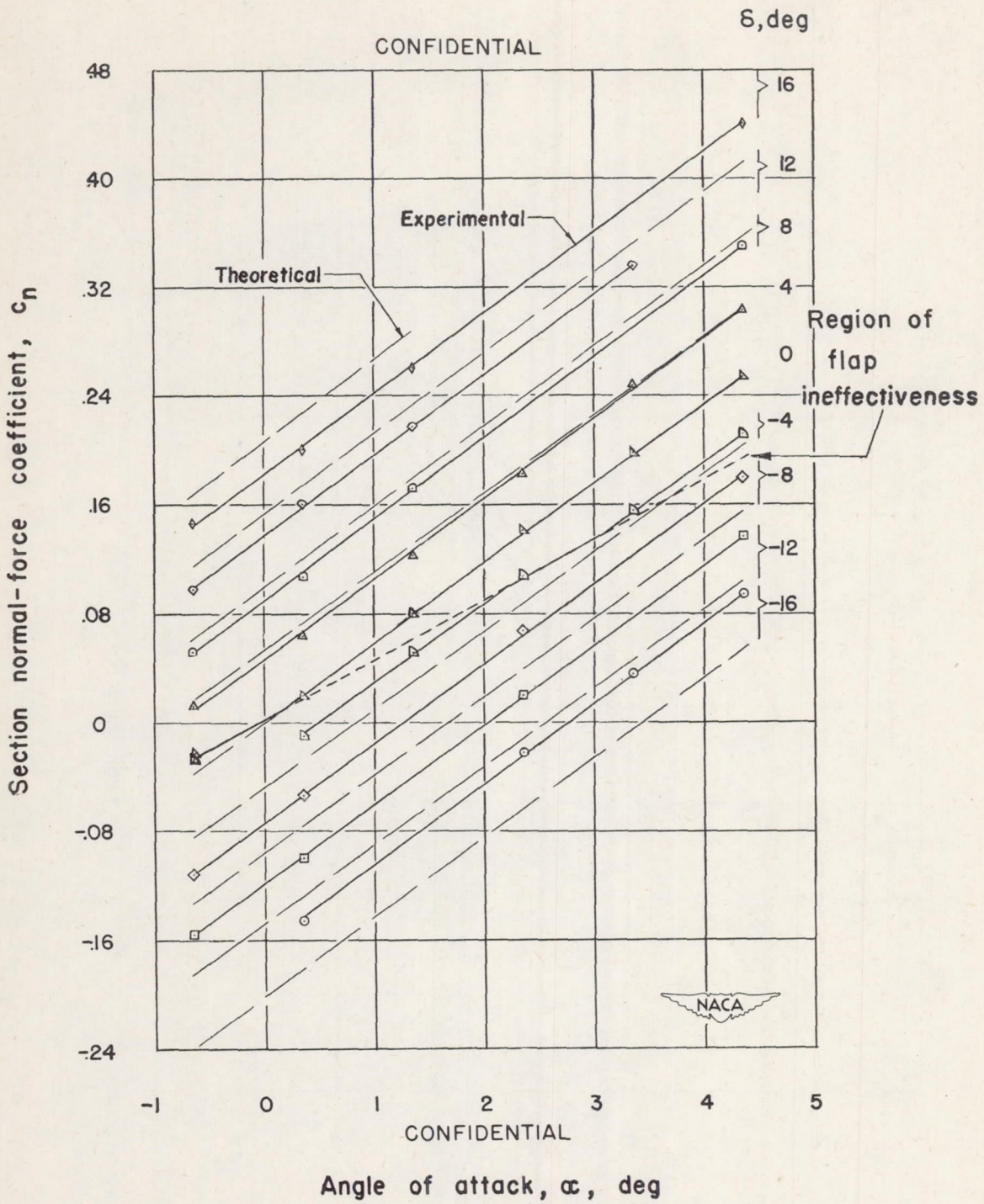

(a) Station 1.

Figure 17.- Variation of section normal-force coefficient with angle of attack. Symmetrical circular-arc airfoil, 9-percent thick; M, 1.62; R, 1.07×10^6.

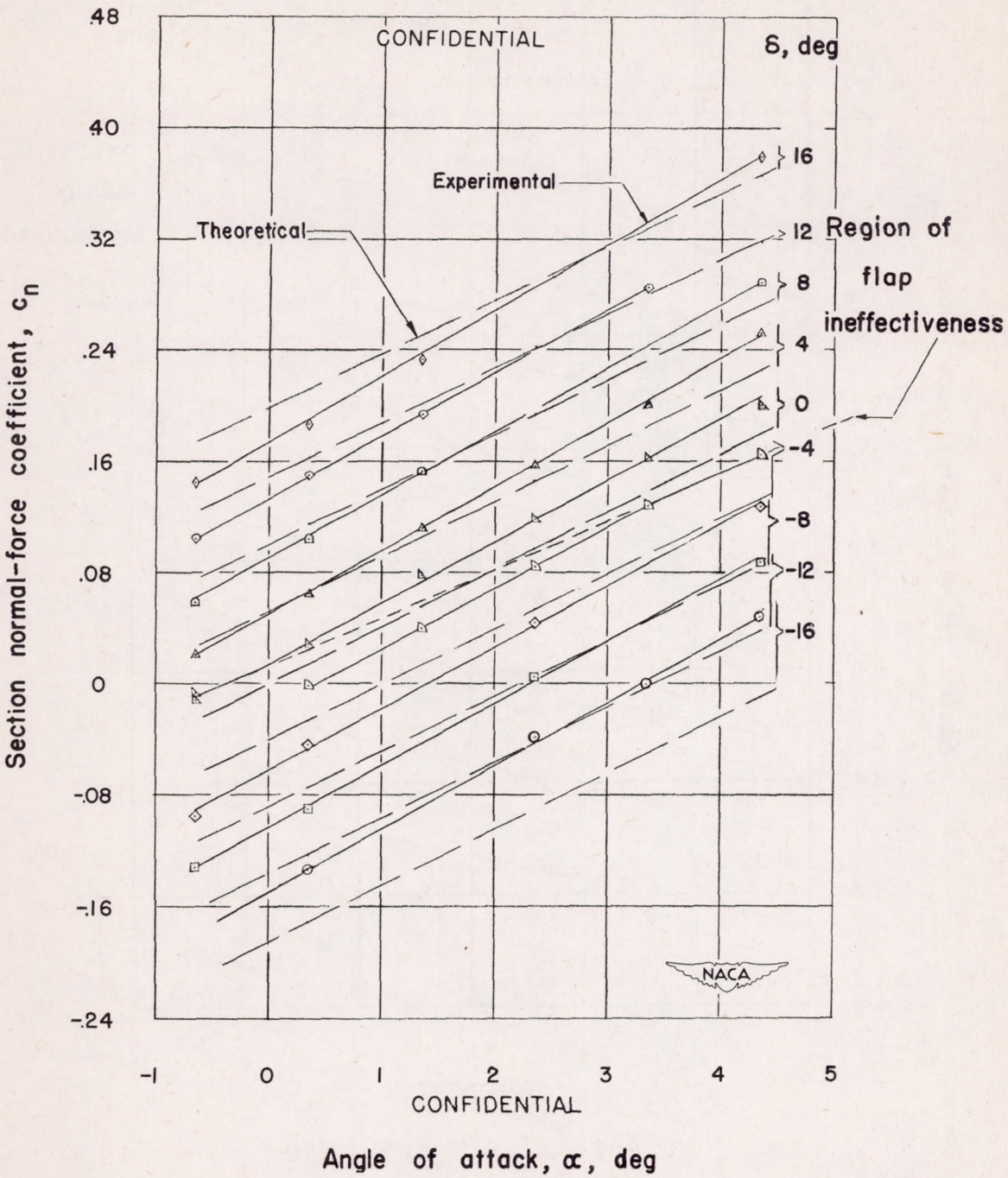

(b) Station 2.

Figure 17.- Concluded.

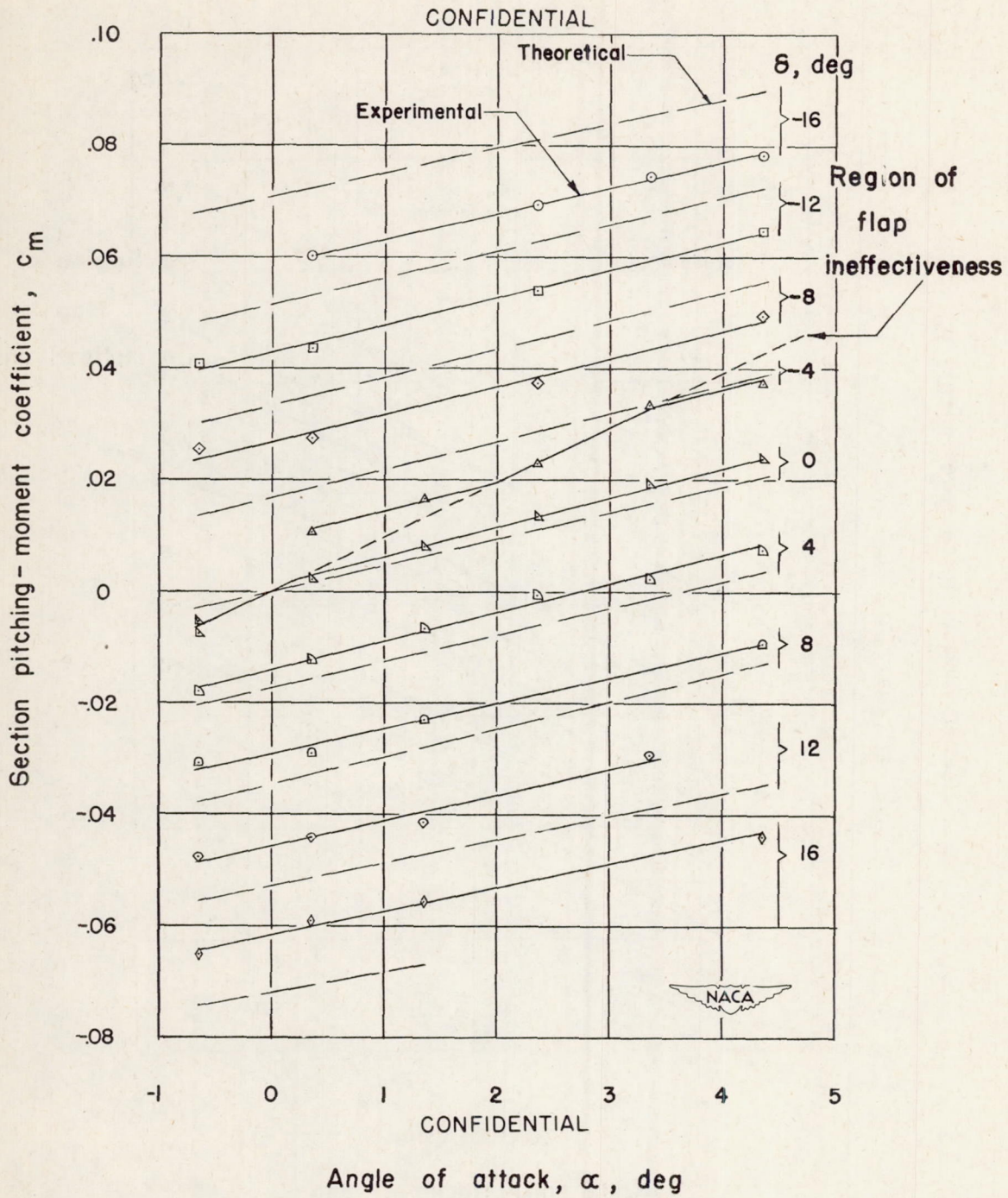

(a) Station 1.

Figure 18.- Variation of section pitching-moment coefficient with angle of attack. Symmetrical circular-arc airfoil, 9-percent thick; M, 1.62; R, 1.07×10^6.

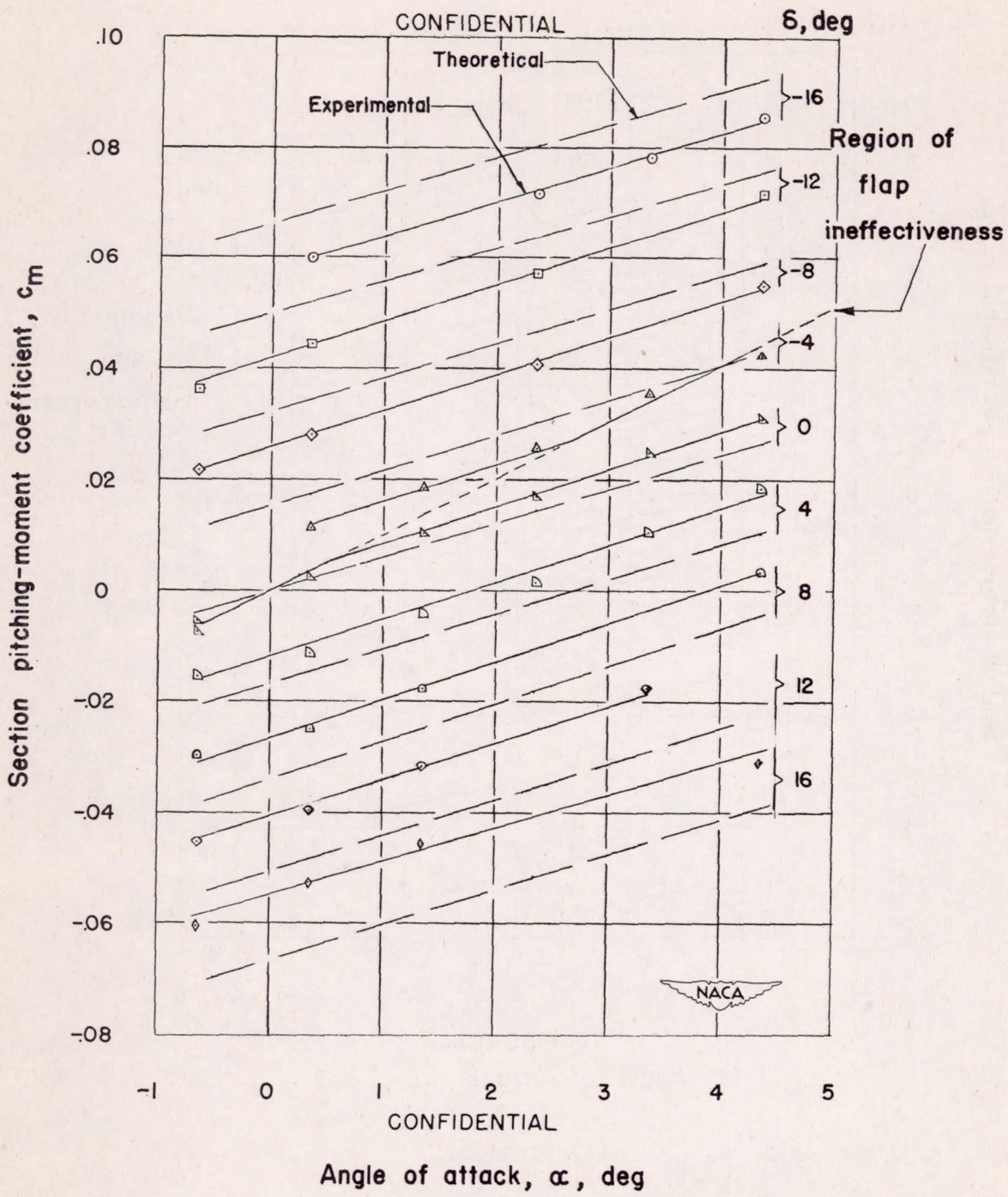

(b) Station 2.

Figure 18.- Concluded.

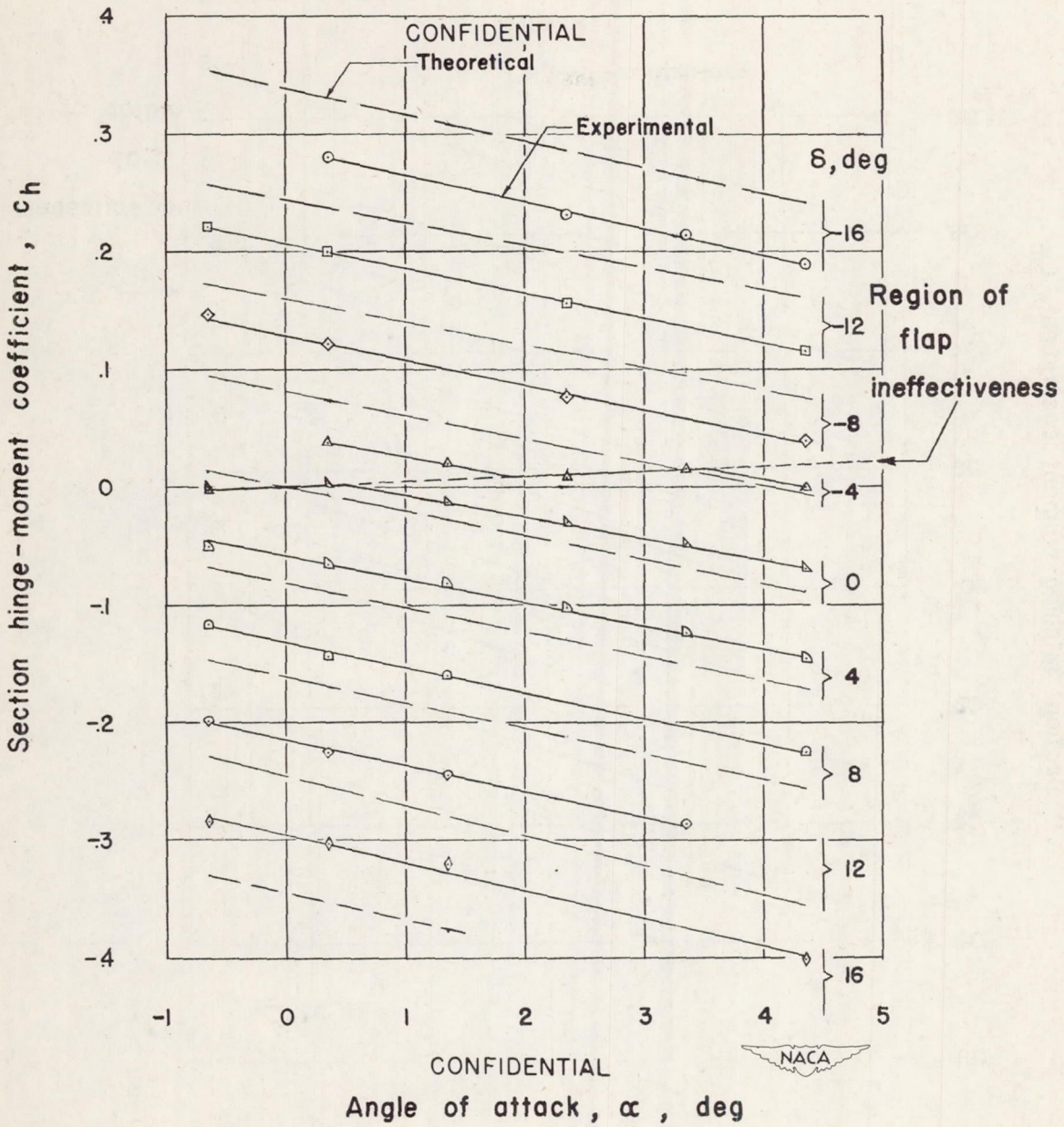

(a) Station 1.

Figure 19.- Variation of section hinge-moment coefficient with angle of attack. Symmetrical circular-arc airfoil, 9-percent thick; M, 1.62; R, 1.07 x 10^6.

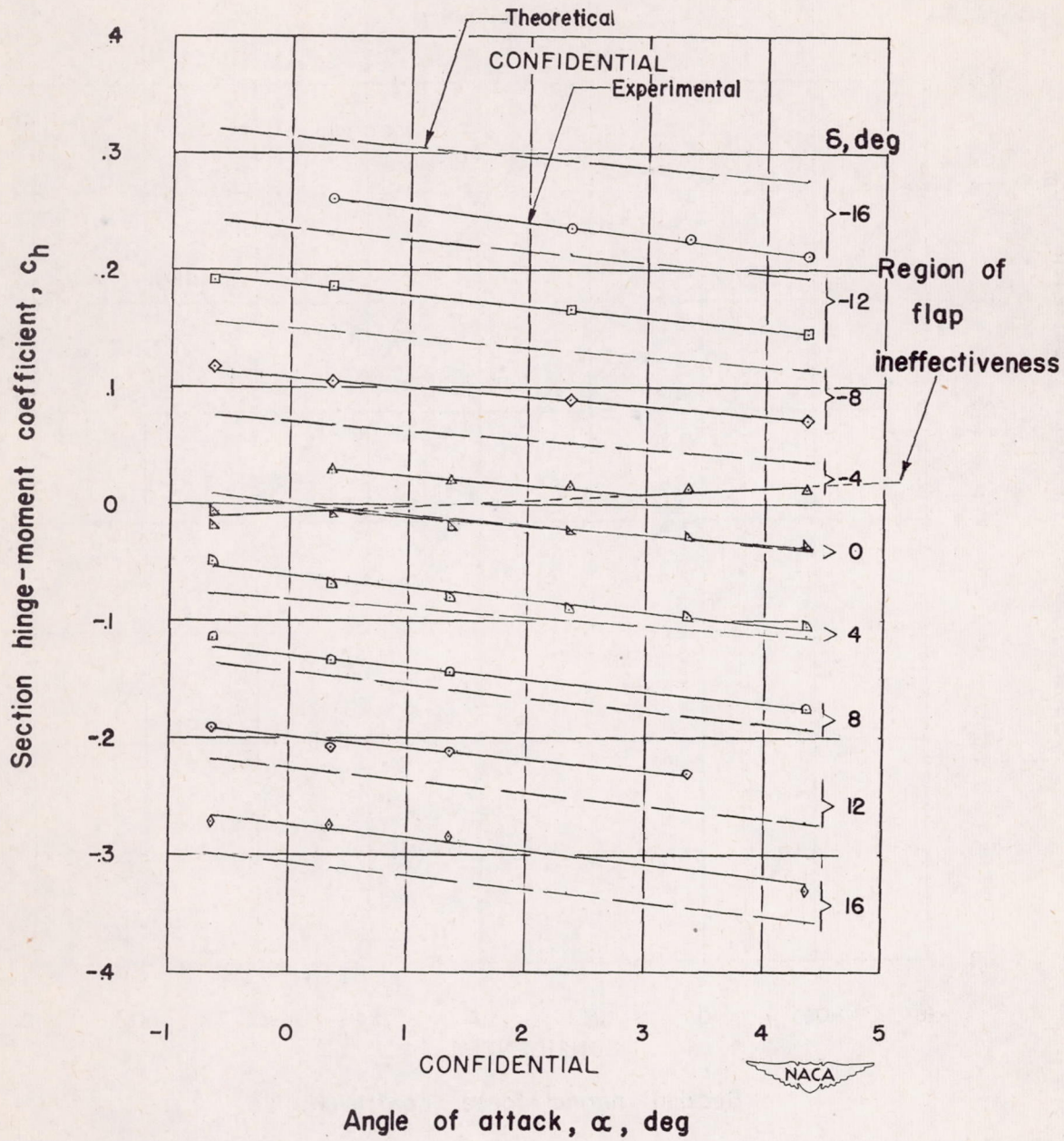

(b) Station 2.

Figure 19.- Concluded.

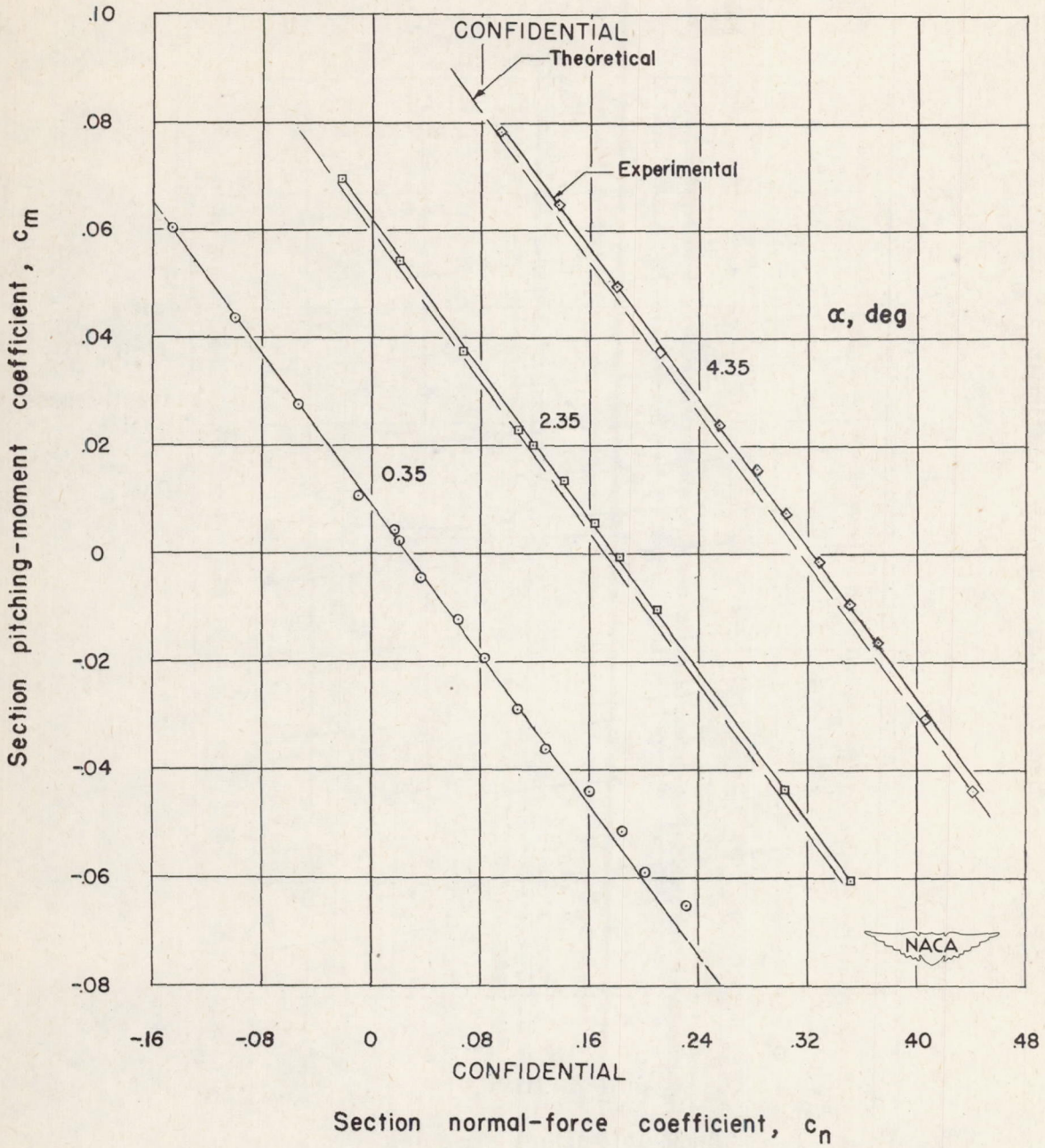

(a) Station 1.

Figure 20.- Variation of section pitching-moment coefficient with section normal-force coefficient for constant angle of attack. Symmetrical circular-arc airfoil, 9-percent thick; M, 1.62; R, 1.07×10^6.

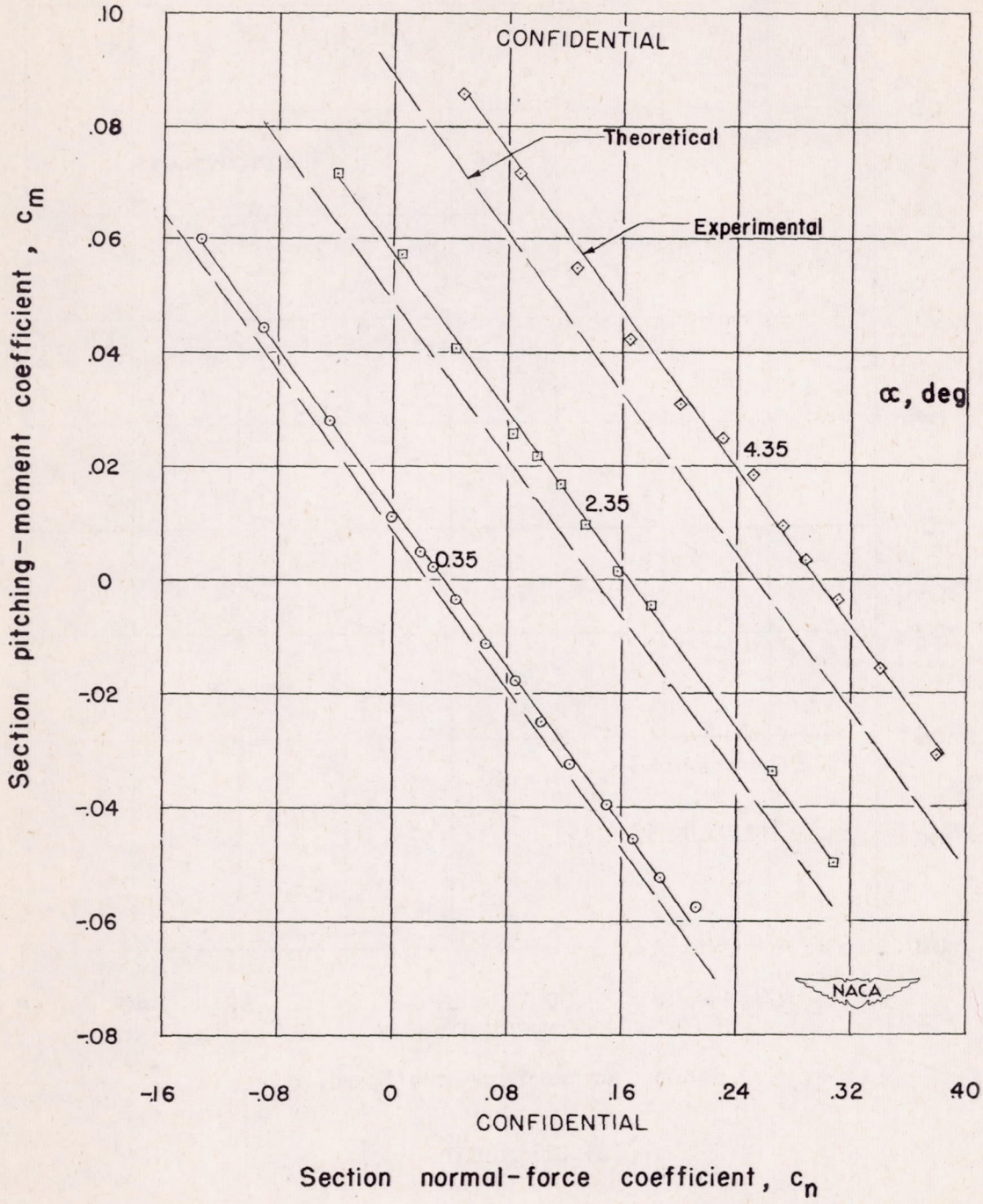

(b) Station 2.

Figure 20.- Concluded.

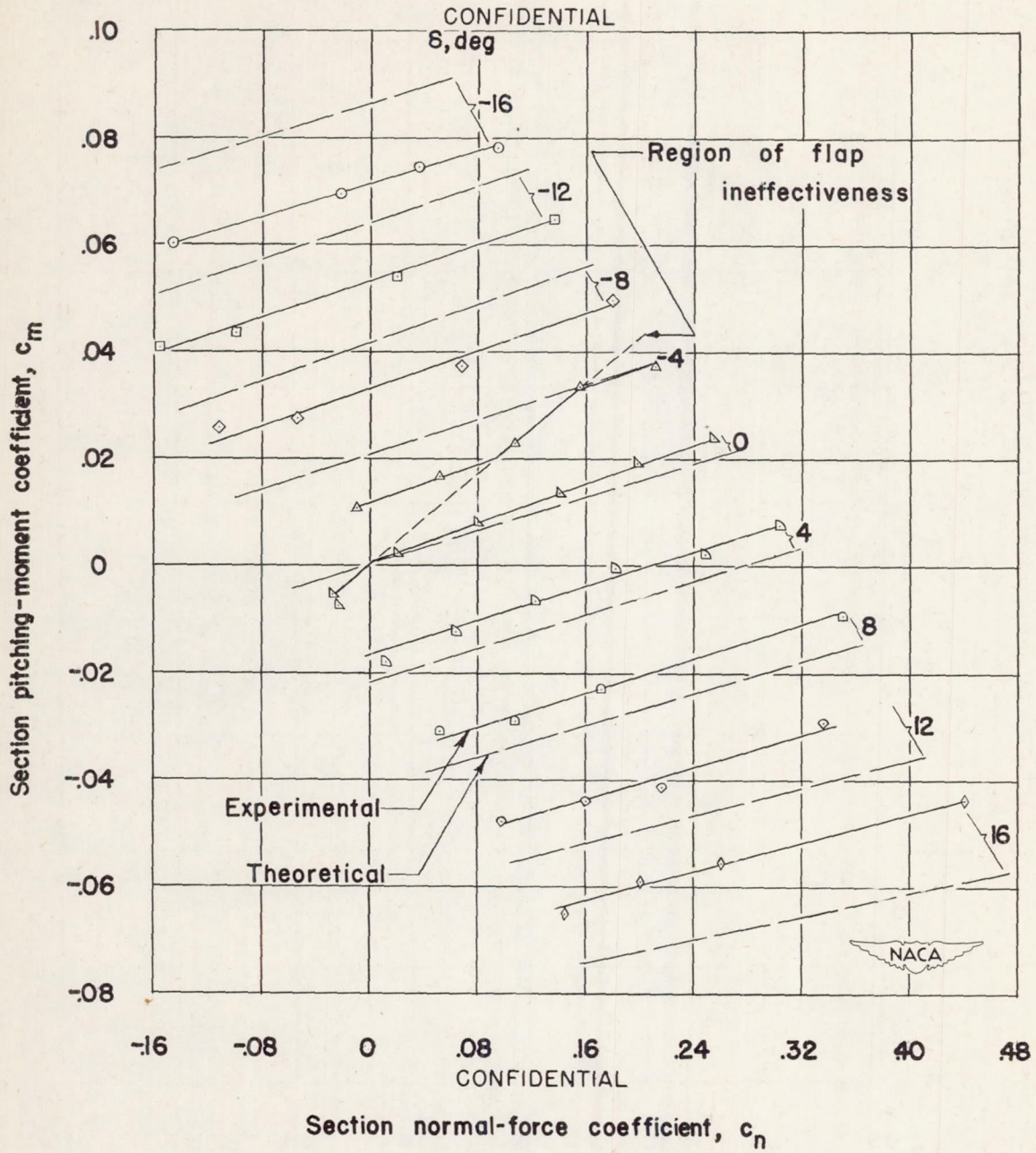

(a) Station 1.

Figure 21.- Variation of section pitching-moment coefficient with section normal-force coefficient for constant flap deflection. Symmetrical circular-arc airfoil 9-percent thick; M, 1.62; R, 1.07 × 10^6.

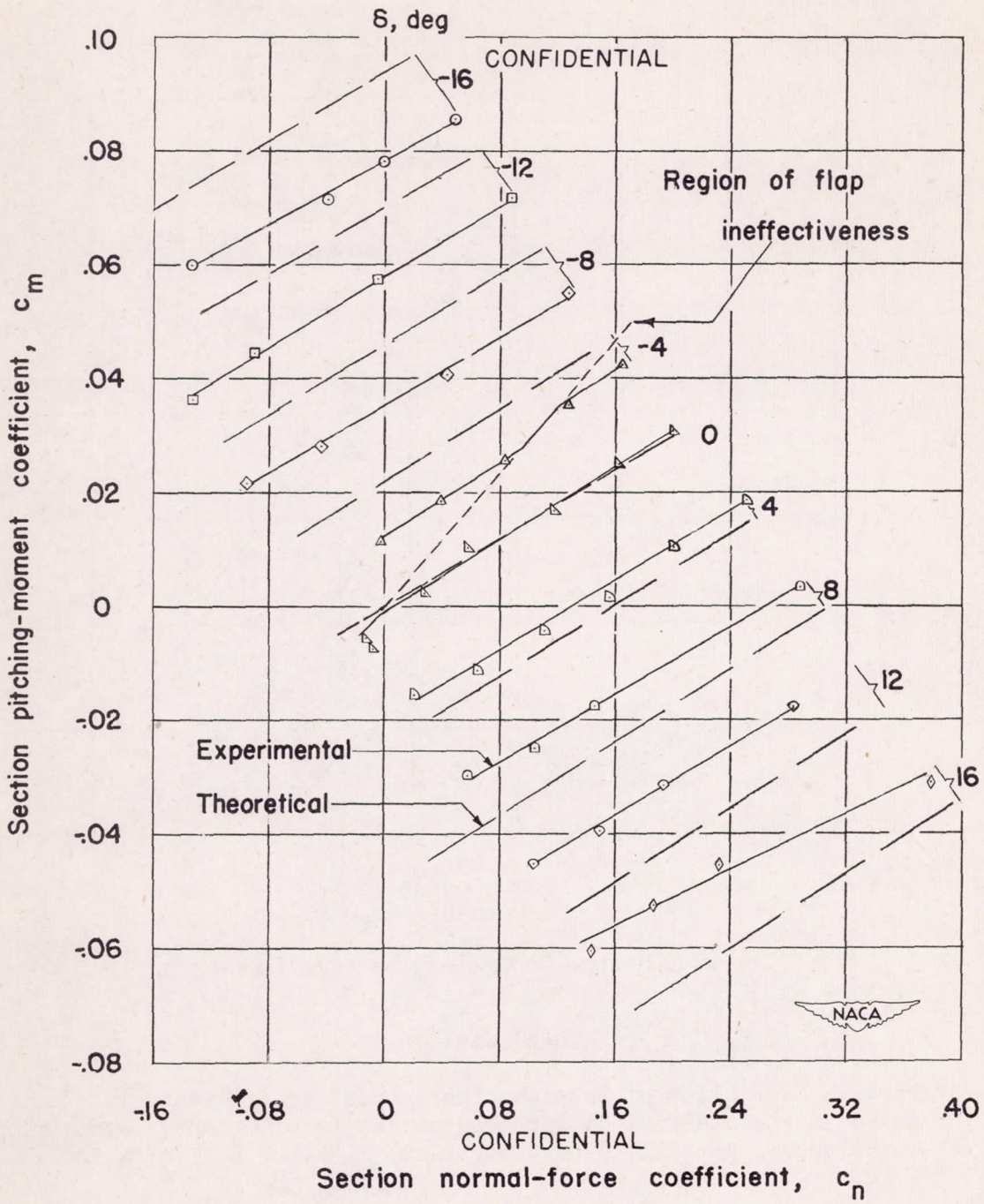

(b) Station 2.

Figure 21.- Concluded.

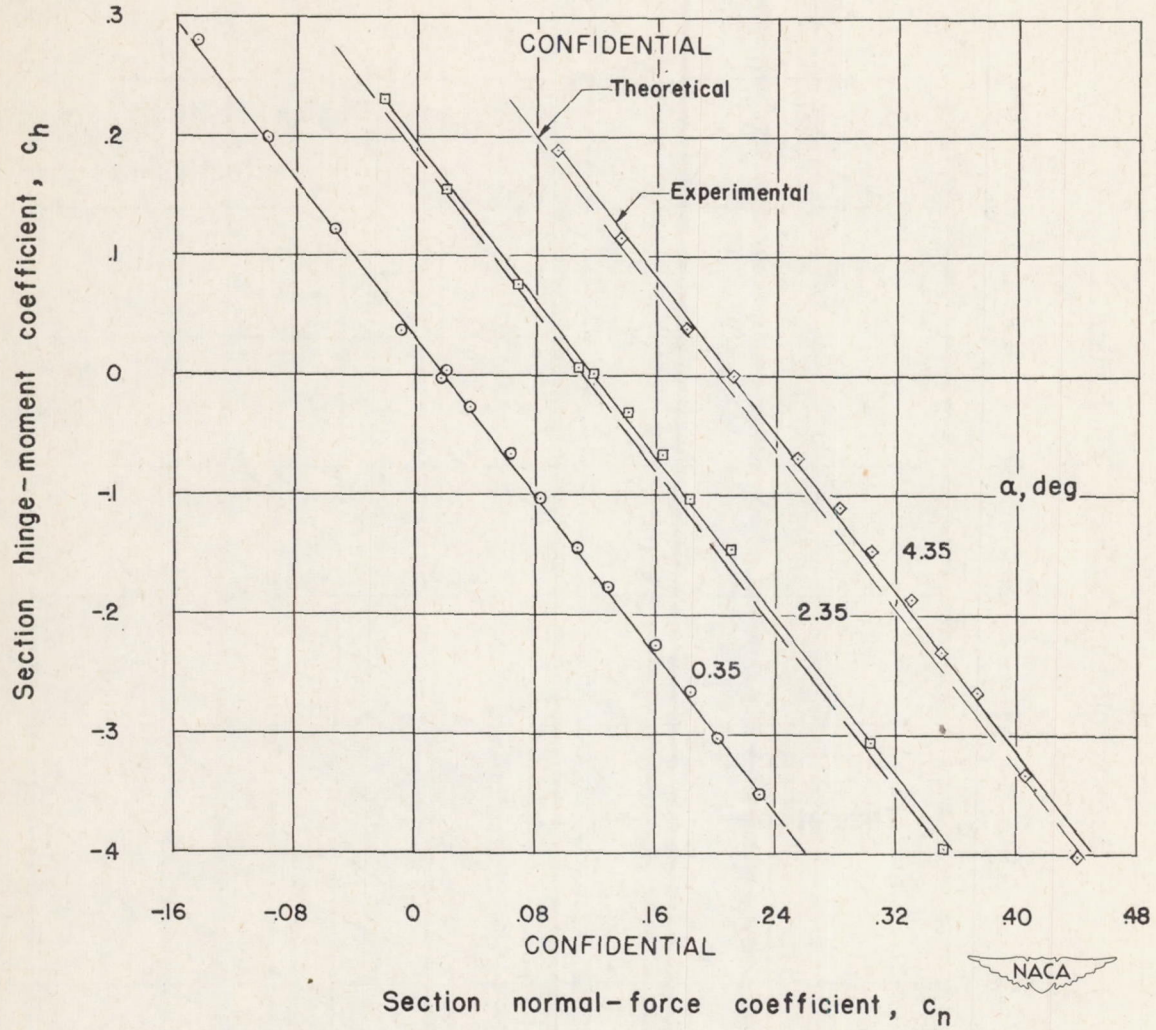

(a) Station 1.

Figure 22.- Variation of section hinge-moment coefficient with section normal-force coefficient for constant angle of attack. Symmetrical circular-arc airfoil, 9-percent thick; M, 1.62; R, 1.07 x 10^6.

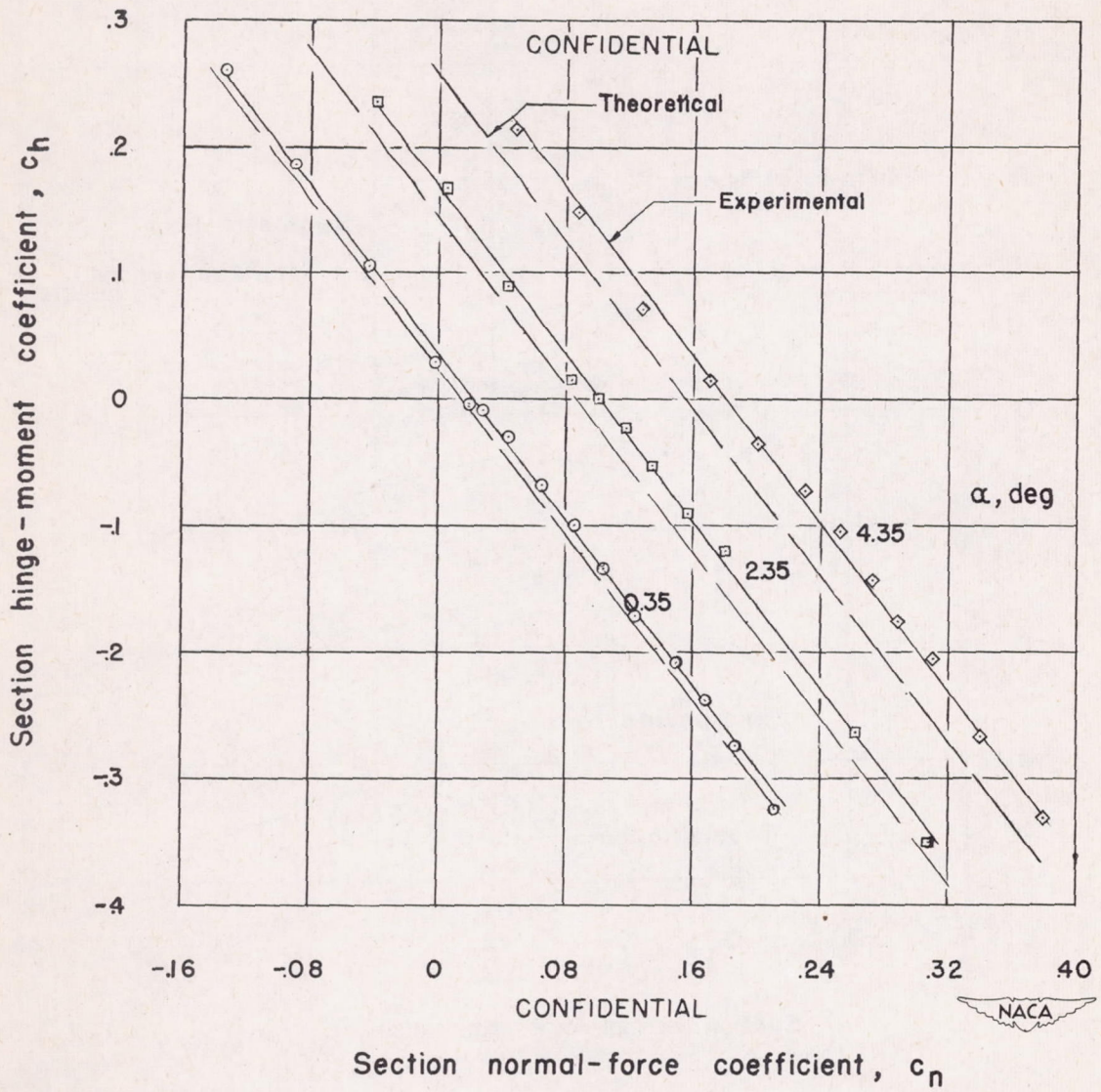

(b) Station 2.

Figure 22.- Concluded.

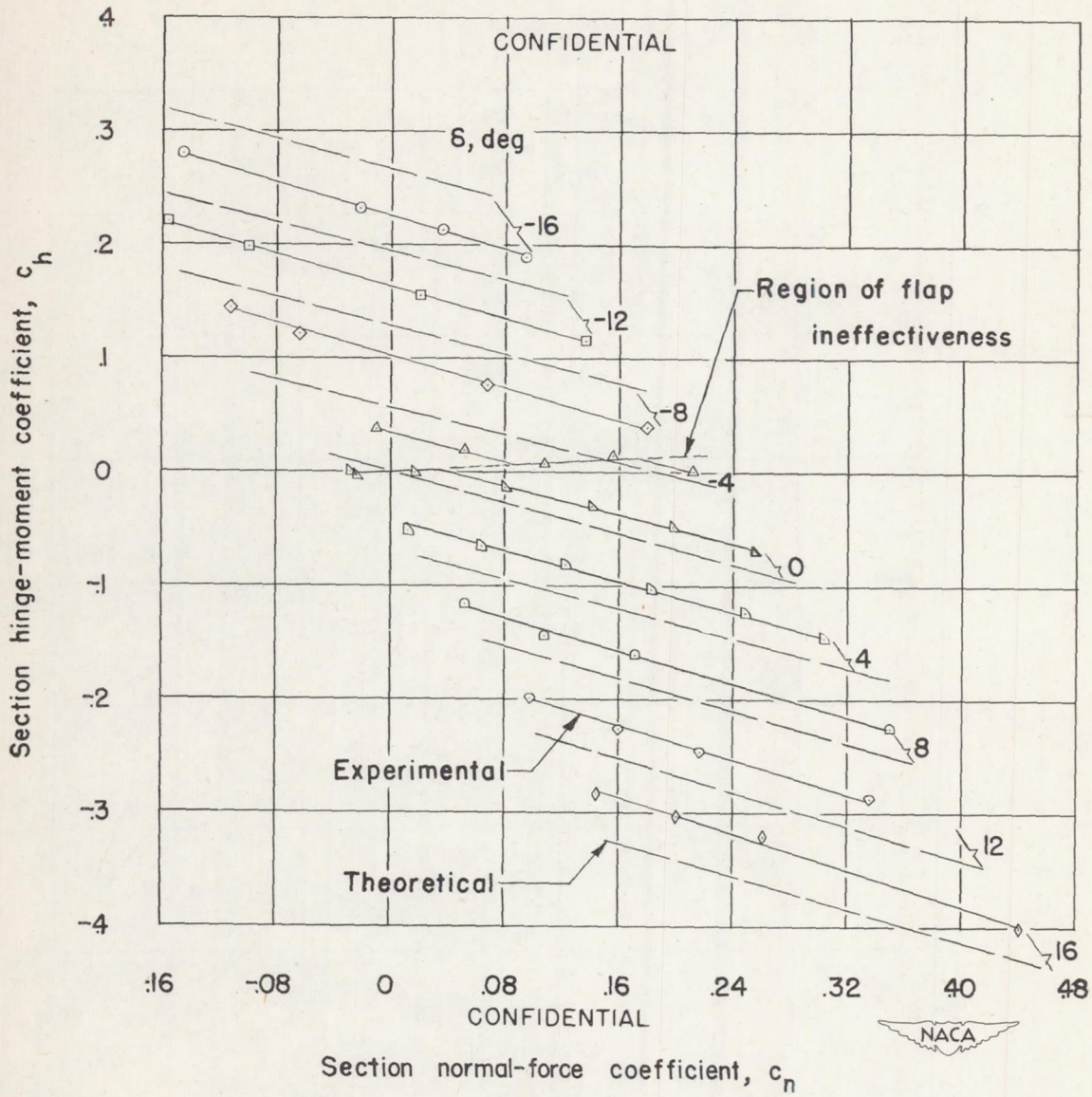

(a) Station 1.

Figure 23.- Variation of section hinge-moment coefficient with section normal-force coefficient for constant flap deflection. Symmetrical circular-arc airfoil, 9-percent thick; M, 1.62; R, 1.07×10^6.

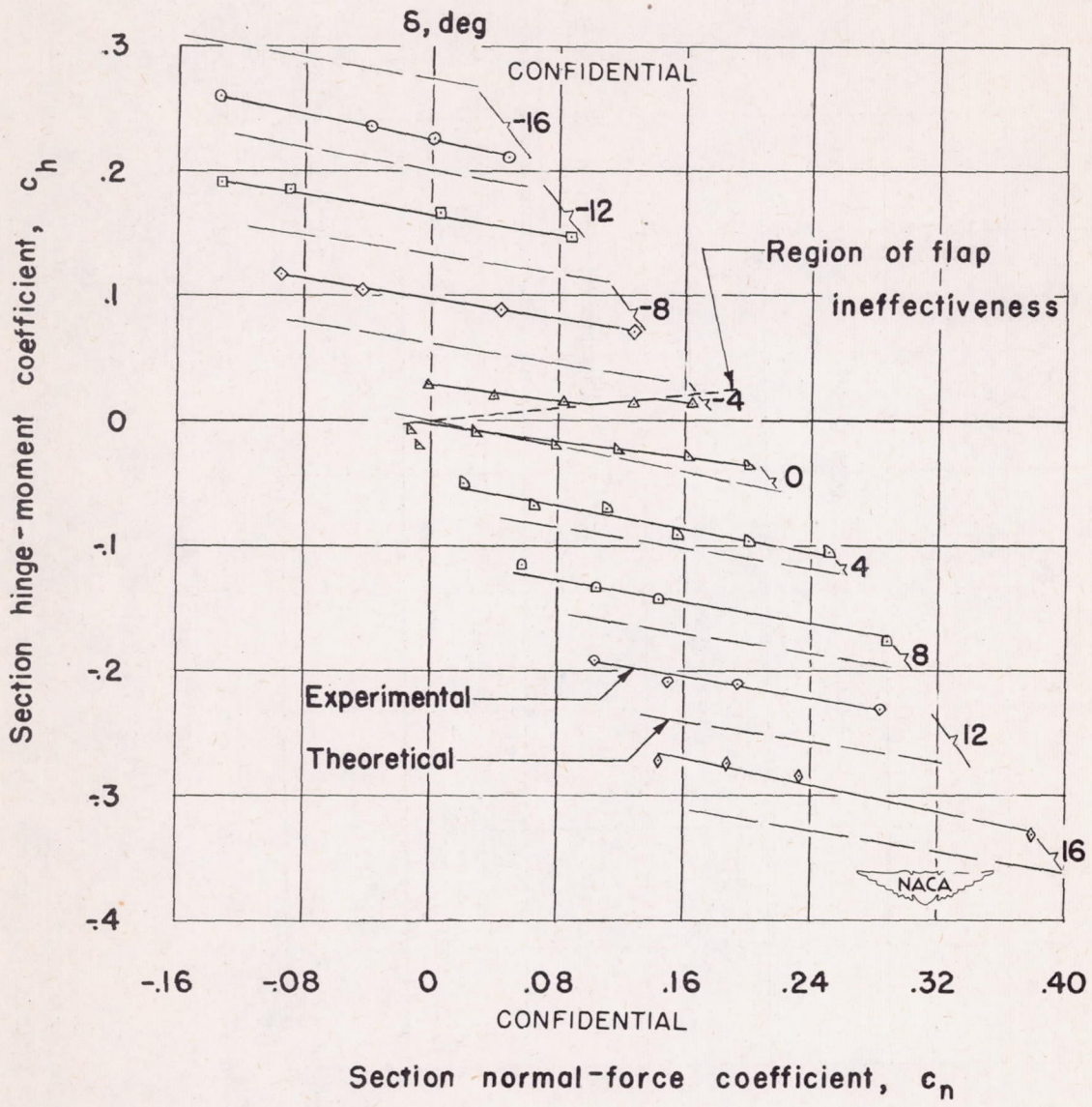

(b) Station 2.

Figure 23.- Concluded.

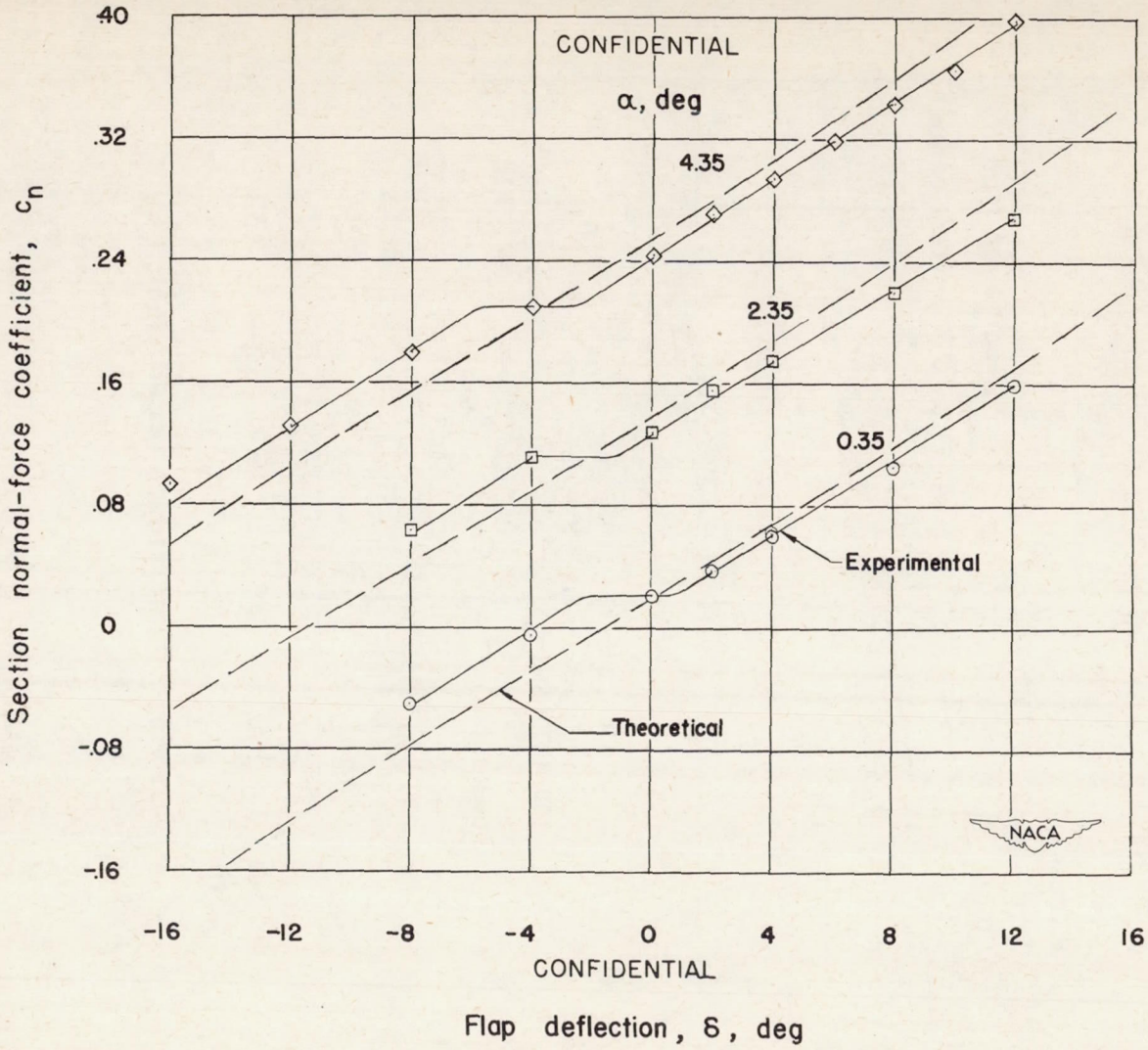

Figure 24.- Variation of section normal-force coefficient with flap deflection. Symmetrical circular-arc airfoil, 9-percent thick; station 1; M, 1.62; R, 0.55×10^6.

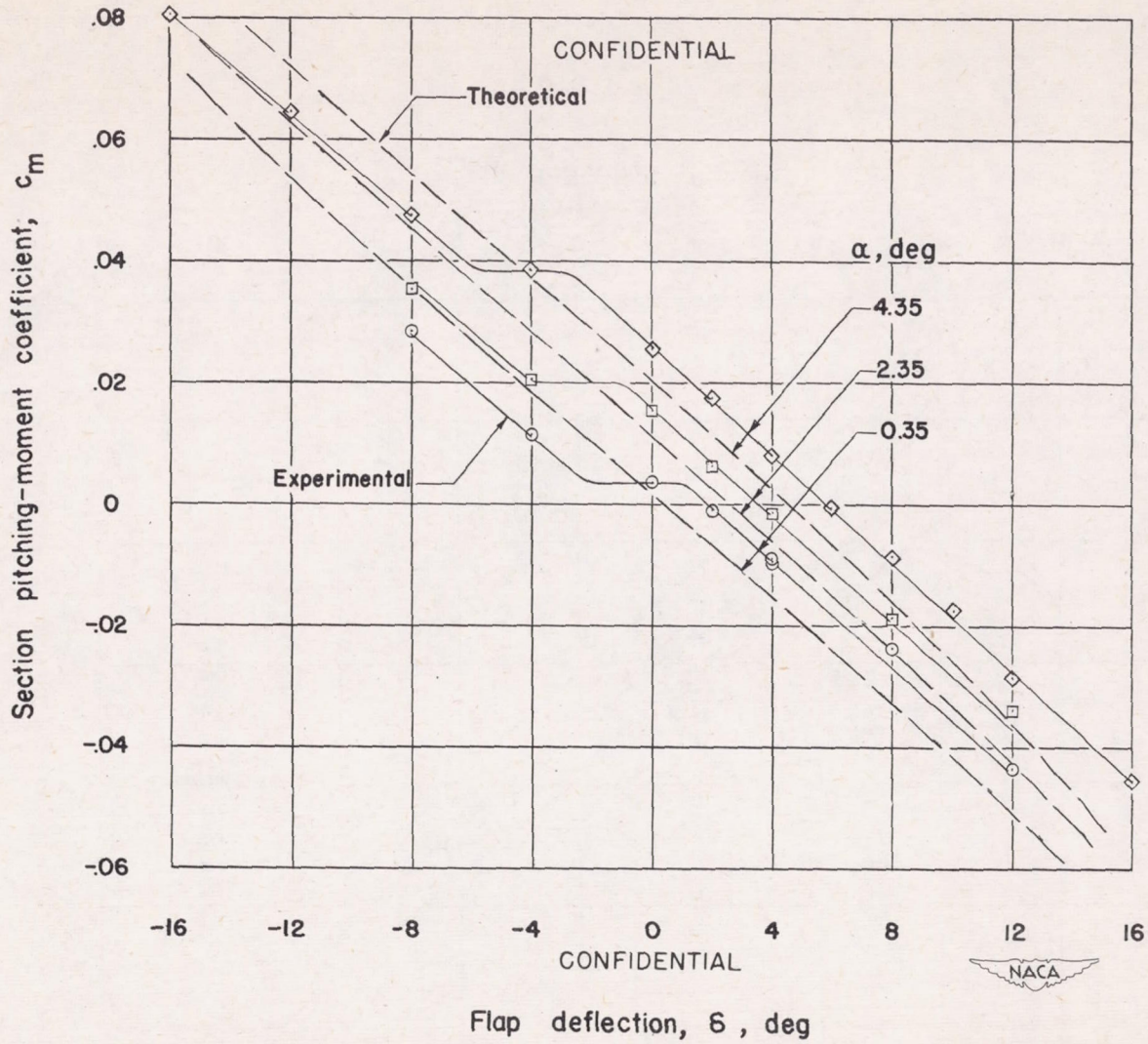

Figure 25.- Variation of section pitching-moment coefficient with flap deflection. Symmetrical circular-arc airfoil, 9-percent thick; station 1; M, 1.62; R, 0.55×10^6.

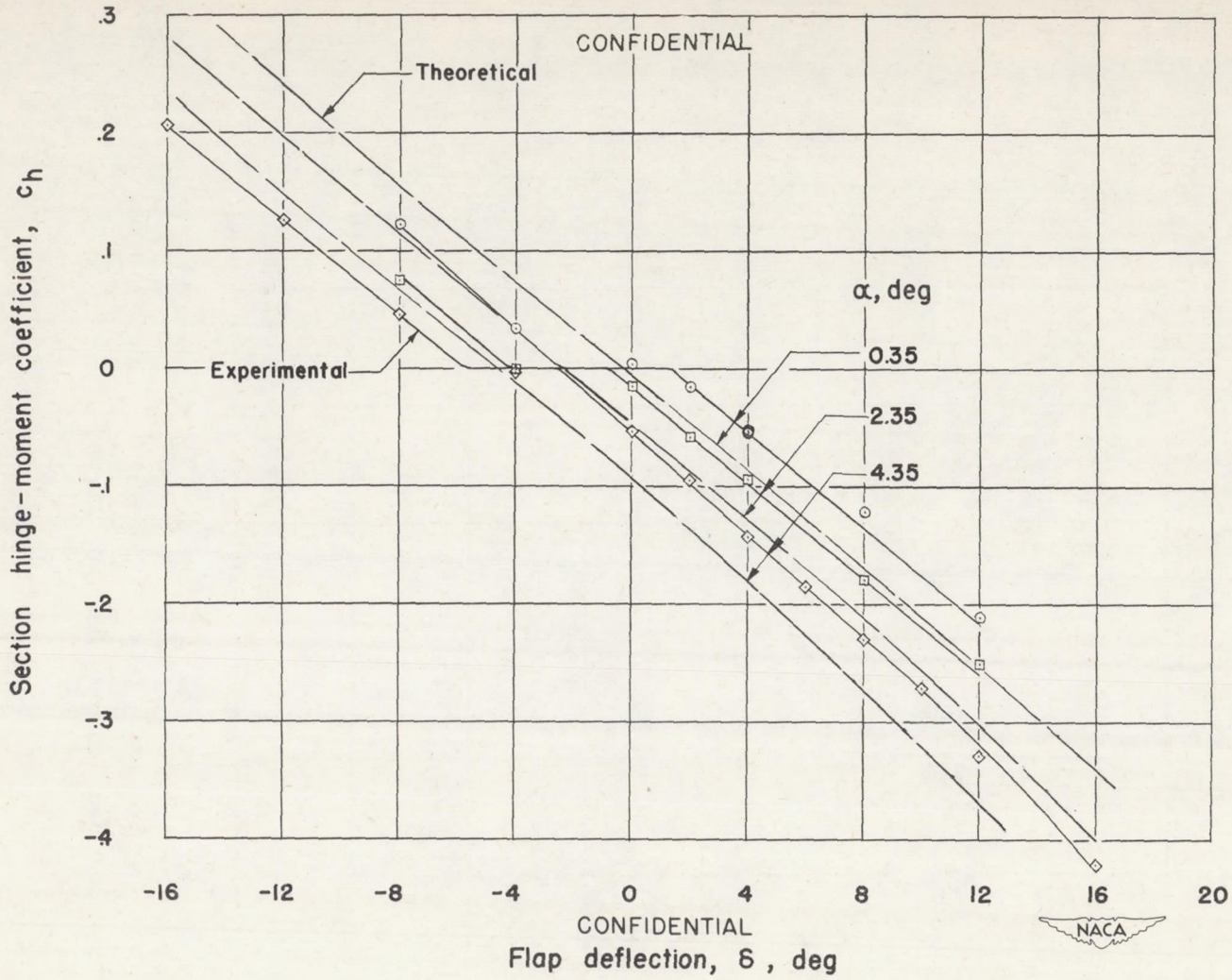

(a) Station 1.

Figure 26.- Variation of section hinge-moment coefficient with flap deflection. Symmetrical circular-arc airfoil, 9-percent thick; M, 1.62; R, 0.55 × 10^6.

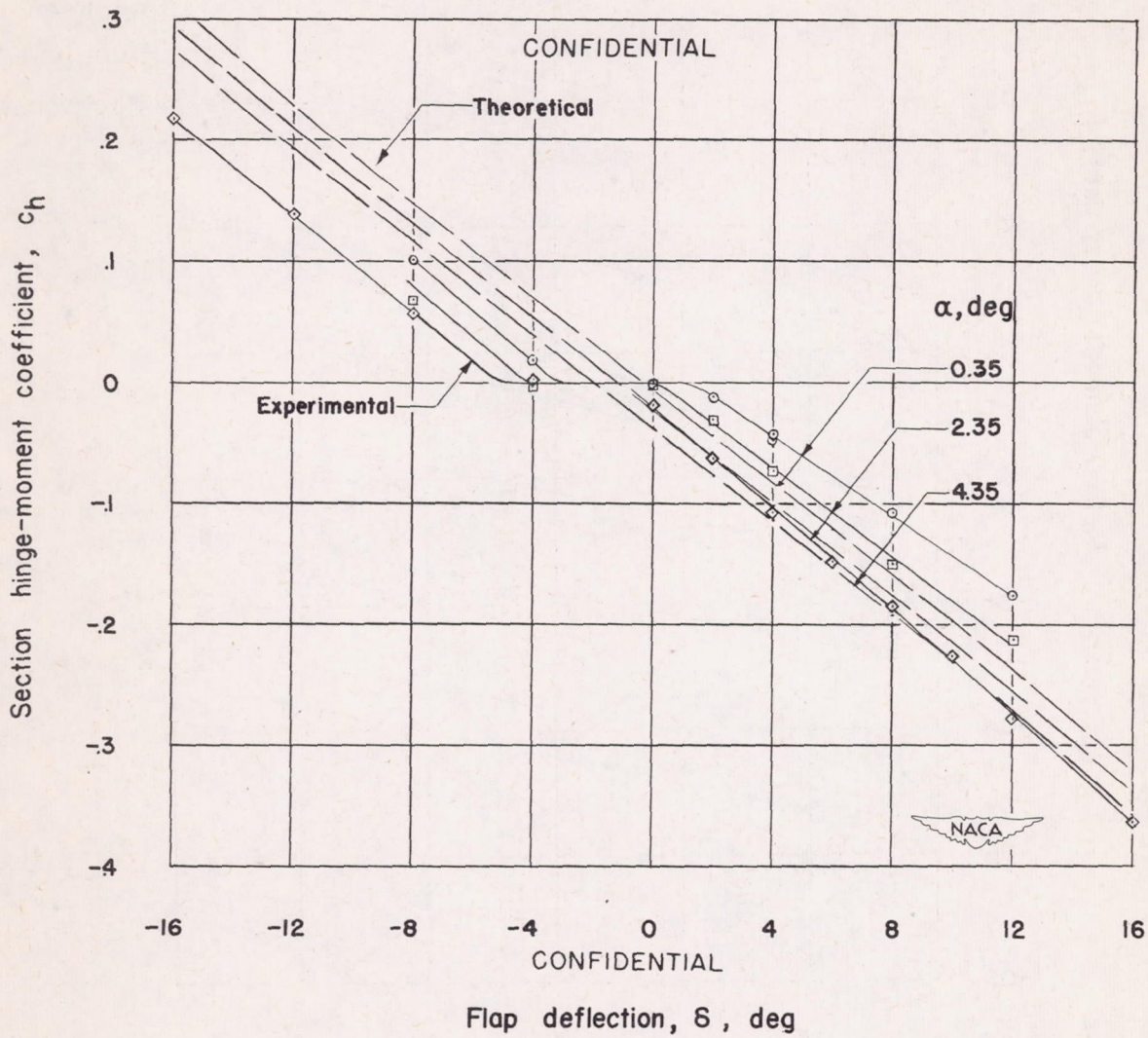

(b) Station 2.

Figure 26.- Concluded.

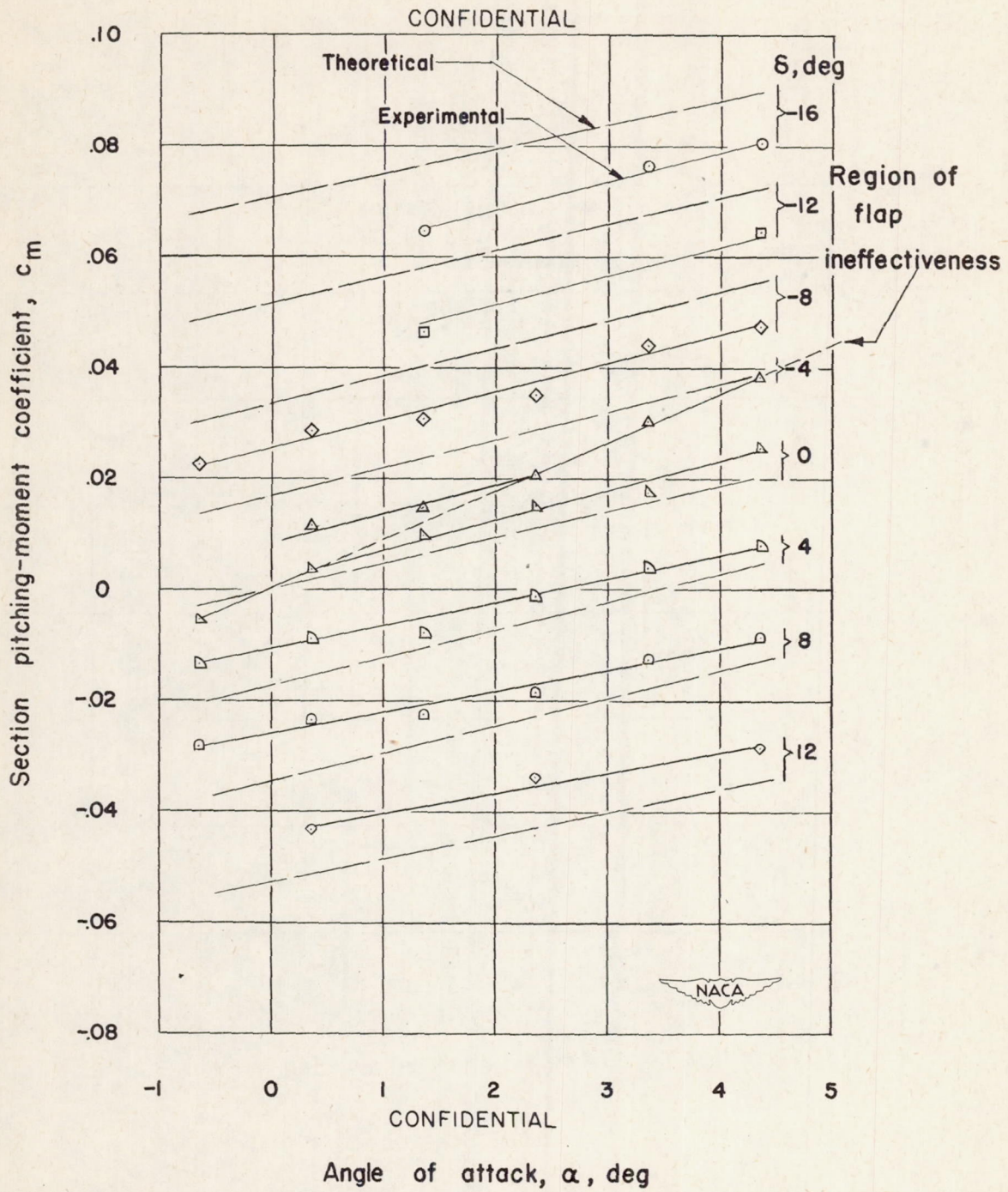

Figure 27.- Variation of section pitching-moment coefficient with angle of attack. Symmetrical circular-arc airfoil, 9-percent thick; station 1; M, 1.62; R, 0.55×10^6.

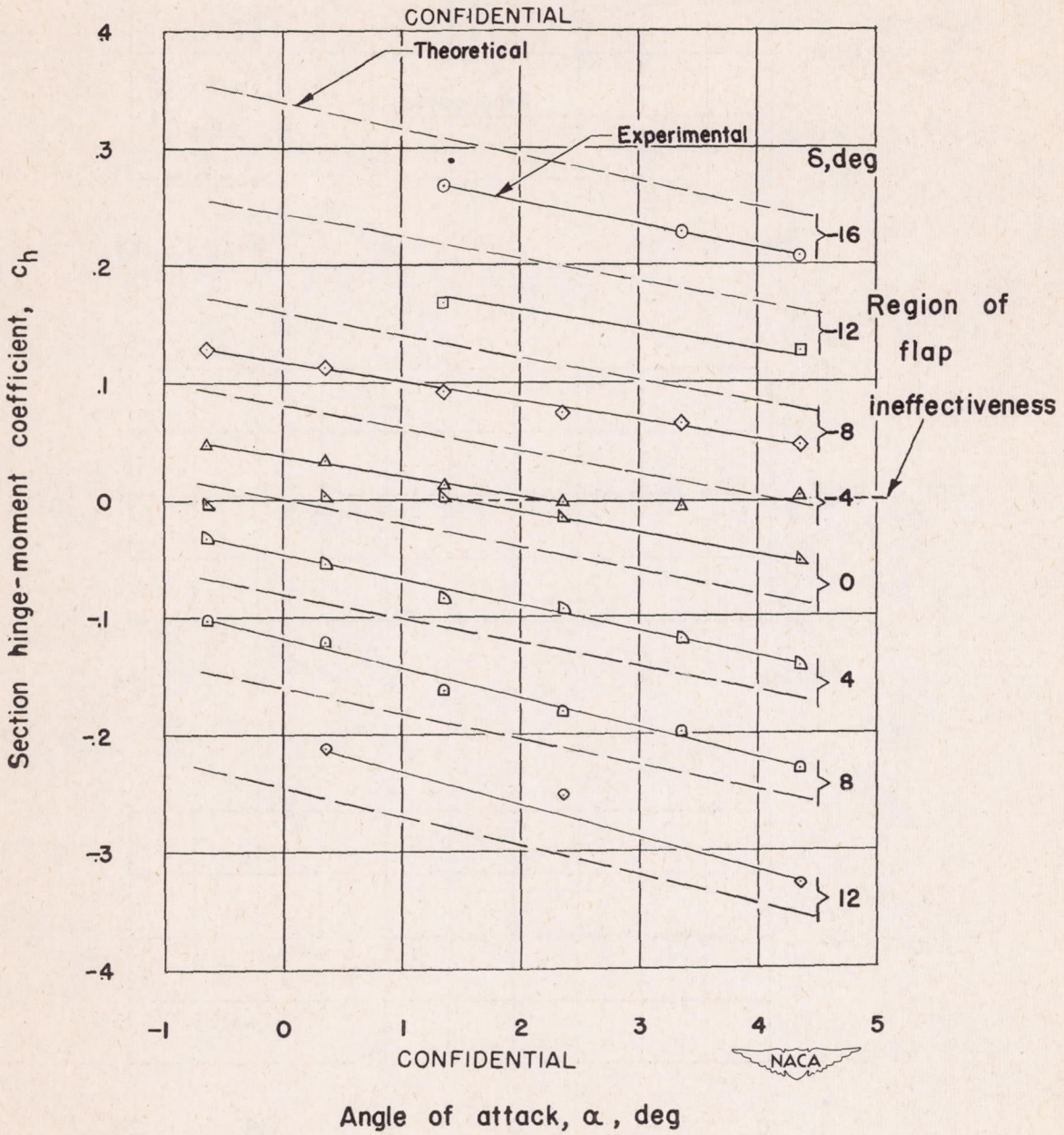

Figure 28.- Variation of section hinge-moment coefficient with angle of attack. Symmetrical circular-arc airfoil, 9-percent thick; station 1; M, 1.62; R, 0.55×10^6.

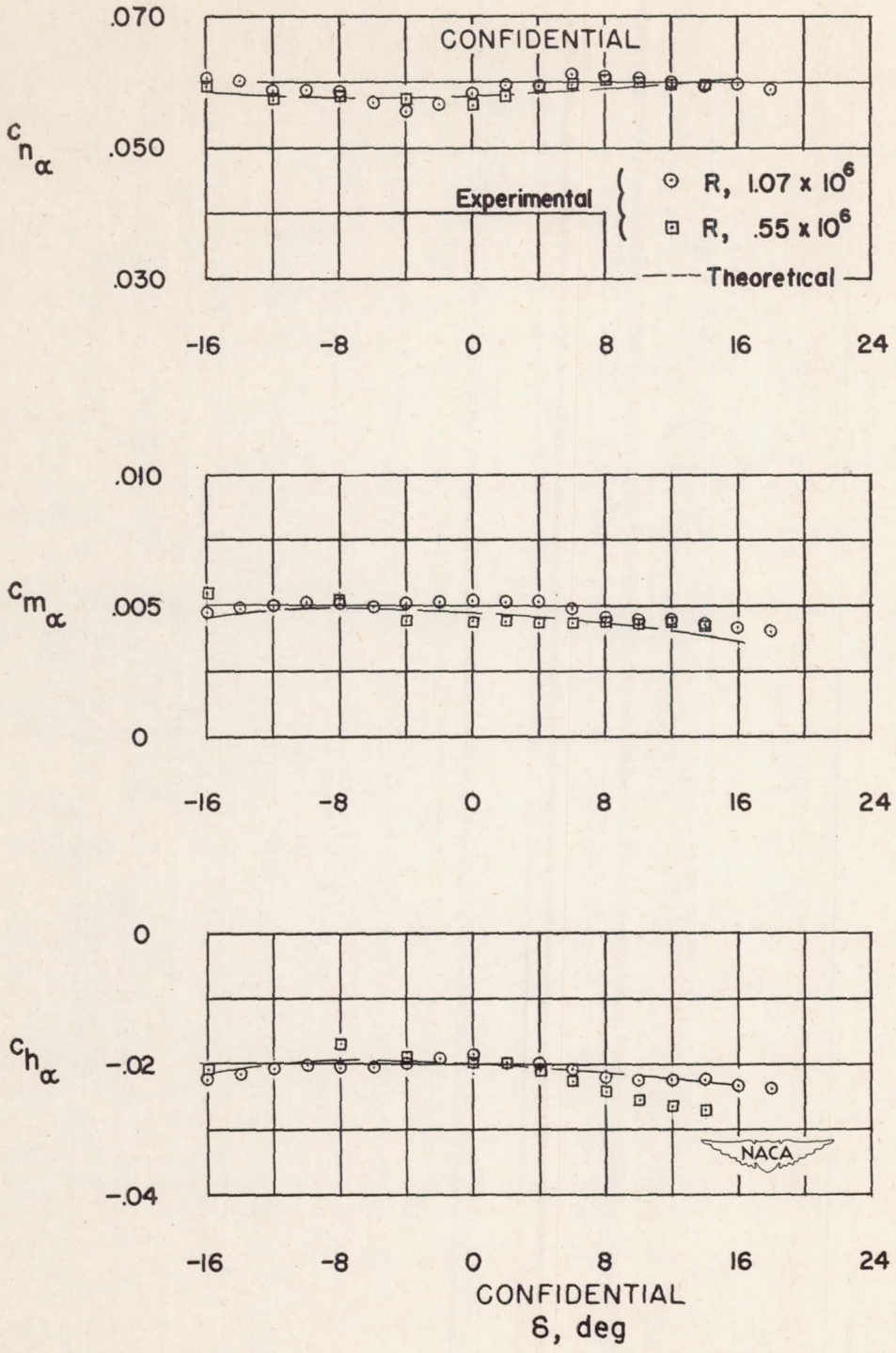

(a) Station 1.

Figure 29.- Variation of slope parameters with flap deflection. Symmetrical circular-arc airfoil, 9-percent thick; M, 1.62.

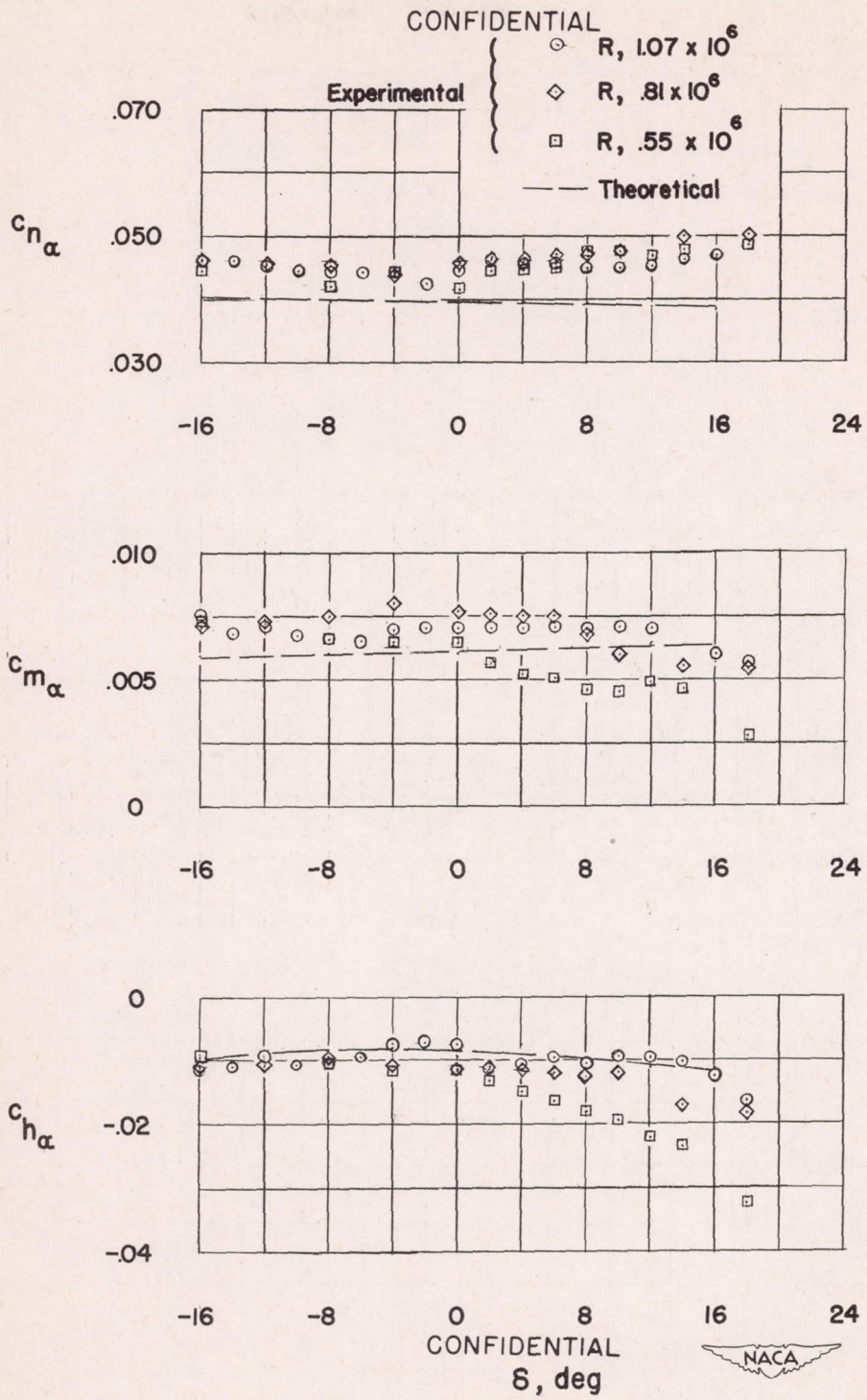

(b) Station 2.

Figure 29.- Concluded.

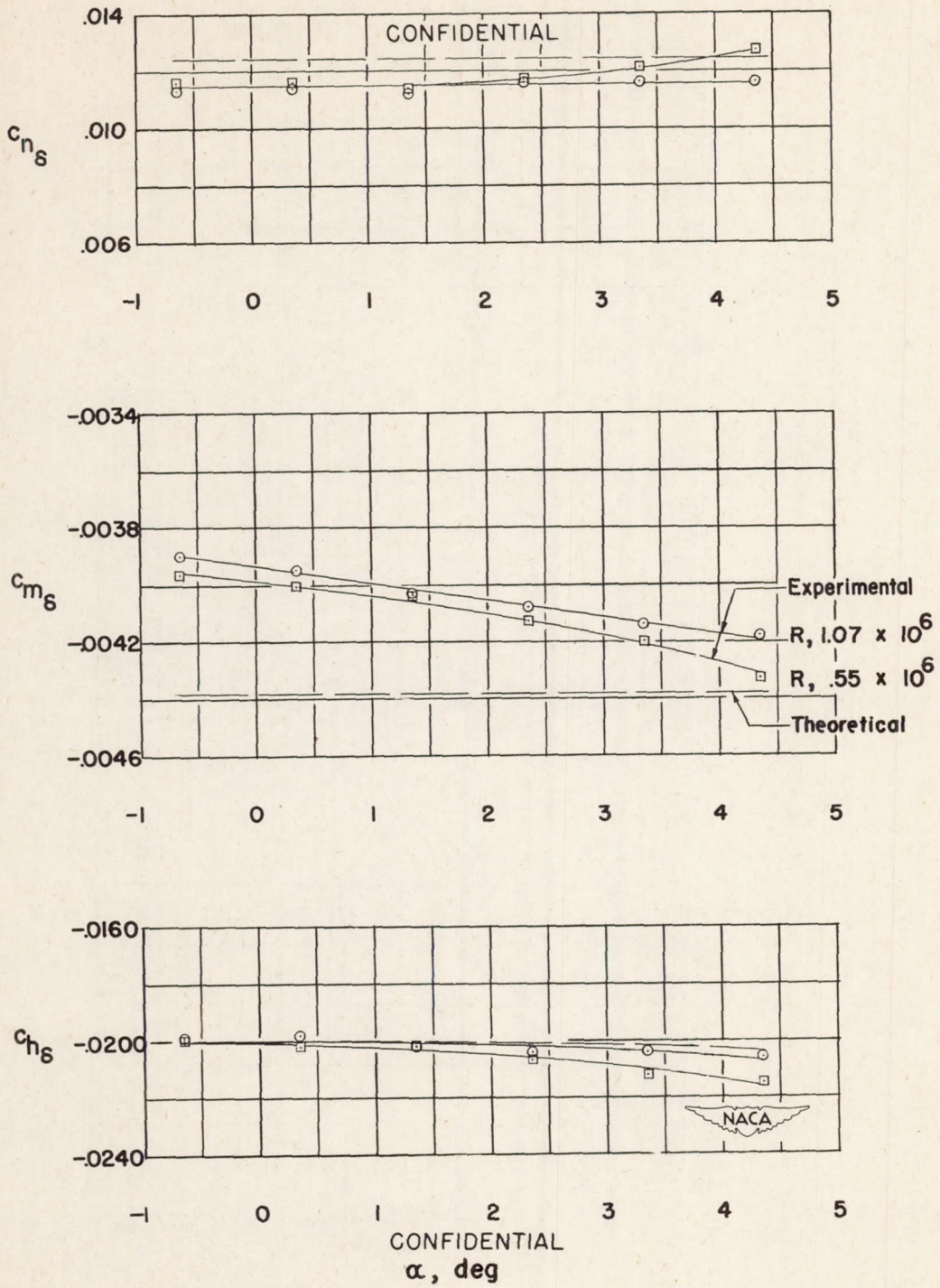

(a) Station 1.

Figure 30.- Variation of slope parameters with angle of attack. Symmetrical circular-arc airfoil, 9-percent thick; M, 1.62.

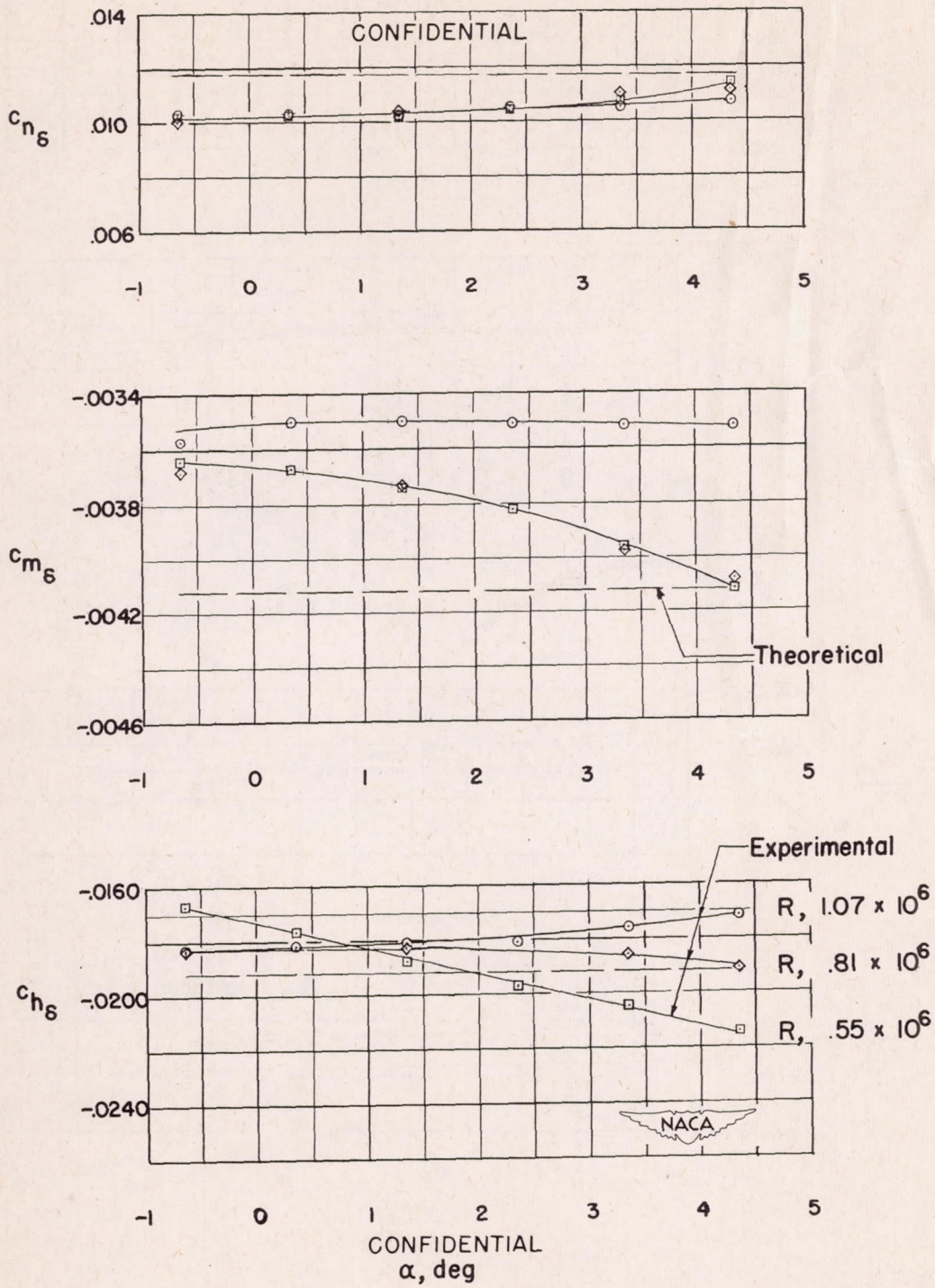

(b) Station 2.

Figure 30.- Concluded.

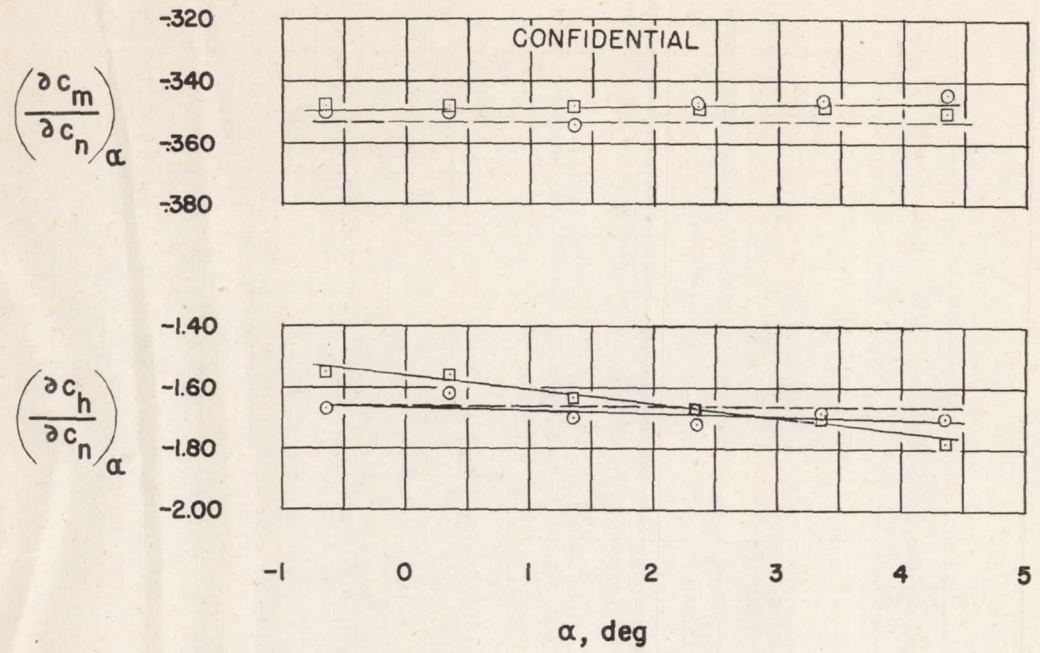

(a) Station 1.

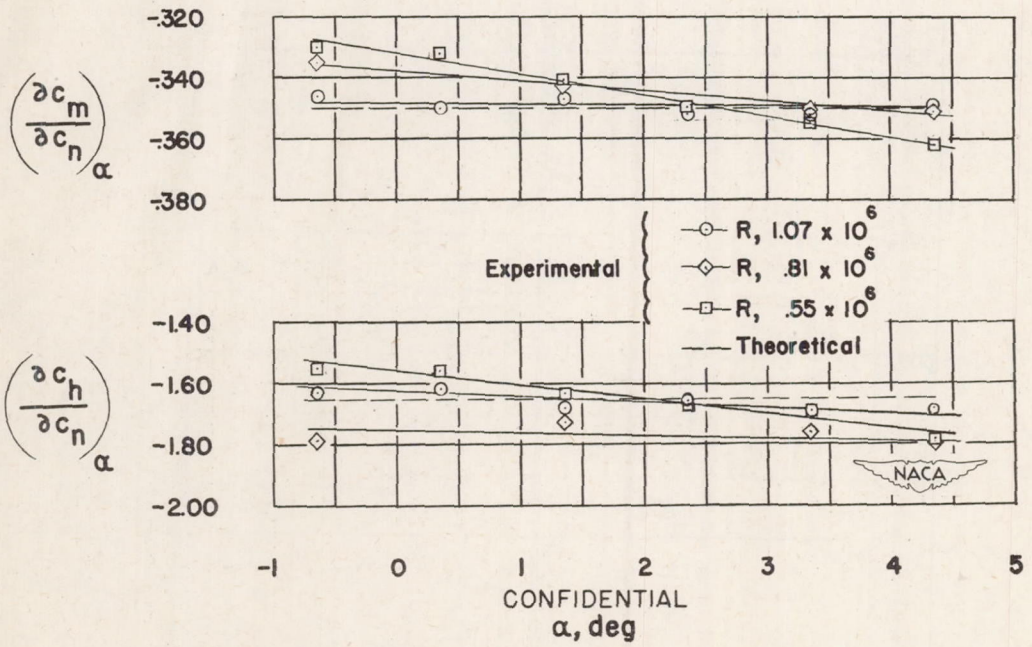

(b) Station 2.

Figure 31.- Variation of slope parameters with angle of attack. Symmetrical circular-arc airfoil, 9-percent thick; M, 1.62.

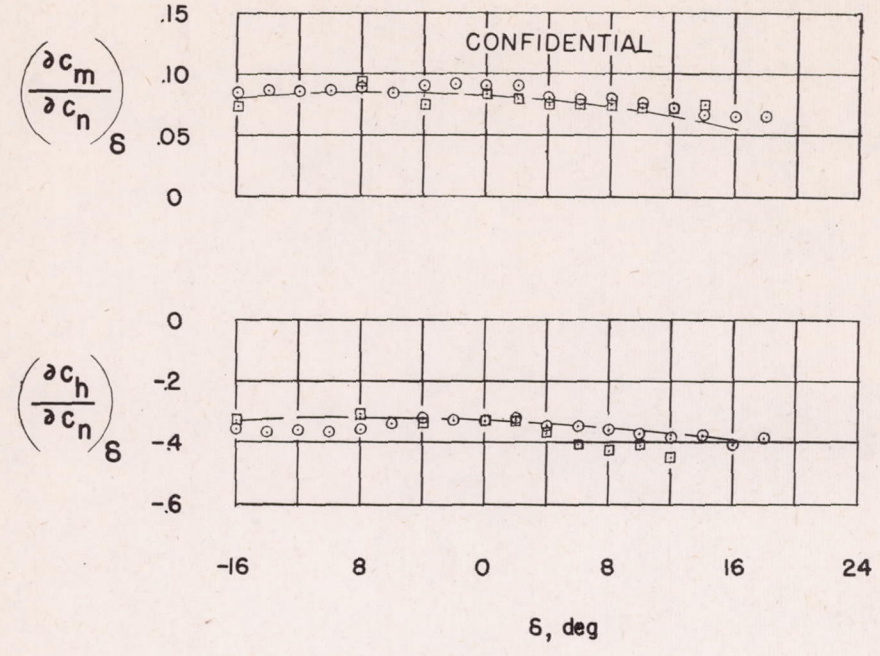

(a) Station 1.

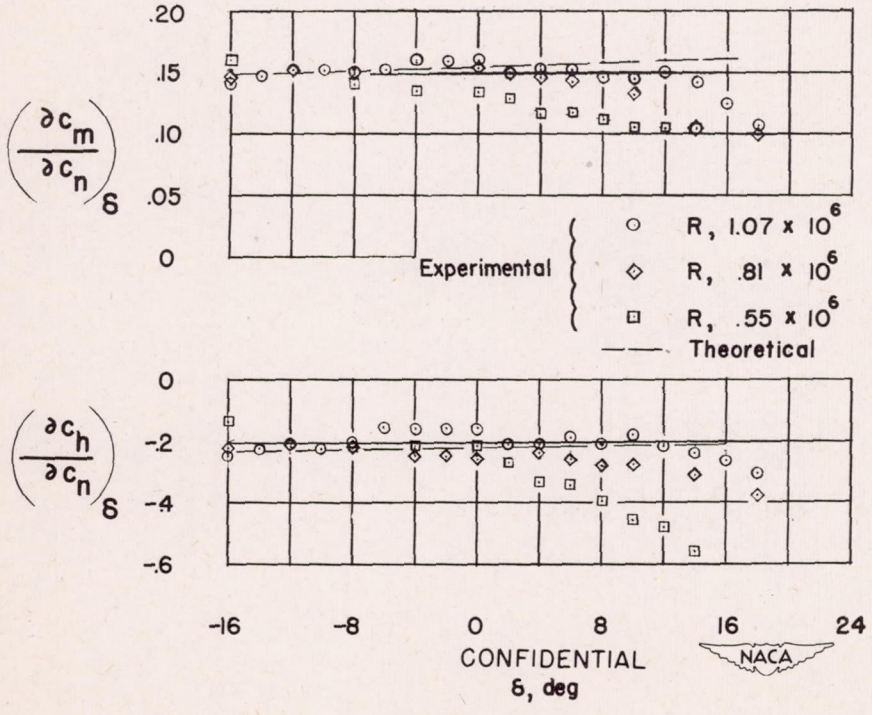

(b) Station 2.

Figure 32.- Variation of slope parameters with flap deflection. Symmetrical circular-arc airfoil, 9-percent thick; M, 1.62.